In-cell analysis of FK506 binding protein 51-glucocorticoid receptor-heat shock protein 90 interaction at single residue resolution

TECHNISCHE UNIVERSITÄT DARMSTADT

Intrazelluläre Untersuchung von FK506 Bindeprotein 51-Glucocorticoidrezeptor-Hitzeschock Protein 90 Interaktionen mit aminosäure-genauer Auflösung

Vom Fachbereich Chemie
der Technischen Universität Darmstadt

zur Erlangung des Grades
Doctor rerum naturalium (Dr. rer. nat.)

Dissertation von
Asat Baischew, M.Sc.

Erstgutachter: Prof. Dr. Felix Hausch
Zweitgutachter: Prof. Dr. Harald Kolmar

Darmstadt 2023

Baischew, Asat : In-cell analysis of FK506 binding protein 51-glucocorticoid receptor-heat shock protein 90 interaction at single residue resolution
Darmstadt, Technische Universität Darmstadt
Jahr der Veröffentlichung der Dissertation auf TUprints: 2023
Tag der mündlichen Prüfung: 24.04.2023

Tag der Einreichung: 9. März 2023

Tag der mündlichen Prüfung: 24. April 2023

Erklärung laut Promotionsordnung

§8 Abs. 1 lit. c PromO

Ich versichere hiermit, dass die elektronische Version meiner Dissertation mit der schriftlichen Version übereinstimmt und für die Durchführung des Promotionsverfahren vorliegt.

§8 Abs. 1 lit. d PromO

Ich versichere hiermit, dass zu einem vorherigen Zeitpunkt noch keine Promotion versucht wurde und zu keinem früheren Zeitpunkt an einer in- oder ausländischen Hochschule eingereicht wurde. In diesem Fall sind nähere Angaben über Zeitpunkt, Hochschule, Dissertationsthema und Ergebnis dieses Versuchs mitzuteilen.

§9 Abs. 1 PromO

Ich versichere hiermit, dass die vorliegende Dissertation selbstständig und nur unter der Verwendung der angegebenen Quellen verfasst wurde.

§9 Abs. 2 PromO

Die Arbeit hat bisher noch nicht zu Prüfungszwecken gedient.

Darmstadt, _____

Asat Baischew

Table of contents

1. Abstract 1

1.1. Zusammenfassung 1

1.2. Abstract 3

2. Introduction 4

2.1. FK506-binding proteins 4

2.2. FKBP51 a Hsp90 cochaperone 7

2.3. FKBP51 inhibits GR activity 10

2.4. Characterization of protein-protein interaction by amber suppression 12

2.4.1. Expansion of the genetic code 12

2.4.2. Photocrosslinking to study protein interaction 14

3. Results and discussion 19

3.1. Chapter 1: Identification of FKBP51 interaction partner by amber suppression enabled photocrosslinking 19

3.1.1. Cloning of the FKBP51 library 19

3.1.2. Establishing of amber suppression 21

3.1.3. Screening the FKBP51 surface for interaction partner 23

3.1.4. Identification of FKBP51 interaction partner 24

3.1.5. Pin-pointing residues important for interaction 28

3.1.6. Crosslinking as a stabilizer 35

3.1.7. Systematic mapping the FKBP51 surface 38

3.1.7.1. FKBP51 interacts with Hsp90 beyond FKBP51^{TPR} 38

3.1.7.2. FKBP51 directly interacts with the Hsp90 cochaperone p23 43

3.1.7.3. FKBP51 directly interacts with the glucocorticoid receptor 46

3.2. Chapter 2: In detail study of the GR-FKBP51 interaction 50

3.2.1. High-throughput cloning approach of the GR TAG library 50

3.2.2. ELISA as a tool to investigate the GR-FKBP51 interaction 52

3.2.2.1. Establishing ELISA for a high-throughput crosslinking screening 52

3.2.2.2. Screening the GR for FKBP51 interactions 60

3.2.3. Exploration of GR-p23 contacts 67

3.3. Chapter 3: Pharmacological studies reveals the architecture of the FKBP51-Hsp90-apoGR complex 70
3.3.1. FKBP51 and rapamycin 70
3.3.2. The FKBP51 inhibitor SAFit2 reveals a multi-layered interaction of GR and FKBP51 74
3.3.3. FKBP51 and p23 interact with apoGR in a Hsp90-dependent manner 76
4. Conclusion 83
5. References 87
6. Materials and methods 104
6.1. Materials 104
6.1.1. General chemicals 104
6.1.2. General plastics and materials 104
6.1.3. Cell culture plastics 105
6.1.4. Devices 105
6.1.5. Software 105
6.1.6. Antibodies 106
6.2. Generation of the TAG library by Golden Gate reaction 106
6.2.1. PCR 106
6.2.2. Agarose gel electrophoresis 107
6.2.3. Golden Gate reaction 107
6.2.4. Transformation 108
6.2.5. Plasmid DNA isolation 108
6.2.6. Production of the FKBP51 TAG Twin Strep FLAG library 109
6.3. Cell culture 109
6.3.1. Growth condition and cell passaging 109
6.3.2. Cell counting 109
6.3.3. Cell culture plate coating 110
6.3.4. Amber suppression of FKBP51 mutants 110
6.3.5. Amber suppression with isotopically labelled pBpa 110
6.3.6. Amber suppression of glucocorticoid receptor mutants 111
6.3.7. UV crosslinking and cell lysis 112
6.4. Western blot 112

6.5. Immunoprecipitation 112
6.6. Coomassie staining and gel drying 113
6.7. Size exclusion chromatography 113
6.8. Sample preparation for mass spectrometry analysis 113
6.8.1. SDS PAGE 113
6.8.2. In gel digest 114
6.8.3. Peptide isolation 114
6.8.4. Mass spectrometry analysis at the Munch Group in Frankfurt 114
6.8.5. Data analysis 115
6.8.6. In-house mass spectrometry analysis 115
6.9. Silver staining 116
6.10. ELISA 116
6.10.1. ELISA coating 116
6.10.2. ELISA 117
7. Extended Figures 118
8. Abbreviations 125
9. Bibliography 126
10. Acknowledgment 127

1. Abstract

1.1. Zusammenfassung

Die Immunophiline FKBP51 und FKBP52 spielen eine Schlüsselrolle bei der Hsp90-vermittelten Reifung von Steroidhormonrezeptoren, die für Stressverarbeitung und eine korrekte geschlechtsspezifische Embryonalentwicklung entscheidend sind. Ein wichtiger Vertreter ist der Glucocorticoidrezeptor (GR), dessen Aktivierung durch FKBP51 unterdrückt und durch FKBP52 beschleunigt wird. Trotz ihrer wichtigen Rolle sind die molekularen Wirkungsweisen von FKBP51 und FKBP52 nur unzureichend verstanden, da die dynamischen Interaktionen der FKBP-vermittelten GR-Regulierung experimentell schwer zu analysieren sind.

In dieser Arbeit wird der systematische Einbau einer photoreaktiven Aminosäure in menschliche HEK-Zellen vorgestellt, der die Erfassung der dynamischen FKBP51-GR-Hsp90-Interaktionen ermöglicht. Photoreaktive, unnatürliche Aminosäuren werden durch die Erweiterung des genetischen Codes ortsspezifisch eingebaut und fungieren als Sensor für die räumliche Nähe von Proteinen, um die Interaktion mit einer aminosäure-genauen Auflösung zu erfassen. Dies wird zuerst an FKBP51 durchgeführt, wobei die Interaktionsfläche zwischen FKBP51 und Hsp90 weit über die bekannte FKBP51-TPR-Domäne vermittelte Interaktion hinaus gezeigt wird. Sie umfasst zusätzlich die FK1- als auch die FK2-Domäne von FKBP51. Darüber hinaus wird das Hsp90-Cochaperon p23 als direkter Interaktionspartner von FKBP51 identifiziert, was darauf hindeutet, dass für eine funktionierende Hsp90-Maschinerie ein Multiproteinkomplex erforderlich ist.

Die Entwicklung einer geeigneten Hochdurchsatzanalyse für die Charakterisierung von Proteininteraktionen mittels ELISA ermöglicht die detaillierte Aufklärung der GR-FKBP51-Interaktionsfläche. Die identifizierten Crosslink-Stellen sind abhängig von einer funktionierenden Hsp90-Cochaperon-Maschinerie und werden durch die Aktivierung des GR gestört. Die Crosslinks zeigen ein charakteristisches Muster und erlauben die relative Orientierung sowie die Interaktionsflächen innerhalb der FKBP51/p23-apoGR-Komplexe zu definieren.

Des Weiteren ermöglicht der hier entwickelte ELISA die Quantifizierung der intrazellulären Aktivierung des GR durch Dexamethason. Es wird gezeigt, dass die GR→FKBP52 Crosslinks fünfmal empfindlicher für die Aktivierung des GR sind als die GR→FKBP51 Crosslinks. Die ELISA-Daten zeigen, dass die GR-Aktivierung des FKBP52-Hsp90-GR-Komplexes im Vergleich zum FKBP51-Hsp90-GR-Komplex schneller ist. Dies bestätigt die bekannte aktivierende Wirkung von FKBP52 auf den GR sowie der inhibierenden Wirkung von FKBP51.

Durch den Einbau von Photocrosslinkern in eine umfassende FKBP51 und GR Mutantenbibliothek wird in dieser Arbeit die Architektur und funktionelle Charakterisierung der FKBP51- und p23-Hsp90-apoGR-Preaktivierungskomplexe gezeigt.

1.2. Abstract

The large immunophilins FKBP51 and FKBP52 play key roles in the Hsp90-mediated maturation of steroid hormone receptors, which is crucial for stress-related disorders and correct sexual embryonic development, respectively. A prominent regulatory target is the glucocorticoid receptor (GR), whose activation is repressed by FKBP51 and facilitated by FKBP52. Despite their vital roles, the molecular modes of action of FKBP51 and FKBP52 are poorly understood since the transient key states of FKBP-mediated GR-regulation have remained experimentally elusive. This work presents a systematic incorporation of a photoreactive amino acid inside human cells that allows capture of the transient FKBP51-GR-Hsp90 interactions. A photoreactive, unnatural amino acid is site specifically incorporated by amber suppression and acts as a proximity sensor to map the interaction at single residue resolution. This is first established for FKBP51, where the FKBP51-Hsp90 interaction interface is explored well beyond the known FKBP51-TPR-domain mediated interaction including both the FK1- and FK2-domain of FKBP51. Additionally, the Hsp90 cochaperone p23 is identified as a direct interaction partner of FKBP51 suggesting that a multi-protein complex is needed for a functional Hsp90 machinery.

Creating a suitable, high-throughput analysis for mapping protein interaction via ELISA allows the elucidation of the GR-FKBP51 interaction interface in great detail. The identified crosslinking sites all depend on a functional Hsp90 chaperone cycle, are disrupted by GR activation, and cluster in characteristic patterns, defining the relative orientation and contact surfaces within the FKBP51/p23-apoGR complexes.

Moreover, the developed ELISA enables quantification of in-cell activation of the GR by its synthetic agonist dexamethasone. GR→FKBP52 crosslinks were found to be 5-fold more sensitive to GR activation compared to GR→FKBP51 crosslinks. The ELISA data show that GR activation is facilitated in the context of a FKBP52-Hsp90-GR complex compared to GR in a FKBP51-Hsp90-GR complex. This in accordance with the well-documented GR-facilitating effect of FKBP52 and the GR-repressing effect of FKBP51.

Taken together, this work presents the architecture and functional annotation of FKBP51-, and p23-containing Hsp90-apoGR pre-activation complexes, trapped by large scale in-cell photocrosslinking.

2. Introduction

2.1. FK506-binding proteins

FK506-binding proteins (FKBPs) are a class of proteins that are named after their ability to bind the immunosuppressive natural product FK506. FK506 (see Figure 1) is a polyketide isolated from a soil sample taken near Mount Tsukuba in Japan that is produced by *Streptomyces tsukubaensis* (Tanaka et al., 1987). The name arises from the molecule's identification number FK506009 given by the Japanese pharma company Fujisawa. FKBPs additionally bind another immunosuppressive natural product, rapamycin (see Figure 1, named after their origin of discovery the Easter Islands, in the native tongue Rapa Nui). FKBPs are thus part of the immunophilins protein class.

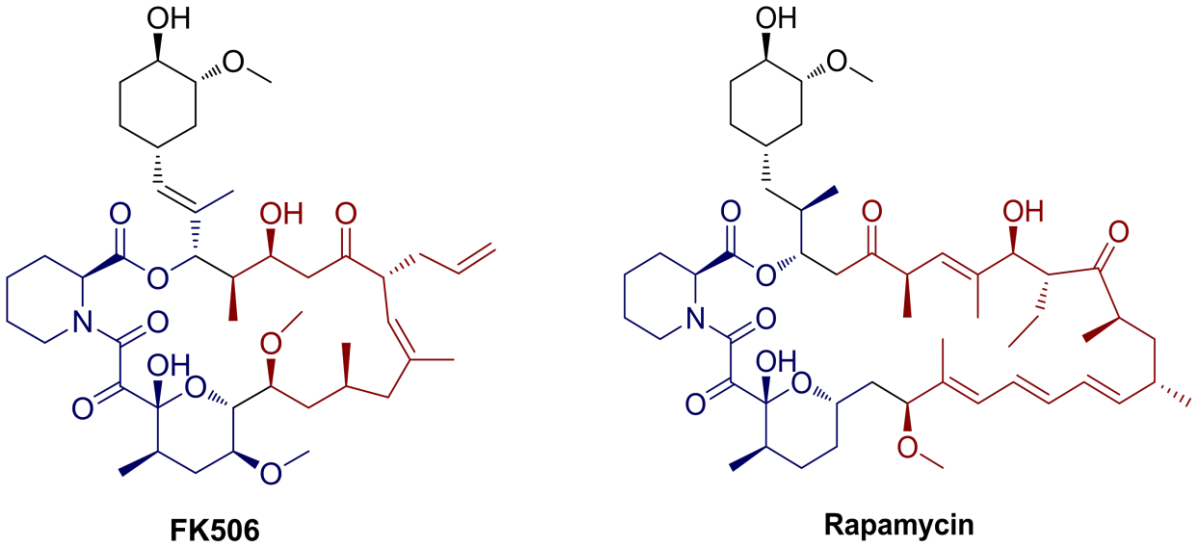

Figure 1: Chemical structure of the natural FKBP ligands FK506 and rapamycin. The FKBP binding domain is highlighted in blue and the effector domain is highlighted in red.

The most prominent and smallest protein of this FKBP family is the 12 kDa small FKBP12, which comprises five antiparallel β-sheet wrapping around an α-helix. This fold the FK domain. FK domains often have a prolyl-peptidyl-isomerase activity and catalyzes the *cis-trans* isomerization of a peptide bond preceding a proline. The *trans* conformation of the peptide bond features a higher stability due to the lower steric hindrance between the amino acids on neighboring sides of the bond than in the *cis* conformation (Weiss et al., 1998). Therefore, most peptide bonds occupy the *cis* conformation in less than 0.01%. The exception is a proline, where the peptide bond where is more favorable in a *cis* conformation with an occupancy of 5%. This conformational change produces an increased variety in protein folding, making *cis-trans* interconversion a rate-limiting step in protein folding (Weiss et al., 1998). So far at least 15

FKBPs have been identified in humans with various cellular functions and distributions (Galat, 2008; Rulten et al., 2006). For example, FKBP12 is present in the cytoplasm and stabilizes the ryanodine receptor (Brillantes et al., 1994; Jayaraman et al., 1992). FKBP12 is thought to stabilize ryanodine receptor 1 (RyR1), while the close homolog FKBP12.6 stabilizes RyR2 (Brillantes et al., 1994). Nevertheless, this generalization seems controversial as FKBP12.6 is described as activator of skeletal RyR1, while FKBP12 may act as an activator of the cardiac muscle RyR2. (Venturi et al., 2014) These associations could explain hypertension and endothelial dysfunction as a side effect after prolonged FK506 or rapamycin treatment (Long et al., 2007). However, FKB12 is most prominently known for the formation of a ternary complex by a molecular glue mechanism enabling the immunosuppressant effect of FK506 and rapamycin. Here , the binding domain of either of the molecules connect FKBP12 and the effector domain, recruiting calcineurin or mTOR, respectively (Banaszynski et al., 2005; Sabers et al., 1995; Steiner et al., 1992). Another family member is FKBP51, which was first characterized as a protein contributing to glucocorticoid insensitivity in squirrel monkeys. Those primates have elevated cortisol levels, however, show no signs of glucocorticoid excess. Compared to humans, FKBP51 expression in squirrel monkey is 13 times higher. This is thought to inhibit the glucocorticoid activity by weakening the hormone binding affinity of the receptor 11-fold (Denny et al., 2000; Reynolds et al., 1999). FKBP51 is described to be involved in many other molecular pathways but remains best characterized as a cochaperone of Hsp90 in the steroid hormone receptor (SHR) maturation cycle (Baischew et al., 2023; Hähle et al., 2019).
FKBP51 consists of three domains: an N-terminal FK1 domain (residue V33−K138) that mediates peptidyl-prolyl-*cis-trans* isomerase (PPIase) activity and is able to bind immunosuppressants, an enzymatically inactive FKBP-like FK2 domain (residue G147−E251), and a C-terminal tetratricopeptide repeat domain (TPR) (residue T261−M412) as well as a C-terminal extended helix 7 (eH7) (residue F413−456V) that can both bind the C-terminal domain of the heat shock protein 90 (Hsp90) (Sinars et al., 2003). The structure is depicted in Figure 2. FKBP51 has a close homolog, FKBP52, with a shared sequence of 60% and a sequence similarity of 75%. FKBP52 acts partially in an antagonistic manner to FKBP51 (Hähle et al., 2019). The domains of both proteins fold similarly, but the relative orientation of the domains may differ, e.g., the FK1 domain of both immunophilins are rotated against each other. Further, the hinge regions bridging FK1 and FK2 domain have different conformations as well (Wu et al., 2004). The FK1 domain of FKBP51 shares a sequence similarity of 50% with FKBP12 and shows a comparable structure with five antiparallel β-sheets centering an α-helix. Within a hydrophobic pocket at the N-terminal part of the central α-helix, FK506 binds by forming hydrogen bonds to the amino acid residues D68, Q85, I87, and Y113 (Bracher et al., 2011).

A proline rich loop (residues S118−P123) stretches over the binding pocket. The FK2 domain shows a FK1-like structure but has neither PPIase activity nor does it bind immunosuppressive ligands (Bracher et al., 2011). However, it has been suggested that the FK2 domain is involved in protein interactions and possesses scaffolding function (Sinars et al., 2003). The TPR domain consists of 7 α-helices that are responsible for binding to the C-terminal EEVD motif of Hsp90 (Hähle et al., 2019). The TPR domain is conserved and characteristic for a class of Hsp90 binding proteins including the immunophilins, Protein Phosphatase 5 (PP5) (Chen et al., 1996) and Hsp90-Hsp70 organizing protein (Hop/Sti1) (Chen et al., 1996; Lässle et al., 1997), all competing for Hsp90 binding (Nair et al., 1997; Owens-Grillo et al., 1995; Ratajczak & Carrello, 1996). The TPR domain is followed by the C-terminal domain (~60 amino residues from E400−end) that is shown to significantly contribute to Hsp90 binding (Cheung-Flynn et al., 2003). A recent cryo-EM of the Hsp90-FKBP51-p23 complex (see Figure 2) shows FKBP51 binding to the closed ATP-bound state of Hsp90 dimer with extensive contact to the C-terminal Hsp90 dimer interface through its C-terminal helix extension. This identified the C-terminal helix 7 as a key recognition element that explains a 2:1 stoichiometry of Hsp90 and FKBP51 (Lee et al., 2021).

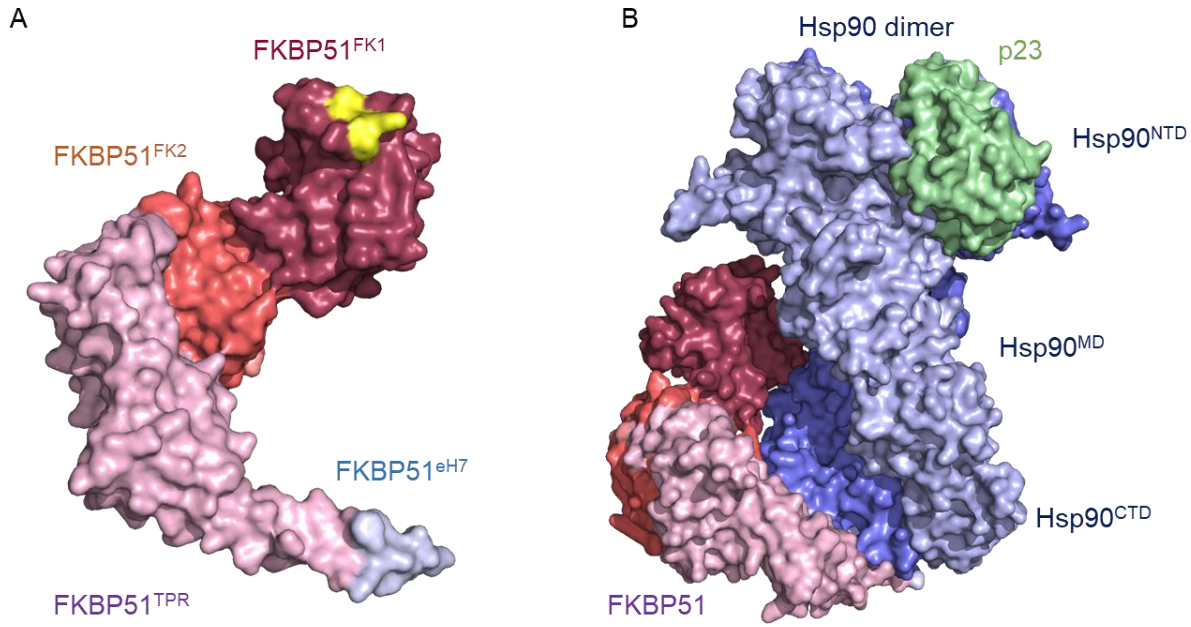

Figure 2: Structure of full-length FK506-binding protein 51 (A, PBD-ID: 5NJX) and cryoEM structure of the Hsp90-FKBP51-p23 complex (B, PBD-ID: 7L7J). The FK1 domain is colored dark red and the proline rich loop is colored in yellow, FK2 domain is colored in salmon, and TPR domain is colored in light pink with the C-terminal extended helix 7 colored in pale blue. Hsp90 dimers are colored in blue with p23 colored in light green.

The *fkbp5* gene, encoding FKBP51, received great attention as a correlation was discovered between single nucleotide polymorphisms and the recurrence of depressive episodes and rapid response to antidepressant treatment of major depressive disorder (Binder et al., 2004). Furthermore, FKBP51 acts as an important regulator of endocrine stress responses and has emerged as a potential drug target for stress-related disorders (Schmidt et al., 2012). This includes depression and post-traumatic stress disorder as well as metabolic disorders (Balsevich et al., 2017) like obesity and diabetes, and chronic pain (Maiarù et al., 2016). Importantly, no potentially adverse effects have been observed in FKBP51$^{-/-}$-mice so far, suggesting FKBP51 as a novel and potentially safe drug target (Sabbagh et al., 2014). Instead FKBP51-deficient mice underline the important role of FKBP51 as a regulator of the hypothalamus–pituitary–adrenal axis, a key stress response system in mammals (Hartmann et al., 2012; O'Leary III et al., 2011; Touma et al., 2011). In contrast, FKBP52$^{-/-}$ mice have a severely compromised embryonic development, which is explained by reduced androgen and progesterone receptor signaling (Sivils et al., 2011). Interestingly, selective inhibition of FKBP51 by the compounds of the SAFit family displays similar effects as the knock down of FKBP51 and shows promising effects in animal models (Gaali et al., 2015; Maiarù et al., 2016)

2.2. FKBP51 a Hsp90 cochaperone

FKBP51 was discovered as a cochaperone of the progesterone receptor (PR) and Hsp90 interaction partner 30 years ago (Smith et al., 1990; Smith, 1993). Since then it is described as a cochaperone that regulates the transcriptional activity of several steroid hormone receptors (SHR) (Schülke et al., 2010; Stechschulte & Sanchez, 2011; Storer et al., 2011). Prominently, FKBP51 decreases the activity of both glucocorticoid receptor and the progesterone receptor but cell-type specifically increases the activity of the androgen receptor (Ni et al., 2010; Periyasamy et al., 2010; Schülke et al., 2010). Cochaperones are roughly defined as cofactors with scaffolding and regulatory functions on molecular chaperones such as Hsp90, which is a highly abundant protein in the cytosol. Chaperones are conserved proteins that operate as key components of the protein folding machines. Here, Hsp90 is exceptional in a sense that it functions in the later stages of folding by binding to partially folded protein intermediates (Jakob et al., 1995). For Hsp90, these proteins are so called "client" proteins and are typically identified by their loss of activity in response to inhibition of ATP hydrolysis on Hsp90 (Schneider et al., 1996; Whitesell et al., 1994). During the ATP hydrolysis cycle, Hsp90 undergoes nucleotide-induced conformational changes and thereby supports energy-intense rearrangements of clients (Krukenberg et al., 2011; Prodromou et al., 2000). Hsp90 acts as a homodimer that dimerizes in the open (apo) state through its C-terminal domain (CTD),

thereby adopting a V-shaped conformation (Krukenberg et al., 2008). The nucleotide binding sites at the N-terminal domain rearrange during ATP binding. ATP hydrolysis leads to the dimerization of both domains to a close conformation (Ali et al., 2006). Furthermore, the Hsp90 middle domain has a wide contact interface with the client which is threaded through the Hsp90 lumen providing a mostly hydrophobic tunnel. The movement of Hsp90 through the ATP hydrolysis circle is regulated and accompanied by a variety of cochaperones that have been most intensively studied for the model client GR, especially its ligand binding domain (LBD). (Lorenz et al., 2014; Morishima et al., 2000; Nathan & Lindquist, 1995; Picard et al., 1990; Pratt & Toft, 1997; Smith & Toft, 2008).

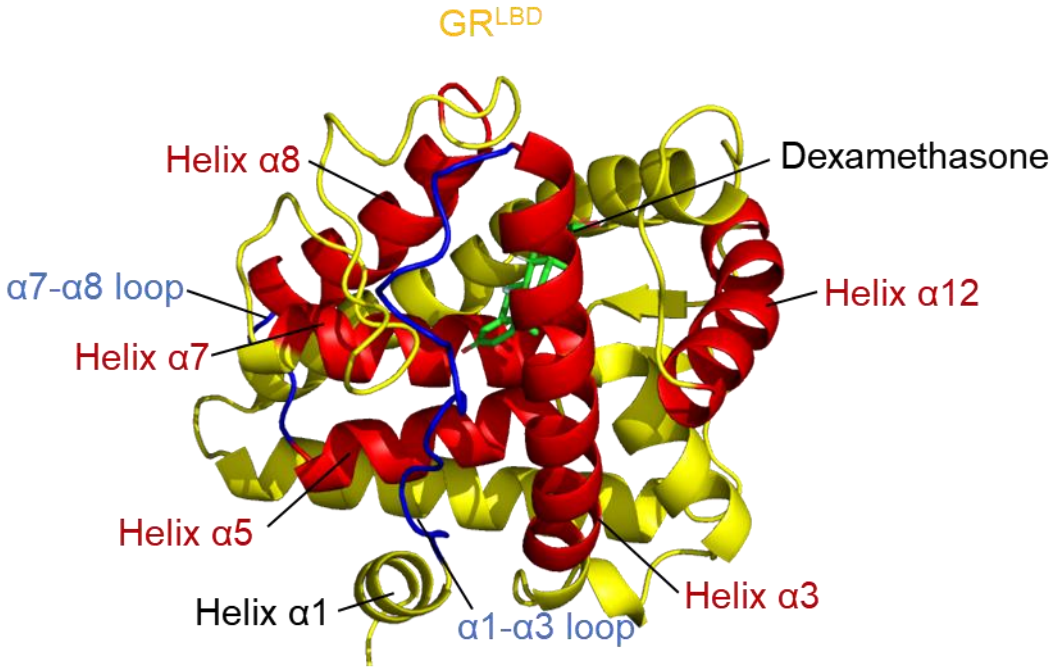

Figure 3: Structure of the dexamethasone-bound GR^{LBD} (523–777, PDB-ID: 7KRJ). α-helices shown in red and yellow and key loops highlighted in blue.

GR activity is regulated through the C-terminal ligand binding domain (LBD) with a helical structure and a ligand binding pocket in the center of the domain (see Figure 3). It is speculated that the ligand unbound LBD is more dynamic while ligand binding provides stability with the ligand deeply embedded in the structure (Bain et al., 2007). GR maturation and activation is a dynamic process from an inactive GR to a loading and then a mature complex (Pratt et al., 2006) (see Figure 4). It is generally accepted that in order to stabilize and activate the GR, a complex of heat shock proteins is required, including Hsp90, Hsp70, Hop, Hsp40 and p23 (Kirschke et al., 2014; Pratt & Toft, 1997). Recent cryo-EM structures give potential new insights into the structural basis of both the client-loading mechanism as well as the client-

maturation (Noddings et al., 2022; Wang et al., 2022). A schematic overview of the proposed GR maturation process through the Hsp90 machinery is shown in Figure 4.

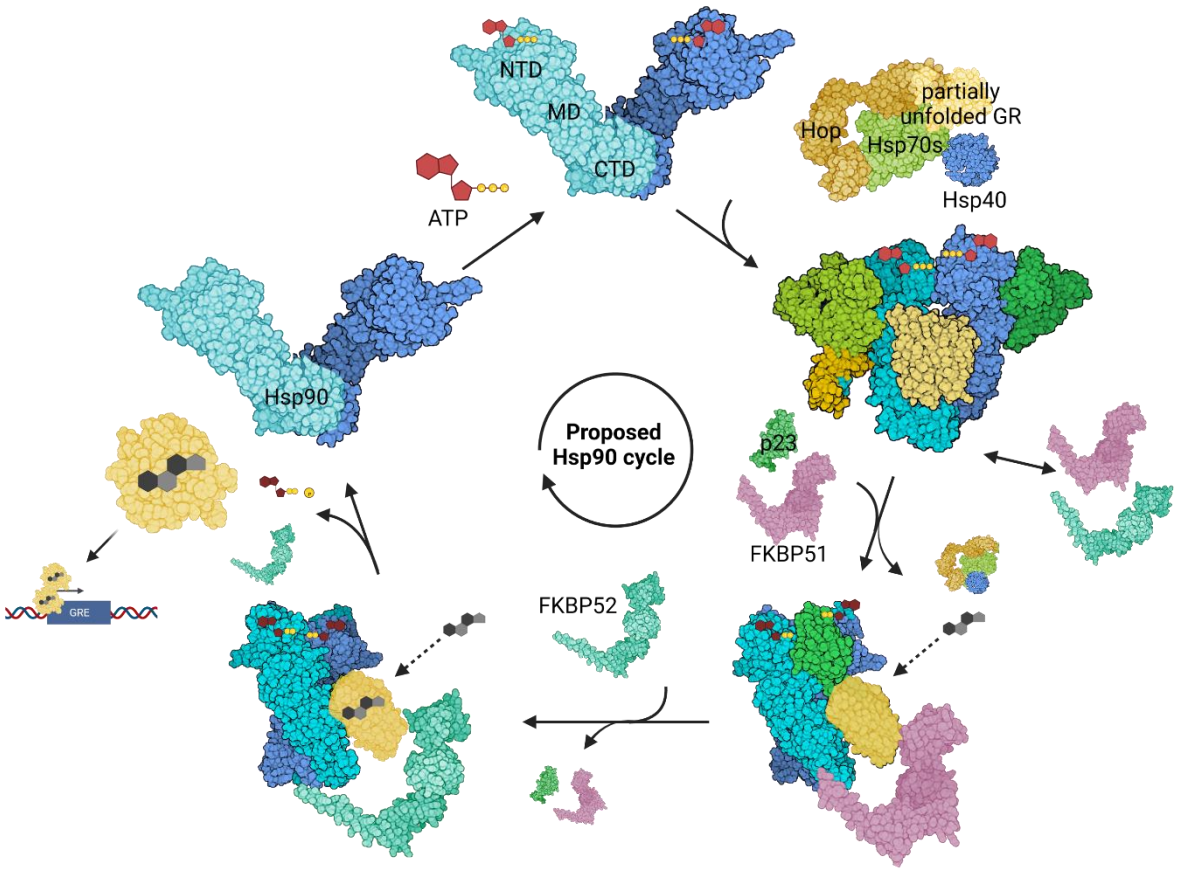

Figure 4: Schematic overview of the proposed Hsp90 cycle with GR as model client. Hsp90 undergoes conformational changes during ATP binding and hydrolysis, from an open stage via a semi-closed client-loading complex through a closed conformation of the client-maturation complex followed by client release accompanied by ADP release. The time point of ligand binding to the GR is implied by a dashed arrow. A different binding of cochaperones is required for client loading and shuttling through the Hsp90 cycle. Through the Hsp90 cycle partially unfolded GR is chaperoned to a fully folded, ligand-bound, active conformation.

First, GR LBD is thought to be inactivated through partially unfolding by Hsp70 whereas Hsp90 partially reverses this inactivation. For full recovery both Hsp90 cochaperones Hop and p23 are essential (Kirschke et al., 2014). In the proposed client-loading complex, the Hsp70-bound LBD is delivered by Hop to the client binding site of a semi closed Hsp90 with a second Hsp70 bound (Kirschke et al., 2014; Wang et al., 2022). For the progress from the loading complex to the maturation complex, the Hsp90 ATP hydrolysis as well as the release of both Hsp70 and Hop is necessary. In the proposed maturation complex comprising LBD, Hsp90 and p23, the LBD is restored to a folded, ligand bound conformation and the N-terminus of the LBD is threaded

through the lumen of the closed Hsp90 dimer (Noddings et al., 2022). The LBD is further stabilized through direct p23 interaction which requires the closed Hsp90 stage (Dittmar et al., 1997; Morishima et al., 2003). This is thought to be accompanied by immunophilin binding (Ebong et al., 2016). The active, ligand-bound GR is translocated to the nucleus to act as transcription factor on DNA (Grossmann et al., 2012).

2.3. FKBP51 inhibits GR activity

FKBP51 has been established as a key regulator in GR signaling. This is achieved by inhibiting GR activity through lowering hormone binding affinity of the receptor and delaying nuclear translocation (Denny et al., 2000; Wochnik et al., 2005). The hormone-bound GR strongly induces the *fkbp5* gene, yielding a direct negative feedback loop (Baughman et al., 1997). However, the molecular mechanism by which FKBP51 inhibits the GR activity remains poorly understood, due to the dynamic and transient nature of the interaction. In that regard, it is becoming increasingly clear that the molecular functions of both FBKP51 and FKBP52 cannot be fully uncovered without considering their mutual antagonism. Even though the FK1 domain of FKBP51 exhibits PPIase activity, it likely has no major impact on GR regulation. The FKBP51 FD67DV mutant, which has a 90% reduced PPIase activity, remains to inhibit GR activity with no difference to the wild type (Barent et al., 1998). Studies in both yeast and mammalian cells claim to have identified a single residue at position L119 in the N-terminal FK1 domain as being a critical difference between FKBP51 and FKBP52 (Riggs et al., 2007). L119 is located in the binding pocket overhanging loop described above. FKBP51 A116V L119P mutants seem to reverse the inhibitory effect of the wild type, resulting in potentiation of GR activity comparable to wild-type FKBP52 (Riggs et al., 2007). Despite the overall similarity of FKBP51 and FKBP52, it has been discussed that both associate differently with steroid receptors through differences relates to both the Hsp90-binding TPR domain and the C-terminal sequences (Barent et al., 1998; Cheung-Flynn et al., 2003). Difference in the hinge region of the FK1 and FK2 domain were also subject of speculation. FKBP52 can be phosphorylated at Y143 which prevents binding to Hsp90 (Miyata et al., 1997). The hinge region of FKBP51 lacks the phosphorylation site, which may explain why FKBP51 is competitively preferred over FKBP52 in GR complexes (Banerjee et al., 2008; Nair et al., 1997). Native MS studies which tried to partially reconstitutes the GR loading and maturation complex, show that FKBP51 and FKBP52 are interchangeable in early stages of complex formation (Ebong et al., 2016). Substantial differences were observed after release of Hop and Hsp70 where FKBP51 forms a stable complex with Hsp90/LBD/p23. FKBP52 was found to be unable to bind in the presence of p23 but rather binds after p23 release to form the proposed Hsp90/LBD/FKBP52 transfer complex (Ebong et al., 2016).

Further studies speculated on the association of FKBP52 to the dynein-dynactin complex as the distinguishing feature between both immunophilins (Galigniana et al., 2001; Sivils et al., 2011). Suggesting FKBP51 stalls and FKBP52 facilitats transport of the GR/Hsp90 complex to the nucleus. In summary, the current knowledge of the GR pathway, which is controlled by the Hsp90 machinery, is unsatisfactory and leaves many pending questions unanswered. One such question is if FKBP51 directly interacts with the receptors within the Hsp90 chaperone complex in the cytoplasm or influences the receptors indirectly through binding to HSP90. And further, can this interaction be narrowed down to a map of transient FKBP51 interactions. This also includes a more defined picture of the time point and influence of FKBP51 binding.

2.4. Characterization of protein-protein interaction by amber suppression

Protein-protein interactions like FKBP51 interacting with Hsp90 and the GR serve a vital role in bioprocesses and are essential for all living cells (Ryan & Matthews, 2005). Their identification and the deciphering of interaction networks enables a better and more detailed understanding of cellular processes. These interactions are mainly studied by immunoprecipitation, pull-down approaches, yeast-two-hybrid assay, or Förster resonance energy transfer (FRET) methods. Mapping and characterizing transient interaction networks, however, remains highly challenging, since transient protein–protein interactions are by definition dynamic and depend on different stimuli and environmental conditions. A powerful tool is the covalent capture of interaction partners which serves as a snapshot of an interaction. This can be achieved through site-specific incorporation of unnatural amino acids carrying chemical moieties that allow light induced crosslinking in close proximity.

2.4.1. Expansion of the genetic code

Proteins comprise of as much as 20+2 (the rare exceptions selenocysteine and pyrrolysine) proteogenic or canonic amino acids, enough to nearly carry out all the complex process of life. The protein blueprint is encoded in the genetic code. Through exceptional work over the past two decades, this genetic code has been artificially expanded to incorporate unnatural amino acids carrying a versatile range of side chains with different physiochemical and biological properties (Chin, 2017; Liu & Schultz, 2010; Xie & Schultz, 2006). The possibility to incorporate amino acids with defined steric and electronic properties at unique sites in proteins provides powerful chemical tools for exploring protein structures and functions *in vitro* and *in vivo*. The site-specific incorporation is achieved during messenger RNA (mRNA) translation where an unassigned stop codon is suppressed by a transfer RNA (tRNA) loaded with an unnatural amino acid. A general schema is depicted in Figure 5. The suppression of the amber stop codon (UAG), via base pairing interactions between the mRNA codon and the anticodon of the tRNA, allows the chain-terminating triplet to be read as an amino acid by a mutated tRNA. This concept was first shown in *Escherichia coli* where a mutated tyrosyl tRNA, which carries a single base change in its anticodon, allows for a UAG codon to be read as a tyrosine (Goodman et al., 1968). The incorporation of unnatural amino acid, in living organism, requires a tRNA recognizing the amber codon and a corresponding aminoacyl-tRNA synthetase. The amber codon is most often used because it is the least used stop codon in most organisms and natural amber suppression shows no significant cell growth effect (Benzer & Champe, 1962; Garen & Siddiqi, 1962).

It is necessary that both t-RNA and t-RNA-Synthetase are not interfering with their endogens counterparts which is termed orthogonal. The incorporation of an unnatural amino acid was again first achieved in *E. coli* using a modified archaeal tyrosyl-tRNA and the corresponding tRNA synthetase pair from *Methanocaldococcus jannaschii* which is orthogonal in bacteria to incorporate *O*-methyl-L-tyrosine (Wang et al., 2001). Many efforts were made to improve tRNA-synthetase pairs which at were limited by low incorporation efficiency in mammalian cell. For example, the *E. coli* tyrosyl-tRNA synthetase recognition towards its tRNA can be improved 5-fold by engineering the anticodon-binding region (Takimoto et al., 2009). tRNA was also investigated for improvement, a promotor driven tandem repeat of tRNA cassettes was found to be highly efficient (Coin et al., 2013; W. Wang et al., 2007). Up to now, the genetic code expansion was performed in yeast (Chin et al., 2003), mammalian cells (Sakamoto et al., 2002), and whole animals such as nematodes (Greiss & Chin, 2011) and mice (Ernst et al., 2016; Han et al., 2017). A plethora of diverse unnatural amino acids were incorporated containing spectroscopic probes for labelling proteins intracellularly for structural investigations, posttranslational modifications to study their impact on protein function, biorthogonal handles for functionalization, photoaffinity labels and chemical crosslinkers to map weak and transient protein interactions or to characterize protein interactions in functional states (Chin, 2017; Xie & Schultz, 2006).

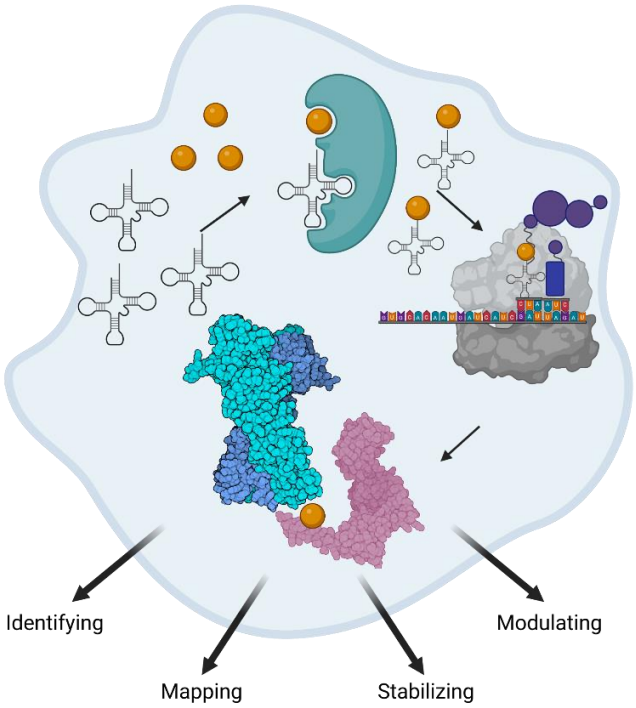

Figure 5: Schematic overview of amber suppressed incorporation of unnatural amino acid to study protein-protein interactions. An orthogonal suppressor tRNA colored in black is loaded with the unnatural amino acid colored orange by an orthogonal tRNA synthetase colored in green. The unnatural amino acid is incorporated via the ribosome colored in grey in response to the amber codon (UAG).

2.4.2. Photocrosslinking to study protein interaction

Photocrosslinkable amino acids are unnatural amino acids that carry a photoactivatable moiety that upon UV-irradiation covalently capture proteins in their vicinity. Therefore, photocrosslinking in combination with biochemical assay or mass spectrometry is a superior strategy for the covalent trapping of transient and low affinity protein-protein interactions in an authentic cellular environment. This is generally not feasible using traditional methods such as immunoprecipitations, pull-down assays or yeast-two-hybrid assays (Berggård et al., 2007; Dunham et al., 2012).

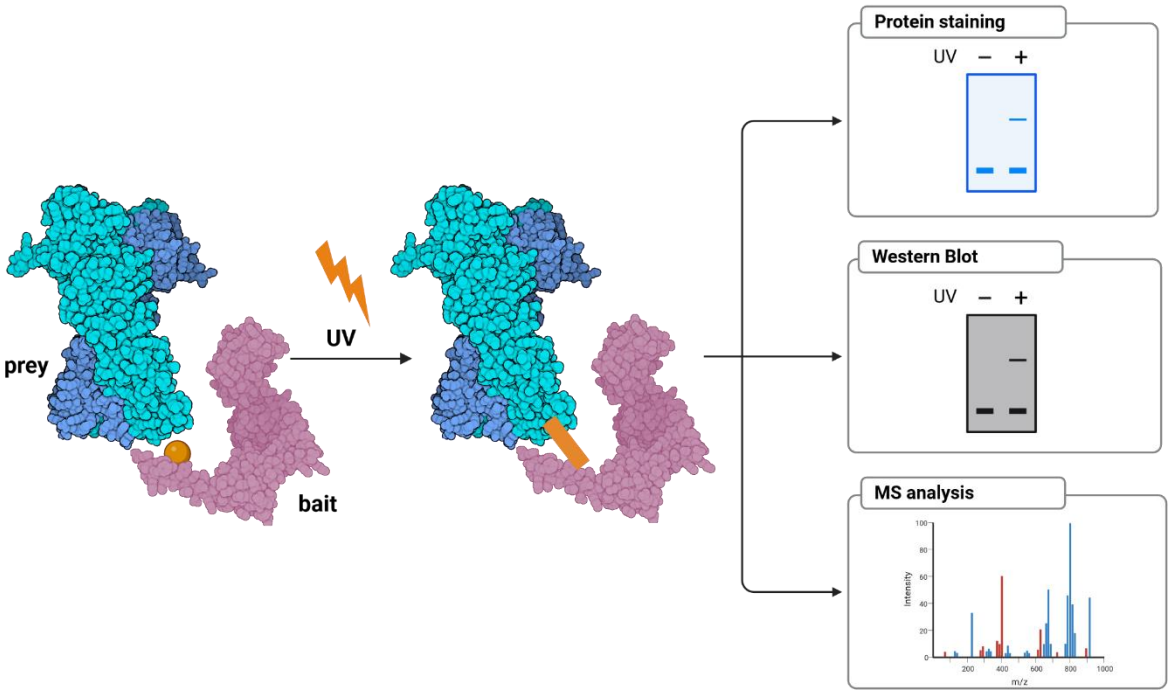

Figure 6: Photocrosslinking for identifying, mapping and characterizing protein-protein interaction. Site-specific incorporated photoactivatable unnatural amino acid covalently captures proteins in their vicinity upon UV irradiation. Analysis of the crosslinked proteins is performed by either SDS-PAGE, Western blot or bottom-up mass spectrometry approach.

Three groups of photosensitive groups have been exploited: benzophenones, diazirines and azides. All are chemical inert and biorthogonal in cells. Advantageously, their small size minimalizes interference with the protein structure and show high and specific crosslinking at longer wavelengths, usually 365 nm, which is thought to be biocompatible (Coin, 2018; Nguyen et al., 2018). The covalent capture by the UV-activated moieties is achieved via a fast (100−120 μs) non-specific radical reactions within a radius of a few Å (8−15 Å) (Nguyen et al., 2018). The benzophenone **1** generates a ketyl diradical that reacts with C−H groups in the vicinity, with preference for methionine (Kage et al., 1996; Wittelsberger et al., 2006).

Additionally, the reversible and efficient UV activation, explains the wide usage of the benzophenones regardless of their bulkiness and rigidity (Nguyen et al., 2018). Diazirines **2** generate a reactive carbene radical after the loss of N_2 which reacts with X−H groups (X = C, N, S, O) (Brunner, 1993) with a preference to acidic residues such as aspartate and glutamate (Iacobucci et al., 2018; Jumper et al., 2012; Ziemianowicz et al., 2017). Lastly, the aryl azides **3** crosslinks through a photogenerated nitrene radical, which is prone to bind into both C–H as well as X–H bonds (X = N, S, O). It is also easily quenched by water which tends to lead to lower yield and unspecific crosslinking (Tanaka et al., 2008).

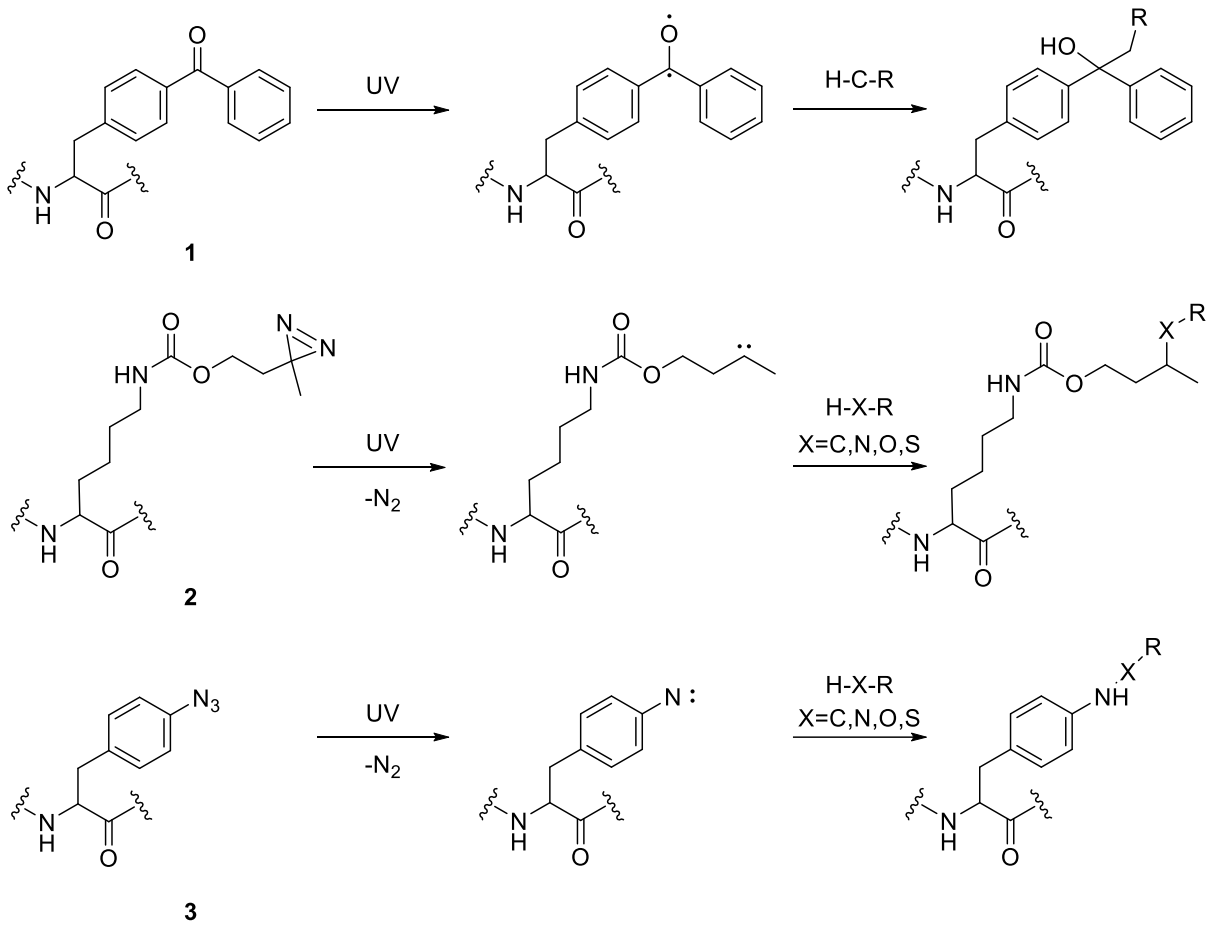

Figure 7:Structure and activation mechanism of frequently used photocrosslinker unnatural amino acids. **1**-para-benzoyl-phenylalanine, **2**-diazirine modified lysine, and **3**-para-azido-phenylalanine.

These photocrosslinking-capable amino acids are powerful tools with high spatiotemporal resolution to study interaction in real time under defined cellular conditions (Nguyen et al., 2018). In general, the biochemical applications of these tools are, (I) Identification of new interaction partners; (II) mapping known protein interactions in a detailed fashion; and (III) stabilization of transient protein interaction for further characterization.

For the first purpose, the approach is to capture low-affinity or transient protein–protein interactions with an artificial covalent bond that would otherwise be missed in standard immunoprecipitation procedures. For HdeA, an acid stress chaperone of *E. coli* important for maintaining protein integrity, client proteins within a wide pH range were identified by photocrosslinking and revealed an unknown ATP-independent mechanism for protein refolding (Zhang et al., 2011). In other studies, the unnatural amino acid *para*-benzoyl phenylalanine (pBpa), a commonly used benzophenone, was incorporated into a yeast histone to elucidate molecular details of the pathway downstream of the histone phosphorylation cascade that induces mitosis (Wilkins et al., 2014).

For the second purpose, the photo-crosslinker is used as a 'proximity-sensor' to pinpoint which positions of the investigated protein are close to the interaction partner in the associated complex. This was extensively applied for G-protein-coupled receptors to show interactions of the natural ligand (Coin et al., 2013; Rudolf et al., 2022; Seidel et al., 2017). For example, the interaction of the corticotropin releasing factor receptor type 1 with its natural 40-mer peptide ligand urocortin-I was mapped at more than 100 residues to reveal, in combination with a crystal structure, a 3D model for receptor ligand binding (Coin et al., 2013). Furthermore, the binding of antidepressant drugs to the human serotonin transporter (hSERT) was investigated on 75 different positions to provide direct evidence of ligand binding within the central-substrate-binding site of the hSERT (Rannversson et al., 2016).

For the third purpose, the formed covalent bond stabilizes the investigated complex in a fashion that allows further investigation. In an *in vitro* experiment, *para*-benzoyl-phenylalanine was incorporated into bacterial expressed liver oncoprotein gankyrin and photocrosslinked with S6 proteasomal protein followed by crystallization. Photocrosslinking allowed crystallization and only minimally disturbs the overall complex structure and showed the actual structure of the crosslink (Sato et al., 2011). So far, the discussed applications of photocrosslinking were mainly analyzed with classical biochemical assays such as Western Blot analysis or Coomassie staining analysis as a detection method. However, analysis of photocrosslinking products can be coupled with mass spectrometry analysis (MS), to identify the captured protein (Coin, 2018). Usually for identification, the analysis of the photocrosslinked protein is performed in a "bottom-up" approach where the crosslinked protein is enzymatically digested, and the peptide mixture is analyzed by a mass spectrometer, typically operated with an online liquid chromatography (LC) system to allow sensitive and robust analysis using the LC separation together with the mass over charge (m/z) separation in the mass spectrometer (Piotrowski & Sinz, 2018). Great efforts have been made that enable selective enrichment and labeling of proteins after crosslinking by

multifunctional unnatural acids, carrying modifiable and cleavable linkers (Nguyen et al., 2018).

For example, the frequently used unnatural amino acid pBpa was modified to bear an independent bioorthogonal alkyne anchor **4** for selective enrichment. Following photocrosslinking, the complex was directly labelled with an azide-modified biotin probe through "click chemistry", which facilitated isolation of the crosslinked complex from whole cell lysate (Joiner et al., 2017). Another approach is selenium-based photocrosslinking unnatural amino acid **5** that allows an oxidative cleavage of the C–Se bond after crosslinking, marking the crosslinking protein with a unique label for MS detection (Lin et al., 2014; Yang et al., 2016). Both ideas were combined in a cleavable unnatural amino acid carrying an alkyne moiety **6** for specific enrichment of low-abundance proteins (He et al., 2017). Additionally, isotopically labeled pBpa were developed with a deuterium **7** and ^{13}C-labeled version **8** to facilitate identification of interacting peptides in the highly complex mass spectra by characteristic isotope pattern (Pettelkau et al., 2014; Wilkins et al., 2008). However, apart from proof-of-concept studies these reagents have not been used extensity.

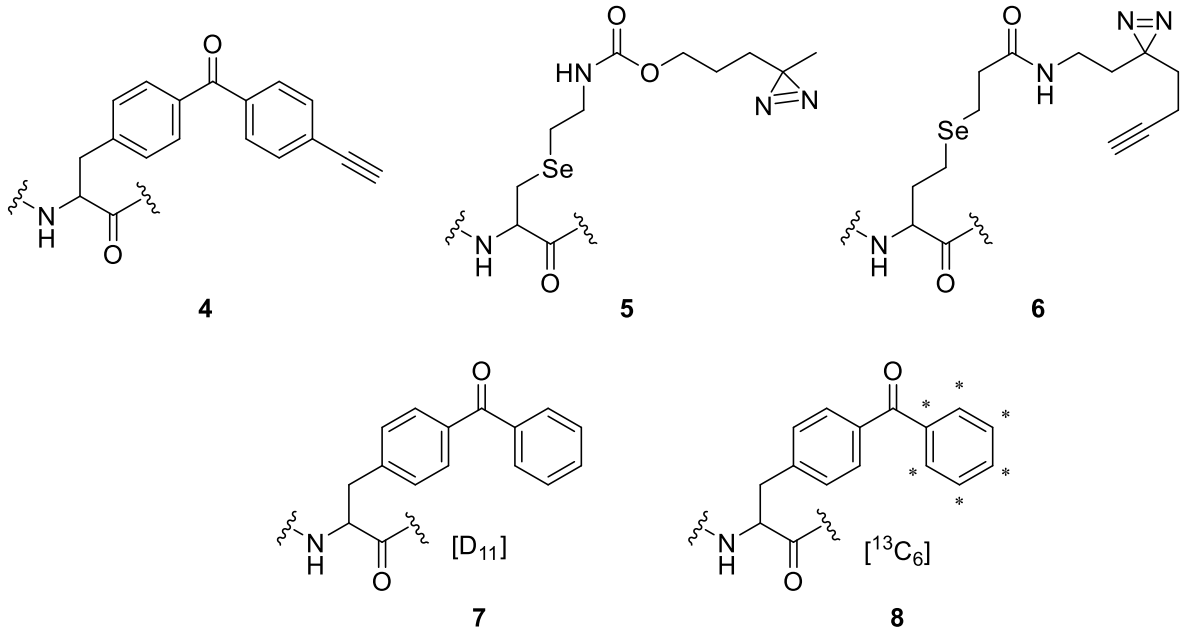

Figure 8: Structure of multifunctional unnatural amino acids. **4**-para-benzoyl-phenylalanine with alkyne handle, **5**-selenium based diazirine modified lysine, **6**-selenium based diazirine with alkyne handle, **7**-deuterated para-benzoyl-phenylalanine, and **8**-^{13}C-labeled para-benzoyl-phenylalanine.

Traditionally, in depth mapping of the interaction interface using site-specific crosslinkers requires genetic insertion of the photocrosslinking and/or chemical crosslinking unnatural amino acids on both bait and prey proteins (Coin et al., 2013). For identification of the site of

crosslinking by mass spectrometry, a challenging problem is the high complexity of mass spectra and usually low yield of photocrosslinking product together with high background signals, especially in mammalian samples. This often precludes routine analysis (Coin, 2018). So far, this approach has not exceeded proof-of-concept study in bacteria or for purified proteins (Dehling et al., 2016; Forne et al., 2012; Schwarz et al., 2013; Yang et al., 2016). In summary, the incorporation of photocrosslinking unnatural amino acids is a powerful tool as a proximity sensor for interactions which allows an in cellular snapshot of transient and dynamic interactions at potentially single residue resolution. Thereby it is holding the potential to answer pending questions about the nature and role of protein interactions, for example about the interaction of FKBP51 and its role in the Hsp90-GR heterocomplex.

3. Results and discussion

3.1. Chapter 1: Identification of FKBP51 interaction partner by amber suppression enabled photocrosslinking

In this chapter, a suitable cloning method for large scale mutant libraries is presented, followed by establishment of the incorporation of a photocrosslinkable unnatural amino acid. In-cell photocrosslinking of FKBP51 revealed an interaction interface of Hsp90-FKBP51 beyond the TPR domain and introduced the cochaperone p23 as a direct interaction partner of FKBP51. Additionally, the glucocorticoid receptor, a model client of the Hsp90 machinery, was investigated as a FKBP51 interaction partner thereby underpinning large scale, in-cell photocrosslinking as an excellent method to study dynamic, multiprotein complex with single residue resolution.

3.1.1. Cloning of the FKBP51 library

For studying the protein interactions of FKBP51 in cellular at single residue resolution, a mutant library of TAG mutants is needed that includes ideally all surface exposed amino acids for a true detailed interaction map. The finding of surface exposed residues as potential crosslink sites was guided by the crystal structure of FKBP51 (Kumar et al., 2017) and comprise more than 200 amino acids. The TAG mutations enable the site-specific incorporation of the photocrosslinking unnatural amino acid in combination with a tRNA/tRNA synthetase pair into the protein (Nguyen et al., 2018). For mapping the interaction interface, the photo-crosslinker is used as a 'proximity-sensor' to pinpoint which positions are close to the interaction partner in the associated complex.

For a library of that size a reliable and fast cloning method is of utmost importance. In the beginning, this was tried with a simple primer-based back-to-back PCR approach (Hemsley et al., 1989) which suffered low yield and extensive cloning. After careful consideration, the cloning strategy was change to a Golden Gate cloning approach with a protocol, termed Golden Mutagenesis that allows the rapid, straightforward, reliable and inexpensive construction of the mutants (Püllmann et al., 2019). The implementation of the technique was facilitated by a web tool application for automated primer design. The concept will be discussed briefly and is depicted in Figure 9.

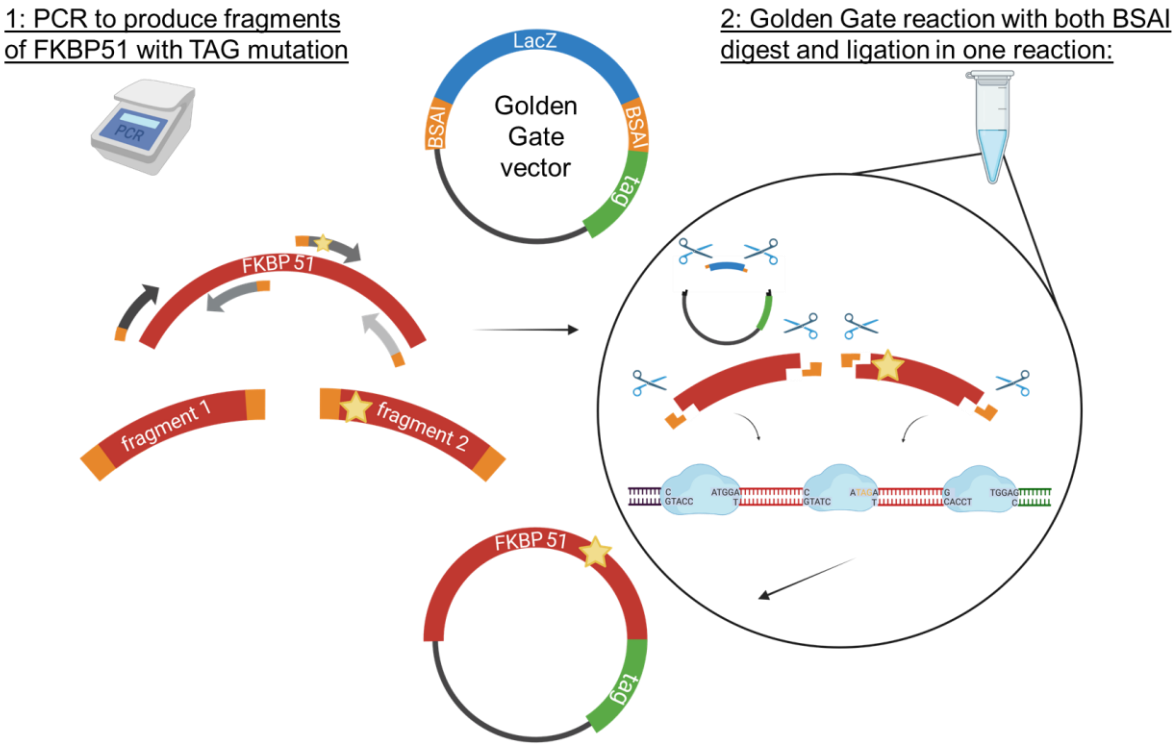

Figure 9: Schematic overview of Golden Gate principle. Eukaryotic expression vector carries two BSAI recognition sites (orange), a LacZ cassette for blue/white screening (blue), and an affinity tag e.g., FLAG or twin Strep FLAG tag (green). Two PCRs produce two fragments of the gene of interest (red) with BSAI recognition site (orange) using specifically designed primers (grey-orange). The introduction of the TAG stop codon is represented by a yellow star. In a Golden Gate reaction, the vector and the two PCR fragments are cut by BSAI and the fragments are ligated into the vector thereby eliminating the BSAI recognition sites. The cloned vector carries the sequence of FKBP51 with the specific TAG mutation and the affinity tag.

The key element is the use of type IIS restriction enzymes such as BSAI, which cut double-stranded DNA molecules outside of their recognition site. This characteristic feature enables an efficient parallel one-pot restriction-ligation procedure. The generated PCR fragments each carry the terminal BSAI recognition sites and usually the second fragment introduce the desired TAG mutation inside of the binding sequence. They are then reassembled in a target eukaryotic expression vector and are directly transformed into an *E. coli* strain. In contrast to some other widespread mutagenesis techniques, amplification of the plasmid backbone via PCR is not necessary for Golden Gate cloning. This circumstance allows the easy introduction of affinity tags at a desired terminus and eliminates the risk of introducing unwanted mutations within the plasmid backbone. After transformation usually two colonies were picked, plasmid DNA isolated and digested to ensure the insertion of the TAG mutated *fkbp5* gene and sent for sequencing to ensure correct introduction of the TAG codon. An efficiency of ~80% positive mutants was achieved with two colonies; this is in contrast to the stated efficiency of 96%

(Püllmann et al., 2019). The technique was used to create a TAG library of a FKBP51 carrying a C-terminal FLAG-tag with 220 mutants. The FLAG tag was chosen to ensure a reliable detection by a tag specific antibody. The position on the C-terminus further ensured detection only after successful amber suppression of the TAG codon. Additionally, the same TAG library was cloned into a FKBP51 carrying a C-terminal twin Strep FLAG tag (discussed later). Noteworthy, this process suffered from relatively low success rate from ~60% for one picked colony. This problem was solved by applying a modified 2 step PCR program starting with a lower annealing temperature of 60°C for 10 cycles which was ramped up the normally applied annealing temperature of 70°C. This was suggested by Adrian Elter (Harald Kolmar lab, TU Darmstadt). Overall, 2 sets of FKBP51 TAG libraries were created, one a FKBP51 C-terminal FLAG and two a FKBP51 C-terminal twin Strep FLAG in a rather time consuming one-mutant-one-tube approach. The cloning was heavily supported by student assistants Marie-Luisa Pfeiffer, Karola Brahmi, Constanze Sixt, Sarah Engel and Janna Treber. In a next step, amber suppression was established and optimized for a comprehensive mapping of FKBP51 interaction partners.

3.1.2. Establishing of amber suppression

In preliminary experiments, two different photocrosslinker were explored for amber suppression of FKBP51. The first one, which was gifted by the Lang Lab (TU Munich/ETH Zurich), was the diazirine lysine derivate AbK (**2**). The second one was the frequently used photocrosslinker unnatural amino acid para-benzoyl phenylalanine (pBpa, **1**), provided by the Coin Lab (Uni Leipzig). The AbK system relies on an improved pyrrolyl tRNA synthetase from *Methanosarcian barkeri* (Chou et al., 2011). The pBpa system uses an optimized *Escherichia coli* tryrosyl tRNA synthetase (Serfling & Coin, 2016). Both systems were tested in eukaryotic HEK293 cells on an eGFP N150TAG mutant, that crosslinks as a dimer. The next step for the establishment of the amber suppression for FKBP51 was to find a crosslink to a known interaction partner.

The pBpa system gave the first incorporation successes as well as an UV induced crosslink. After additional testing, the pBpa system was selected as the most reliable and promising approach. The well-established interaction of FKBP51 to Hsp90 was used as a benchmark for photocrosslinking. As the interaction of FKBP51 to Hsp90 is coordinated through its TPR domain, the focus was first on this domain. In a first screening approach, the position FKBP51 A398pBpa was found as a strong crosslinker forming a complex with the molecular weight of approximately 160 kDa. The amber suppression system was thoroughly tested to ensure

incorporation only in the presence of the FKBP51 TAG mutant, the tRNA/tRNA synthetase, and the unnatural amino acid pBpa (see Figure 10).

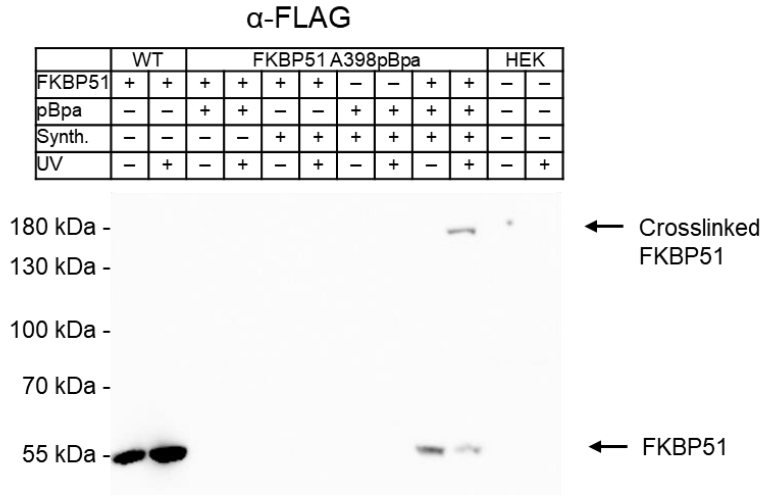

Figure 10:Amber suppression is bioorthogonal for FKBP51. Western blots of the FKBP51 A398pBpa mutant expressed and photocrosslinked in HEK293. UV light-induced FLAG-reactive bands at a size ~160 kDa are indicative of the mutated position being covalently photocrosslinked. WT: FKBP51 without TAG stop codon, HEK not transfected HEK293 cells as control, Synth.: pBpa tRNA/tRNA synthetase, UV: UV irradiation on ice for 30 min before cell lysis.

The first experiments show that the method is bioorthogonal in HEK293 cells, as no amber suppression was observed in the absence of one of the needed components. In the UV-irradiated sample, a shift to a high molecular weight species is observed at ~160 kDa. This band is not observed in the WT sample and represents a successfully amber suppressed and photocrosslinked FKBP51 A398pBpa adduct.

Further, the robustness of the method was tested using different FKBP51 and tRNA/tRNA synthetase plasmid concentrations. Also, the time dependence of the crosslink was evaluated (see Figure 11).

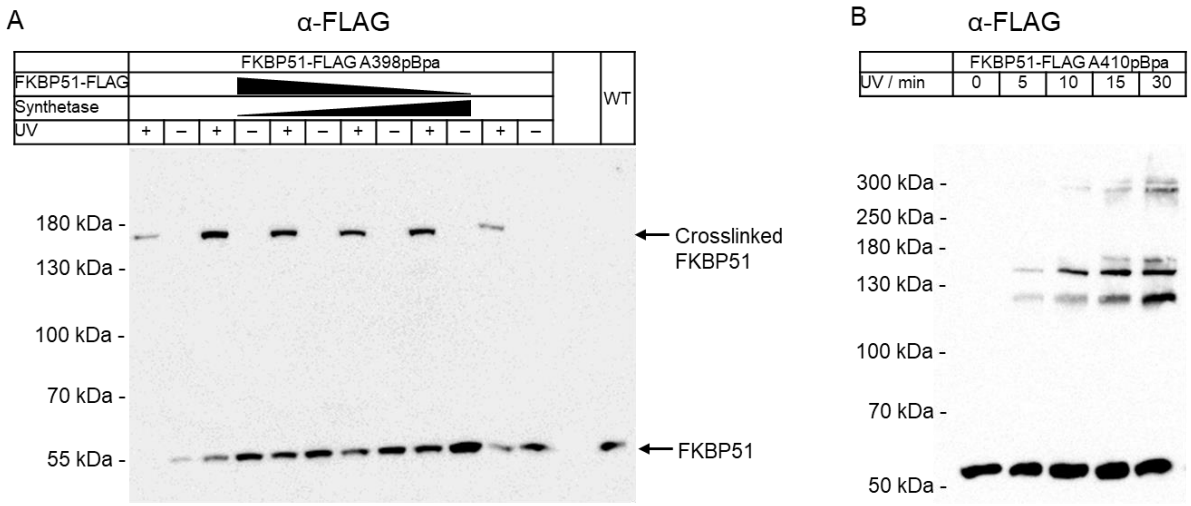

Figure 11: Amber suppression of FKBP51 is robust and UV-induced photocrosslinks are time-dependent. A, Western blot of FKBP51 A398pBpa expressed and crosslinked in HEK293 cells. UV light-induced FLAG-reactive bands at a size of ~160 kDa are indicative of the mutated position being covalently photocrosslinked. Different plasmid DNA concentrations were tested for transfection. B, Western blot of FKBP51 A410pBpa validates time dependency of UV-irradiation for photocrosslinking. Cells were UV-irradiated for the indicated time on ice before cell lysis.

This transfection condition test shows the robustness of FKBP51 amber suppression. If the plasmid concentration is too low, for either FKBP51 or tRNA/tRNA synthetase, a lower amber suppression yield and crosslinking efficiency can be observed. The time-dependency of the UV induced crosslink was confirmed by an increase in strength of the observed FKBP51 crosslinks over time.

The gained experience was translated to a general applicable protocol for photocrosslinking experiments. Therefore, the literature protocol (Serfling & Coin, 2016) was slightly adjusted. Less cells were used for seeding resulting in a surface confluency of ~50% after 24 h instead of a confluency of ~90% after 24 h. For amber suppression, the cells were incubated for 42 h instead of 24 h. Since the longer incubation gave more robust results. After the method adjustment, the FKBP51 library was screened for interaction partners.

3.1.3. Screening the FKBP51 surface for interaction partner

After the establishment of the incorporation of the photocrosslinker pBpa into FKBP51, the surface mutants of FKBP51 were screened for crosslinks. The aim was a detailed picture of the FKBP51 interaction partners as well to investigate the potential of the method. In screening experiments, the FKBP51 TAG library was amber suppressed and at least 10 distinct crosslinks have been observed. These crosslinks were visualized by Western blot analysis.

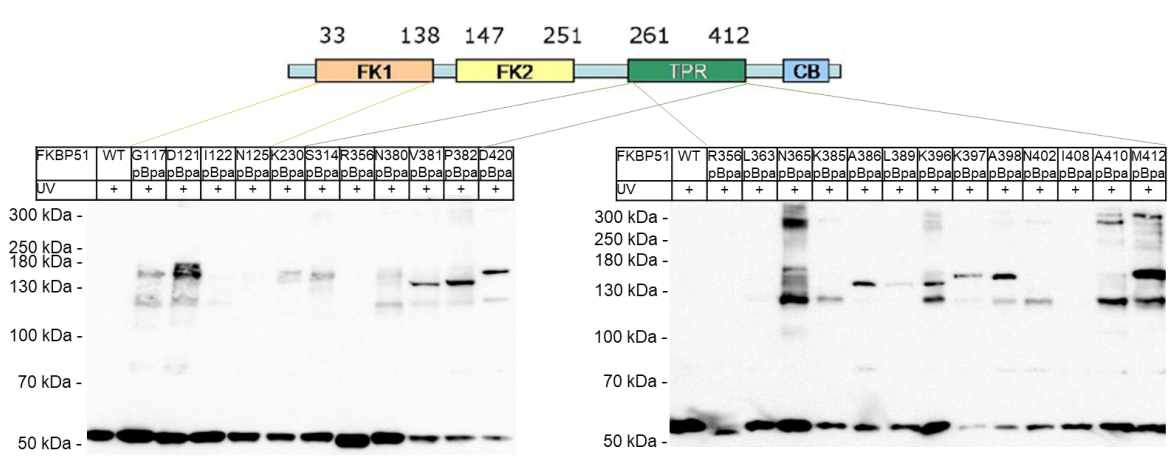

Figure 12: Selected overview of FKBP51 crosslinks. Positions are indicated on the different domains of FKBP51. Western blots were visualized using an anti-Flag Antibody against the FLAG-tagged FKBP51.

3.1.4. Identification of FKBP51 interaction partner

The next step was the identification of the crosslinked interaction partner. This is crucial for the understanding and further study of the FKBP51 interactions. For the analysis, selected FKBP51 mutants that show representative and strong crosslinks were chosen. FKBP51 K60pBpa shows a crosslink ~80 kDa, FKBP51 E75pBpa shows a crosslink ~180 kDa and FKBP51 N365pBpa shows a crosslink at ~130 kDa and ~300 kDa. FKBP51 A398pBpa, which was used as a model, as well as FKBP51 M412pBPa crosslink in a complex at ~160 kDa. The mutants were amber suppressed in a large scale (10 cm cell culture plate), concentrated and enriched by FLAG-immunoprecipitation. The eluted samples were analyzed on an SDS-PAGE followed by either silver staining or Coomassie staining. The benefit of the SDS-PAGE is to lose the high amount of FLAG peptide that is used for elution which would potentially interfere with the analysis, even though it is more labor intense than an in-solution digest approach. The method of choice was a bottom-up proteomics approach using an in-gel digested sample to identify the interaction partner (Zhang et al., 2013). The protein of interest or a mixture protein complex is digested with a protease to peptides which are analyzed by LC/MS-MS (Sinha & Mann, 2020). Here, the peptides are separated by a LC system, ionized in a source, typically by ESI (electrospray ionization) and analyzed by their mass-to-charge ratio (m/z). This reveals the exact mass of the peptide. The peptides are further analyzed by splitting the ions into smaller fragments which is termed tandem MS (MS-MS). This gives rise to the (exact) composition of the peptides e.g., the amino acid sequence. The generated data is matched with a data base of the proteome of the organism of interest e.g., human. The sample preparation was carried out in our lab following a standard protocol provided by the Munch lab in Frankfurt. This included

a reduction and alkylation step, the protein digest and subsequent peptide isolation. The samples were measured by Dr. Georg Tascher (Christian Munch lab, Frankfurt) or Vivien Schoonenberg (Frank Butter lab, Mainz). The complex data analysis was performed using MaxQuant, an open-source proteomics tool, that allows the processing of the generated MS files (Cox & Mann, 2008). Selected data sets were used as read-out for the sample content: the name of the protein, the number of peptides detected, number of unique peptides identified for a certain protein (if two proteins share an identical peptide, it is not count as unique), the coverage of the identified protein and the intensity of the detected peptides as a degree of the concentration of a certain protein in the sample. Proteins were considered as potential interaction partner when the intensity of the peptides were in the same magnitude.

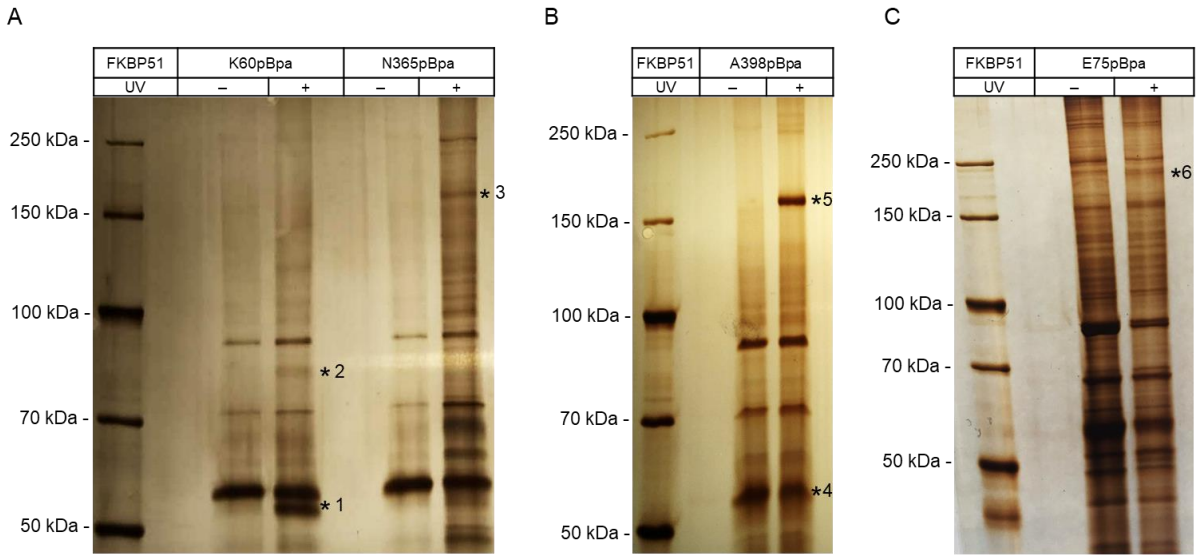

Figure 13: Identification of UV-induced crosslinks. A–C Silver-stained gel for visualization of FKBP51 crosslinks. Selected band (asterisk) were submitted to mass spectrometry analysis.

Distinct bands are visible in silver-stained gels for FKBP51 K60pBpa at ~80 kDa and lower than FKBP51, for FKBP51 N365pBpa at ~160 kDa, while no band is visible at ~130 kDa, and for FKBP551 A398pBpa also at ~160 kDa. Selected UV-induced bands were cut out, digested, and peptides were isolated and analyses by LC-MS. The MaxQuant analysis for each sample is presented in the Table 1.

Table 1: MS analysis reveals direct interaction partner of FKBP51. A representative data set of the MaxQuant analysis is presented and used to identify FKBP51 interaction partner.

Protein name	Peptides	Unique peptides	Sequence coverage	Intensity
FKBP51 K60pBpa <FKBP51 (1)				
FKBP51	37	37	64%	1.54×10^{10}
FKBP51 K60pBpa 80 kDa (2)				
FKBP51	19	19	40%	8.25×10^{8}
p23	3	3	30%	9.66×10^{7}
FKBP51 N365pBpa 160 kDa (3)				
FKBP51	17	17	44%	2.68×10^{8}
Hsp90AA1	18	11	38%	1.77×10^{8}
Hsp90AB1	19	10	40%	9.76×10^{7}
FKBP51 A398pBpa 55 kDa (4)				
FKBP51	68	68	67%	7.69×10^{10}
Hsp90AA1	1	0	2%	0
FKBP51 A398pBpa 160 kDa (5)				
FKBP51	58	58	64%	2.06×10^{10}
Hsp90AA1	63	40	49%	1.83×10^{10}
Hsp90AB1	53	25	45%	1.55×10^{10}
FKBP51 E75pBpa 180 kDa (6)				
FKBP51	56	56	64%	1.82×10^{10}
GR	42	42	48%	1.34×10^{10}

The crosslinks of FKBP51 K60pBpa at a molecular weight of ~80 kDa was identified as the Hsp90 cochaperone p23. p23 is a small protein yet important for the Hsp90 cycle. It enters at a late stage of the Hsp90 chaperoning pathway and enhances maturation of client proteins (Felts & Toft, 2003). Interestingly, a FKBP51 K60pBpa crosslink <FKBP51 band at ~50 kDa was observed and identified as an intramolecular crosslink. This was based on the MS analysis showing only the presence of FKBP51 in the band (the next higher protein detected by its intensity was dermcidin, a common contamination with one magnitude lower than FKBP51) as well as the fact that the band was observed only in the +UV sample. The intramolecular crosslink would result in a more compact species translating into a faster migration through the SDS-PAGE. The same migration behavior was also observed for FKBP51 R356pBpa.

Even though, for FKBP51 N365pBpa a strong crosslink was observed at ~130 kDa (see Figure 12), this did not translate into a strong band visible in the silver staining. The MS analysis failed to identify a crosslink partner. The crosslink was detected over the whole spectrum of mutations, a mapping of the crosslink on the structure of FKBP51 gave no distinct binding interface but rather an equal spread over all domains. As several attempts were made and failed to identify the crosslink, this was not further pursued. The strong crosslink observed for FKBP51 N365pBpa and FKBP51 A398pBpa at ~160 kDa was identified as Hsp90, termed FKBP51→Hsp90. This corresponds roughly to the added mass of both proteins, yet it is not identical. The migration behavior of the crosslinked proteins seems to be slightly different that the sum of the individual proteins (FKBP51 ~55 kDa and Hsp90 ~85 kDa). Based on the height of the crosslink, the position of the mutation and the fact that Hsp90 is known to bind to the TPR domain of FKBP51 this was more a confirmation than a surprise. The crosslink FKBP51 E75pBpa at ~180 kDa was identified as the glucocorticoid receptor, FKBP51→GR. The GR is a model client of the Hsp90 chaperone machinery and is regulated by the FKBP51. The MS data were confirmed by Western blot analysis using protein specific antibodies shown in Figure 14.

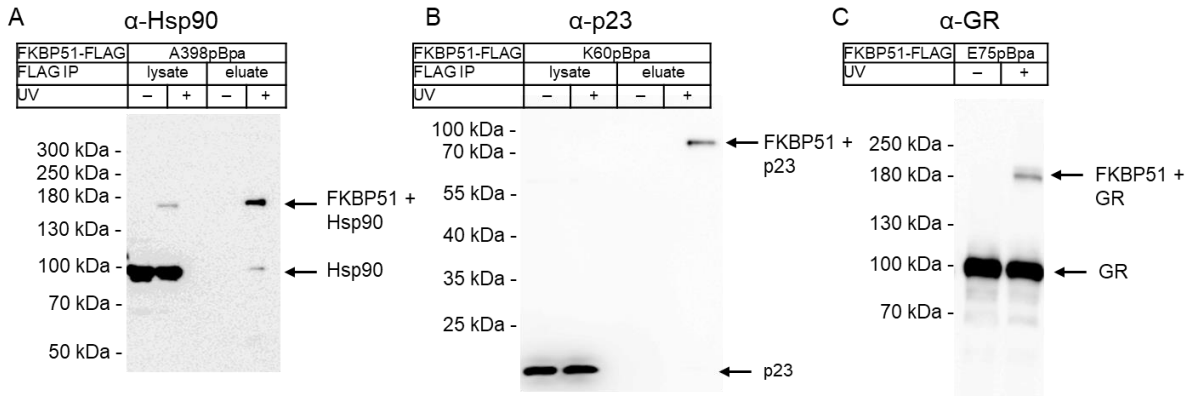

Figure 14: FKBP51 crosslinks to known proteins of the Hsp90/GR heterocomplex. Western blots of selected FKBP51 mutants expressed and crosslinked in HEK293 cells, samples were immunoprecipitated by FLAG-IP and detected with protein specific antibodies as indicated.

FKBP51 was crosslinked to its known interaction partner Hsp90, p23 and the GR through a site specific incorporated pBpa at the position A398, K60, and E75 respectively. The presence of strong crosslinks at specific sites of FKBP51 proves that FKBP51 is tightly bound to members of Hsp90 heterocomplex. The suitability of the method for the detection and identification of FKBP51 interaction partner was shown.

So far crosslinking experiments show at least 10 different band that potentially correspond of direct interaction partner, three of which at ~80 kDa, ~160 kDa and ~180 kDa correspond to

p23, Hsp90 and GR, while the others have not been identified. A systematic mapping of these identified direct interaction partners will give insides into the structure and function of FKBP51 containing Hsp90 complexes.

3.1.5. Pin-pointing residues important for interaction

A great challenge of photocrosslinking remains the identification of the site of the crosslink on the captured protein and great effort has been made to address this challenge by mass spectrometry (Coin, 2018). This would provide a detailed view on the interaction interface on the crosslinked partner, including orientation and exact interaction sites especially if no molecular structure is available. This is often the case for dynamic and multiprotein complexes. One potential approach is the site-specific incorporation of an isotopically labeled UAA. Isotopic labels are frequently used in MS analysis and greatly enhance identification of the (crosslinked) product (Müller et al., 2001). Here, a ^{13}C-labeled photoreactive pBpa (Pettelkau et al., 2014) is used and is preferred over the use of deuterated pBpa (Wilkins et al., 2008) as retention time shifts in reversed phase chromatography can be ruled out. ^{13}C-labeled pBpa (**8**, $^{13}C_6$ pBpa) was synthesized by Tim Heymann and incorporated into FKBP51 by amber suppression, instead of unlabeled pBpa, to install the isotope label. First, the incorporation efficiency and crosslinking behavior was tested (see Figure 15).

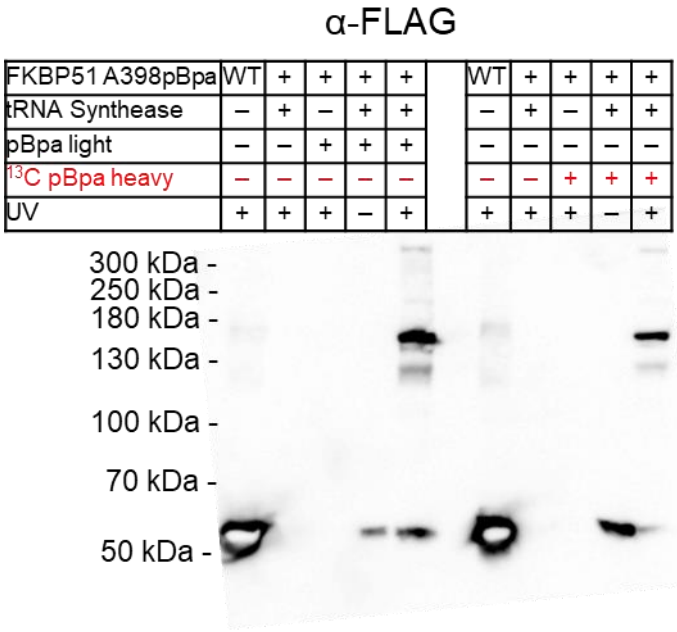

Figure 15: Successful incorporation of an isotopically labeled pBpa into FKBP51. Western blot of FKBP51 A398pBpa expressed and crosslinked to Hsp90 in HEK293 cells. UV irradiation was carried out on ice for 30 min before cell lysis.

No significant difference was observed between the light and heavy version of pBpa in Western blot analysis of crosslinked samples. In both samples, FKBP51 A398pBpa is amber suppressed and shows a UV induced high molecular shift which corresponds to a FKBP51→Hsp90 crosslink. After this proof-of-concept experiment, the goal was to generate samples that allow analysis by mass spectrometry. Two FKBP51 mutants that show strong crosslinks to Hsp90 were selected which are situated in the FKBP51^{TPR} and supposedly crosslink to the C-terminal domain of Hsp90. Therefore, FKBP51 A398pBpa and FKBP51 M412pBpa were amber suppressed in the presence of both the light and heavy pBpa separately or combined in a larger scale (10 cm cell culture plates). This was followed by immunoprecipitation by FLAG IP for sample concentration and purification and subjected to SDS-PAGE analysis using Coomassie staining for visualization. This is shown for FKBP51 A398pBpa as an example for the incorporation of the heavy and light pBpa separately, and FKBP51 M412pBpa for the incorporation of the heavy and light pBpa simultaneously. The heavy species has a mass difference of 6 neutrons which translates to a shift of $m/z = 6$ in the mass spectra for a single charged ion.

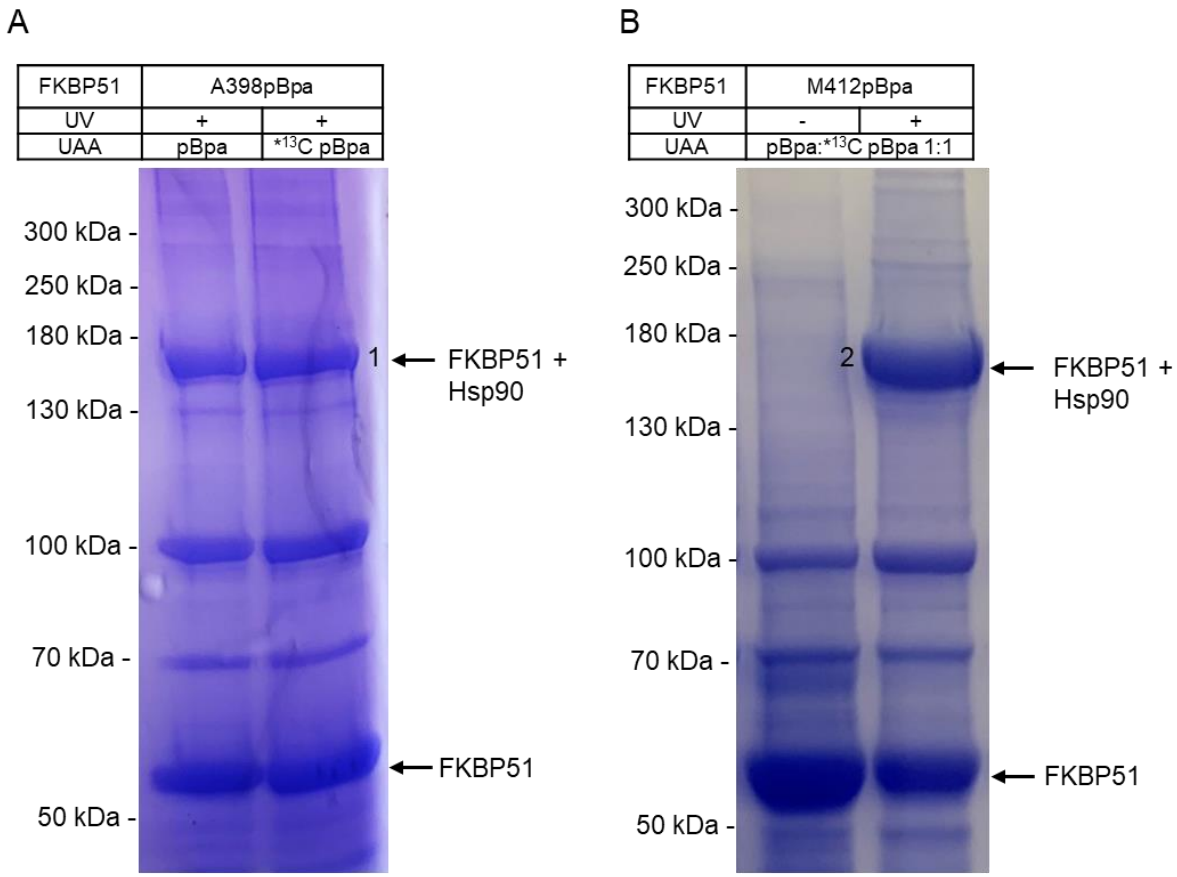

Figure 16: FKBP51→Hsp90 crosslinks analysis by mass spectrometry. Coomassie-stained gel of selected FKBP51 mutants expressed in the presence of an isotopically labeled $^{13}C_6$ pBpa and crosslinked in HEK293 cells. Samples were immunoprecipitated by FLAG-IP. Selected bands were numbered 1 & 2.

The Coomassie staining (Figure 16) reveals a large band at ~160 kDa corresponding to the FKBP51→Hsp90 crosslink as well as the uncrosslinked FKBP51 at ~55 kDa. Further visible are unassigned bands that correspond to coimmunoprecipitated proteins as well as cellular background. The analysis shows the success of both photocrosslinking and immunoprecipitation. Samples were prepared including reduction, alkylation, and tryptic digest, followed by peptide isolation and by LC-MS measurement and data analysis. The MS measurement was carried out by Dr. Georg Tascher (Frankfurt). A high-quality MS-MS spectra, created by fragmentation of a selected precursor peptide ion, is of the outmost importance, to (I) confidently assign the MS-MS spectra to the crosslinked peptide and (II) identify not only the crosslinked peptide but rather the crosslinked residue. In the first step, the quality of the samples was ensured by a MaxQuant analysis to identify the proteins present in the sample (see Table 2).

Table 2: MS analysis confirms the isolation of the FKBP51→Hsp90 crosslink. A representative data set of the MaxQuant analysis is presented and used to identify content of the selected gel bands in Figure 16.

Protein name	Peptides	Unique peptides	Sequence coverage	Intensity
FKBP51 A398pBpa (1)				
Hsp90AB1	66	66	62%	1.82×10^{10}
FKBP51	67	67	80%	2.12×10^{10}
Keratin (P04264)	52	36	57%	1.48×10^{9}
FKBP51 M412pBpa (2)				
Hsp90AB1	69	69	72%	3.61×10^{11}
FKBP51	77	77	90%	4.42×10^{11}
Keratin (P04264)	19	12	23%	1.02×10^{9}

The analysis of the MS measurement shows that indeed the band corresponds to a FKBP51→Hsp90 crosslink. Both proteins show an intensity at the same magnitude and a high sequence coverage. For quality control, the values are shown exemplary for the highest common contamination by the sample preparation Keratin. Here, the advances in sample preparation are seen in comparison to Table 1.

The next and most challenging step is the assignment of the spectra to the crosslinked peptide of interest. This can only be achieved by a software tool as a manual assignment of the complex MS-MS spectra is nearly impossible. For the analysis, MeroX was used, a software which was specifically designed for analyzing the highly complex mass spectrometric datasets that are

obtained after chemical crosslinking of proteins and a subsequent digestion of the created reaction mixtures (Götze et al., 2011, 2014). Even though the software tool was developed for identification of chemical crosslinks, the settings are flexible enough to allow a work-around identifying crosslinks that derived from photocrosslinkable unnatural amino acid. MeroX does not rely on the use of isotopically labeled crosslinker, yet it is an elegant method to potentially distinguish between true crosslink and background thereby adding an extra layer of confidence to the data. Janhavi Atit Kohle (Brian Freeman lab, University of Illinois) and Vincenth Brennsteiner (Georg Winter lab, Vienna) helped with the MeroX settings. The MeroX output is a table of potential identified crosslinks and additionally the corresponding MS-MS spectra are integrated and visualized, including the crosslinked peptides. Based on the fragmentation pattern the exact crosslinked residues can be determined e.g., the amino acid residue pBpa crosslinked to, however this assumes a fully fragmented precursor, where every single amino acid residue is or at least the majority of the residue is fragmented of the precursor. The MeroX output is shown in Figure 17 for two potential crosslinks for FKBP51 A398pBpa→Hsp90 and FKBP51 M412pBpa→Hsp90, including the MS-MS spectra and the visualization of the found crosslinked peptide.

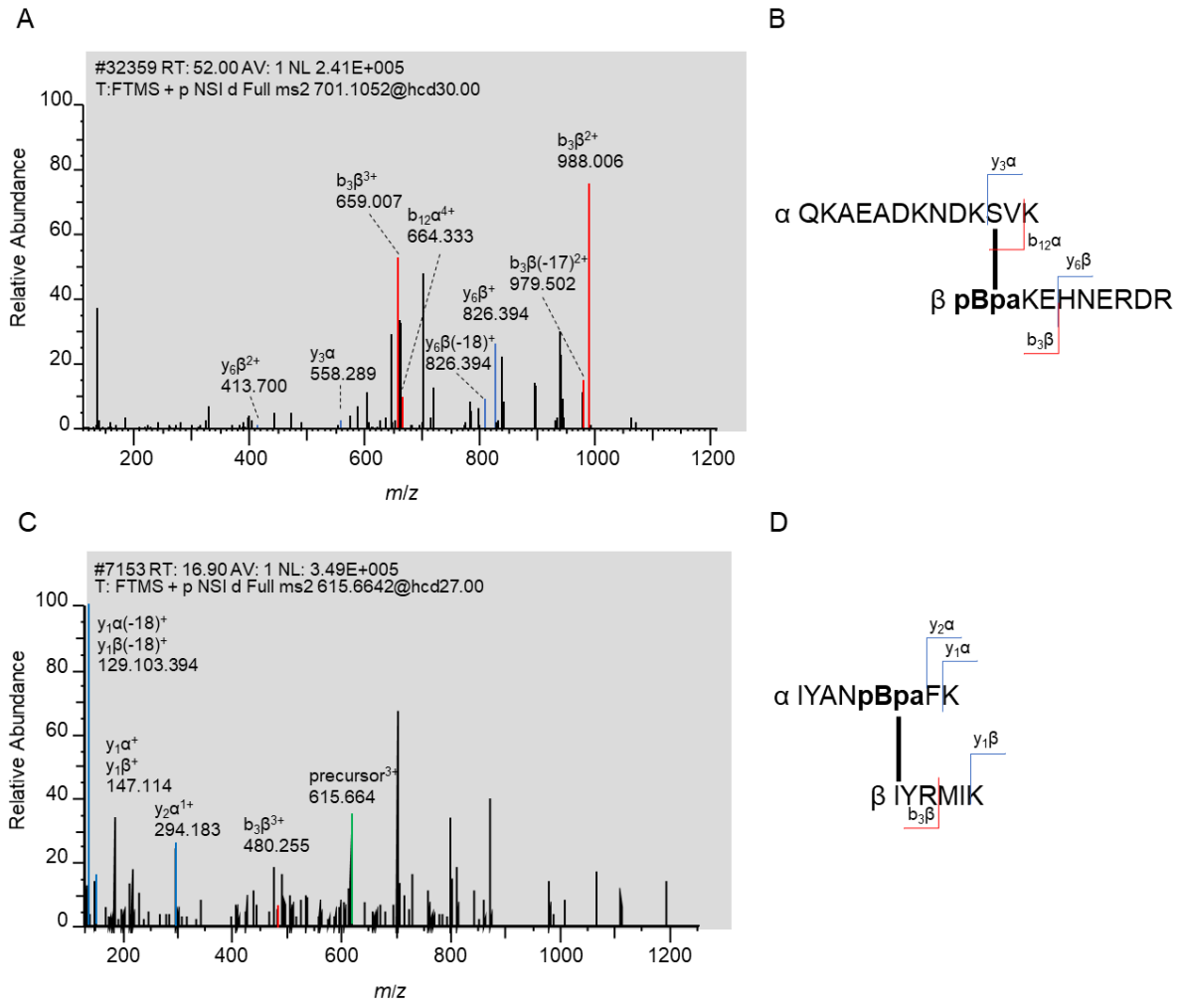

Figure 17: Identification of crosslinked peptides by MeroX. A, MS/MS spectrum of a potential crosslinked FKBP51 A398pBpa→Hsp90 peptide of m/z = 701.1052. C, MS/MS spectrum of a potential crosslinked FKBP51 M412pBpa→Hsp90 peptide of m/z = 615.6642. B + D, Sequence of the potentially crosslinked peptide with fragment ions highlighted. For MeroX read-out see Extended Figure 2.

For FKBP51 A398pBpa, MS-MS data provide evidence that the peptide of FKBP51 398pBpaKEHNERDR was crosslinked to the Hsp90 peptide 648QKAEADKNDKSVK, with 5 fragments of this crosslinked peptide found. Based on the fragmentation pattern pBpa crosslinked to either the C-terminal residues S658, V659, or K660 of Hsp90. For FKBP51 M412pBpa, MeroX identifies the peptide of FKBP51 408IYANpBpaFK as crosslinked to 688IYRMIK. Here, pBpa is suggested to crosslink to either I688, Y689, or R690 of Hsp90. The exact crosslinking site cannot be determined as the fragmentation coverage was not sufficiently high. For example, for the FKBP51 A398pBpa measurement, the precursor ion ($[M+H]^{4+}$ m/z = 700.8546) is still detected in the MS-MS measurement, therefore, the collision energy selected for the fragmentation was too low. This resulted in a poor fragmentation and lowers the quality of the analysis. In general, the quality of the data only allows a first glance on the

potential of this amber suppression coupled with MS analysis. For both potential hits, only the light species of the peptide is detected. This is potentially caused by the low abundance of the heavy ion, which resulted in an exclusion from the MS-MS analysis. Therefore, no MS-MS spectrum was recorded and the peptide cannot be analyzed by MeroX. Indeed, for the FKBP51 A398pBpa→Hsp90 crosslinked peptide, the light species is selected for MS-MS analysis (precursors $[M+H]^{4+}$ m/z = 700.8546) while the heavy species ($[M+H]^{4+}$ m/z = 702.3646) is excluded even though it is present. The MS spectrum of this measurement is shown for the range of m/z = 700.5–704.0.

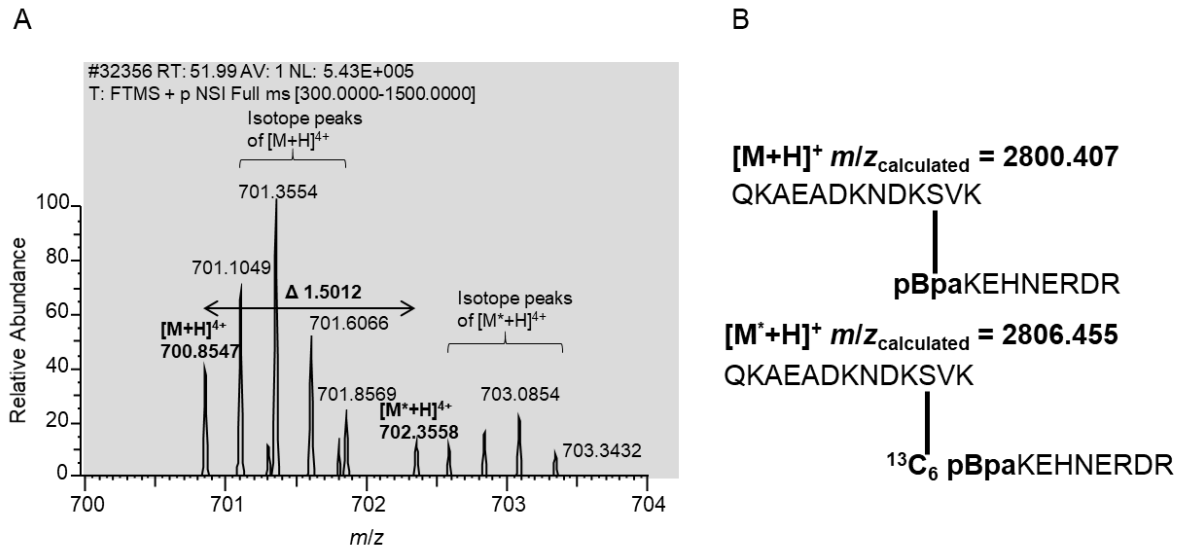

Figure 18: Mass spectrum indicates the presence of a $^{13}C_6$pBpa containing crosslinked peptide. A, selected part of the mass spectrum is depicted and shows two species: the crosslinked peptide with the not $^{13}C_6$-labeled pBpa $[M+H]^{4+}$ and with the $^{13}C_6$-labeled pBpa $[M^*+H]^{4+}$ and their respected naturally occurring isotopes. It indicates the presence of a not labeled and an isotopically labeled species of the same crosslinked peptide, the difference is indicated by an arrow. B, Sequence of the potentially crosslinked peptide and its calculated m/z for $[M+H]^{+}$.

The mass spectrum of the $[M+H]^{4+}$ ion of the potential crosslinked peptide of FKBP51 398pBpaKEHNERDR to the Hsp90 peptide 648QKAEADKNDKSVK is shown in Figure 18. The heavy species of this peptide is potential shown, with the mass shift of the heavy species $\Delta m/z$ = 1.5 (mass difference divided by ion charge; $6\times1.008/4^{+}$). This shows that both light and heavy species were present, however the low abundance of the heavy species, excluded the ion from further measurement.

The identified crosslinked peptide is visualized on the Hsp90-FKBP51 structure in Figure 19.

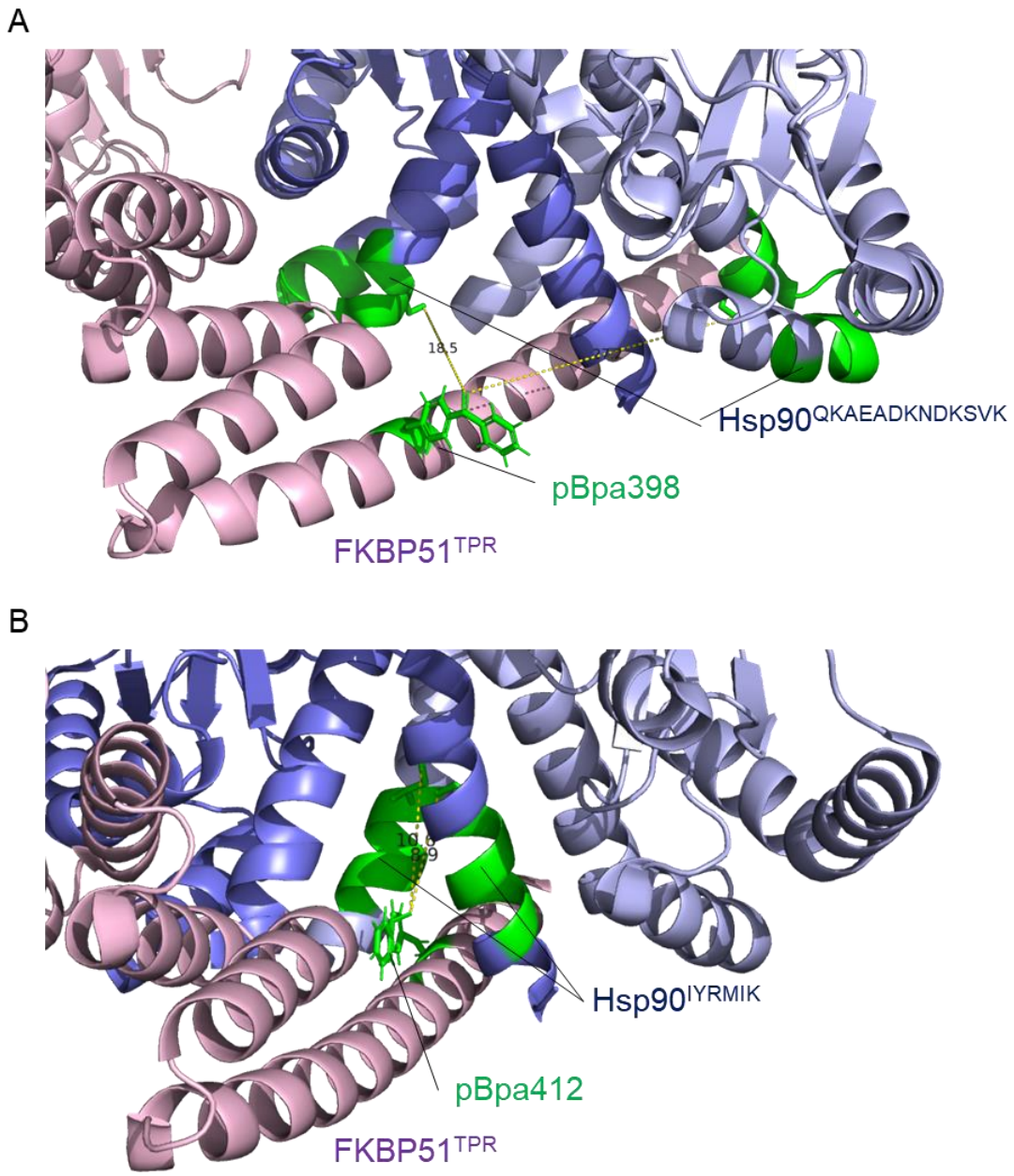

Figure 19: Specific identification of crosslinked peptides confirms FKBP51^{TPR} Hsp90^{CTD} interaction and gives detailed structural insights into the interaction interface. Peptides of the Hsp90 dimer (blue cartoon) identified as potential crosslinking site are visualized (green) on the Hsp90-FKBP51 structure (PDB: 7L7I). The site-specific incorporation of pBpa is indicated on FKBP51 (pale pink cartoon) and the selected position is manually changed to a chemical model of pBpa. Distances (in Å) to the exact crosslinked residues are indicated as yellow dotted lines and show close proximity of the photoreactive moiety of pBpa and the crosslinked residue.

Indeed, for both FKBP51 A398pBpa and FKBP51 M412pBpa potentially crosslinked peptides were identified that fit the Hsp90-FKBP51 structure. Additional potential hits were excluded from the visualization. Both crosslinks are situated in the C-terminal domain of Hsp90 and are in close proximity of the site of pBpa incorporation and in range of the photoreactive moiety.

The experiment laid the groundwork for a reliable identification of crosslinking sites by MS. In general, the MS method has to be improved for further measurements, for example the collision energy for the fragmentation can be increased as well as the numbers of precursors for MS-MS measurements, additionally the LC method can be adopted to meet the different properties of crosslinked peptide e.g., higher mass and polarity. Despite the failure of detection of both isotopically labeled and unlabeled species of the same peptide, the found crosslinked peptides fit well the structure of the complex. This raises the question whether the incorporation of an isotopically labeled pBpa is truly necessary, even though it is an elegant method. These preliminary results show that the incorporation of unnatural amino acids in combination with mass spectrometry has the potential to identify crosslinked peptides and to pinpoint the exact interaction site, which enriches the quality of interaction maps significantly. So far, this has been shown in a rare example, where β-arrestin was crosslinked to the parathyroid hormone receptor. The covalent complex was isolated, analyzed via MS-MS and two crosslinked residues were identified (Clark et al., 2020).

3.1.6. Crosslinking as a stabilizer

The in-cell covalent capture of interaction partner opens the possibility to study the protein, and the complex it may be involved in, in a close to native condition. It can enable the identification and characterization of transient and dynamic interaction partners. However, a detailed biochemical analysis e.g., native mass spectrometry or cryoEM requires larger quantities of a purified protein complex.

Preliminary results suggest that FKBP51→Hsp90 crosslinks stabilize the $(Hsp90)_2$-$(FKBP51)_1$ complex, beyond the covalent bond between $(Hsp90)_1$-$(FKBP51)_1$. The stabilization of the complex through crosslinking opens new opportunities to analyze the structure of Hsp90-FKBP51 complexes, especially in combination with a Hsp90 client such as the glucocorticoid receptor. After crosslinking, the following FLAG-immunoprecipitation experiments yielded partly new or at least enriched interaction partners. That raised the question whether the crosslink can be used as a stabilizer for the isolation of mutant FKBP51-containing complexes. The immunoprecipitated FKBP51 A398pBpa mutant was visualized after SDS-PAGE separation by silver staining and Coomassie staining (see Figure 20).

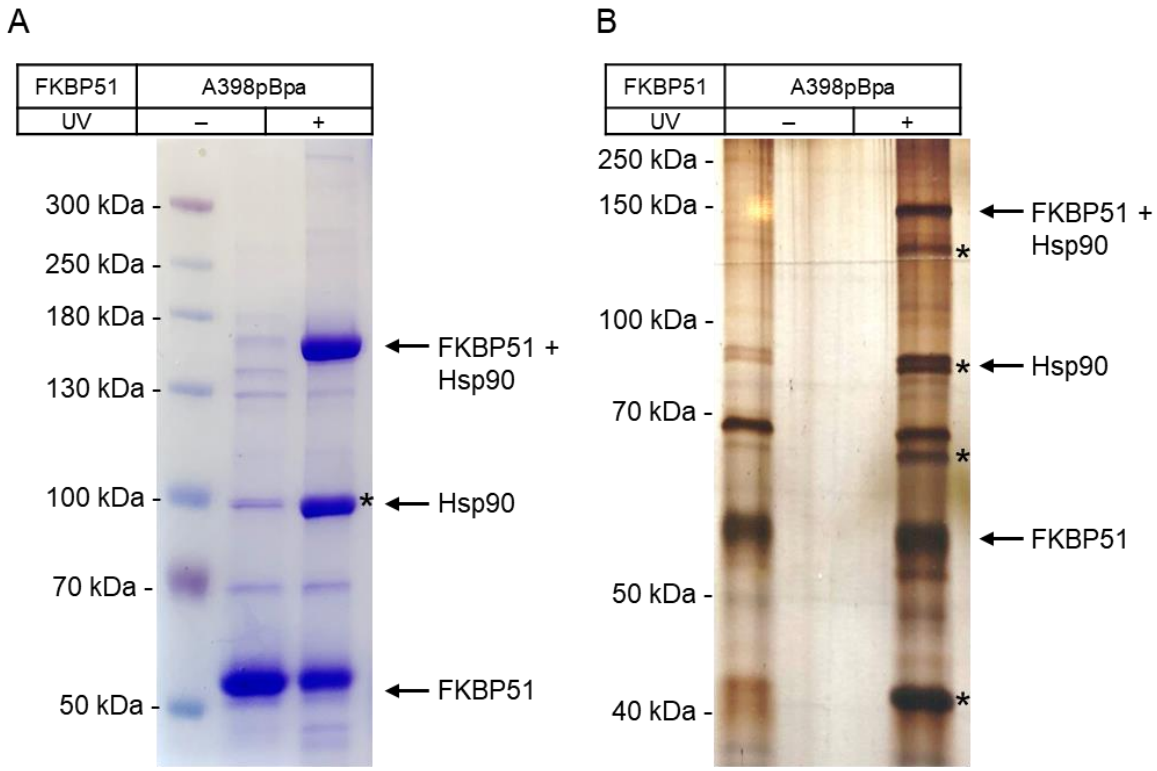

Figure 20: Photocrosslinking as a native interaction stabilizer. A, Coomassie-stained or B, Silver-stained gel of FLAG immunoprecipitated FKBP51 A398pBpa expressed and crosslinked in HEK293 cells. Asterisks indicated proteins that are more dominant in UV-irradiated samples.

In the Coomassie-stained gel (A), the UV induced FKBP51→Hsp90 crosslink is strongly visible at a molecular weight of ~160 kDa and the uncrosslinked FKBP51 at a molecular weight of ~55 kDa. Interestingly, a band at ~100 kDa is predominantly present in the UV irradiated sample. This corresponds to coimmunoprecipitated Hsp90 which was not crosslinked. This led to the speculation that the FKBP51→Hsp90 (monomer) crosslink stabilizes the native Hsp90 (dimer)-FKBP51 complex during cell lysis and the subsequent immunoprecipitation protocol. Similar results are indicated in the Silver-stained gel (B). A band at ~140 kDa, a double band at ~100 kDa, a band <70 kDa, and band at~40 kDa are more strongly visible in the UV-irradiated sample. Potentially, the crosslinked FKBP51 locks the Hsp90 dimer in a stabile complex by strengthening the native interaction to a certain degree.

For follow-up experiments, the stabilized Hsp90-FKBP51 has to be isolated to ensure a purified, intact and homogenous complex. A suitable and heavily used method for the purification of proteins is size exclusion chromatography (SEC), a separation technique that takes advantage of the different migration behavior of protein by their relative size or hydrodynamic volume with respect to the pore size of the column packing (Barth et al., 1994). SEC is a relative method

and requires a calibration of the column by a standard to determine the molecular weight of a protein or protein complex (Barth et al., 1994).

In preliminary experiments, FKBP51 A398pBpa was amber suppressed, crosslinked to Hsp90 and purified by FLAG immunoprecipitation. The eluate of the IP was subjected to SEC separation. The chromatogram of the UV-irradiated sample (+UV) and the control (–UV) is shown in Figure 21.

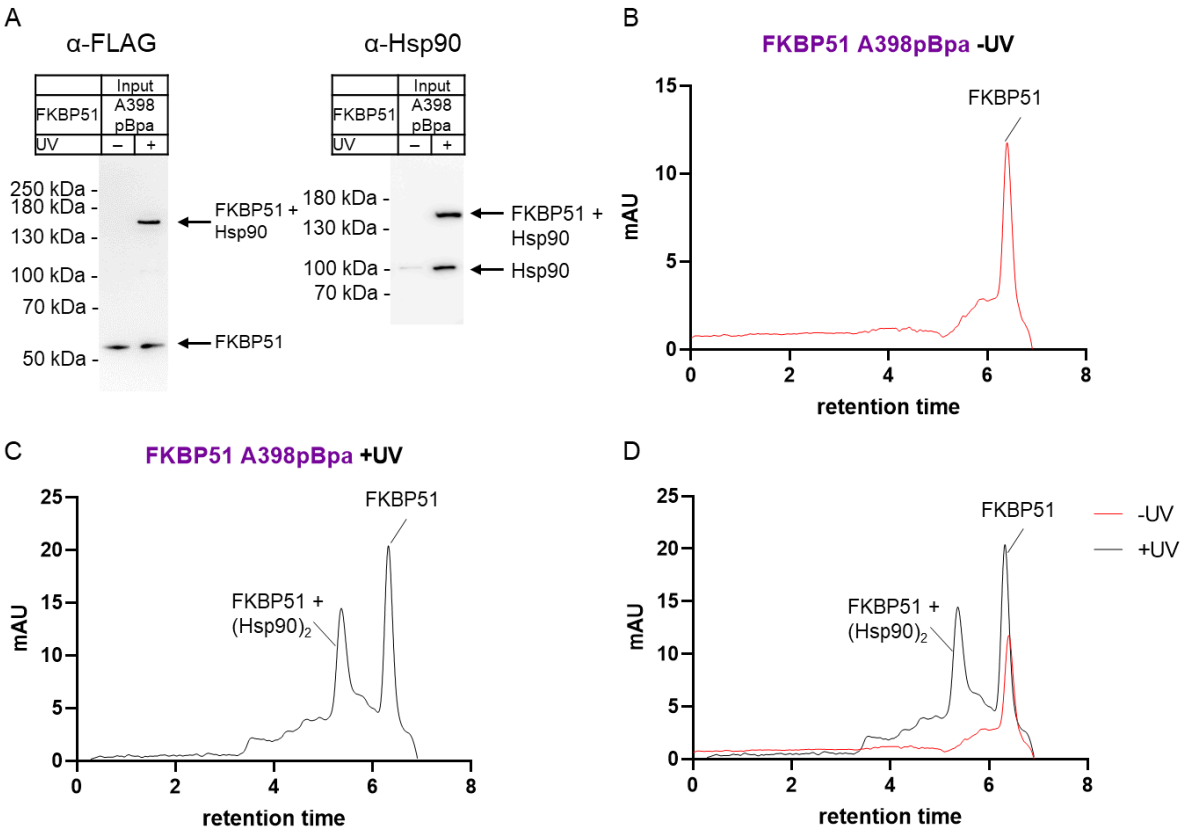

Figure 21: Crosslinked FKBP51→Hsp90 complex detected by size exclusion chromatography. SEC chromatogram of FKBP51 A398pBpa→Hsp90 at an absorption of 280 nm. A, input for SEC detected with both anti-FLAG and anti-Hsp90 antibody, B, –UV C, +UV, D, overlay.

In the chromatogram of the crosslinked FKBP51 two peaks are detected at a retention time of 5.366 min and 6.320 min. For the control sample (–UV) only one peak is detected at rt = 6.398 min. The higher retention time corresponds to a smaller molecular weight of the detected protein. The column was calibrated with a protein standard, which enables a molecular weight determination. The first peak (rt = 5.366 min) corresponds to a molecular weight of ~200 kDa and the second peak (rt = 6.320 / 6.398 min) to ~50 kDa. The retention time shift was frequently observed and is caused by the SEC column. The data suggest the first peak corresponds to a crosslinked stabilized Hsp90 (dimer)-FKBP51 complex, while the second peak

corresponds to the uncrosslinked FKBP51. The SEC presents a similar result to the analysis of FKBP51→Hsp90 by Coomassie-staining SDS-PAGE (Figure 20).
So far, the SEC experiments showed the potential application of isolating a crosslinked stabilized FKBP51 complex. However, the low mAU values, almost at the detection limit, are an indication that the amount of the isolated complex was very low. This has to be significantly improved for further experiment.

3.1.7. Systematic mapping the FKBP51 surface

For mapping the interaction interface, the photo-crosslinker is used as a 'proximity-sensor' to pinpoint which positions of the investigated protein are close to the interaction partner in the associated complex. The identification of direct interaction partners of FKBP51 in the Hsp90-GR heterocomplex and deciphering of interaction interfaces gives detailed spatial information. This can be used to create a molecular model of the interaction, by using crosslinking data to extend the already established yet incomplete model of the Hsp90-GR heterocomplex. This was carried out first for Hsp90.

3.1.7.1. FKBP51 interacts with Hsp90 beyond FKBP51^{TPR}

First, crosslinks to the endogenous Hsp90 were detected using a Hsp90 antibody. However, this approach failed in the sense that the detection was to error-prone and not robust enough for screening the whole library for crosslinks. To facilitate detection of the investigated interaction partner, Hsp90 was overexpressed with a HA-tag. In a first step, positions in the TPR domain of FKBP51 (FKBP51^{TPR}) were investigated, which are predicted to mediate key contacts to the C-terminal domain of Hsp90 (Hsp90^{CTD}) (Lee et al., 2021). Then with mutants in both the FK1 and FK2 domain were investigated. An exemplary Western blot analysis is shown in Figure 22.

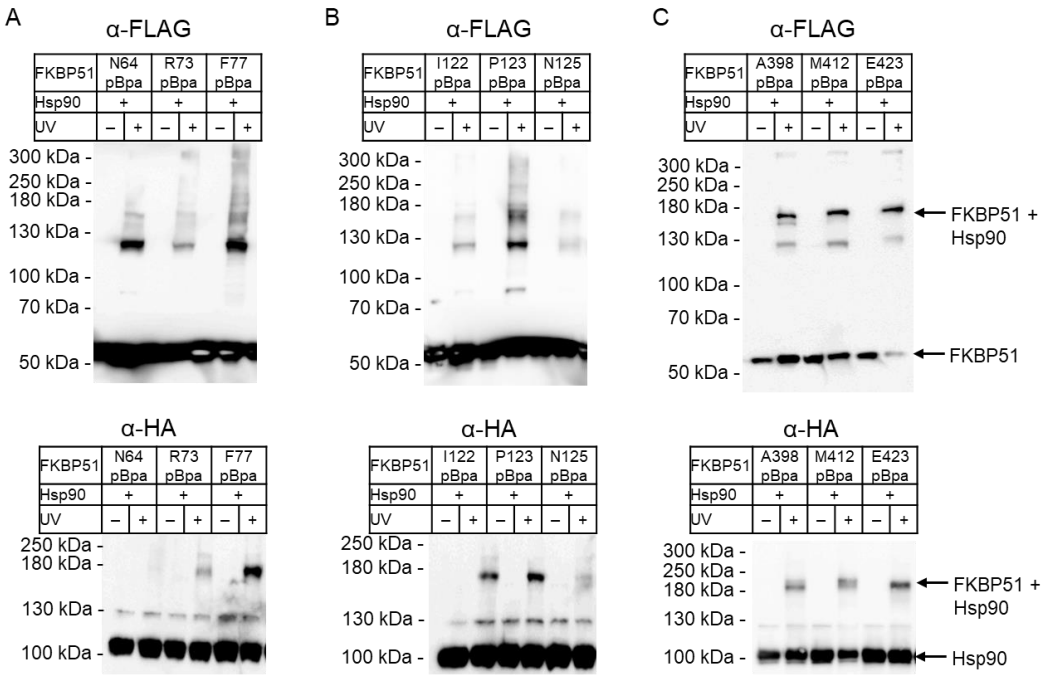

Figure 22: In-cell photocrosslinking confirms multiple interaction sites between FKBP51 and Hsp90. A + B, FKBP51^{FK1} mutants, C, FKBP51^{TPR} mutants, Western blots of exemplary FKBP51 pBpa mutants expressed and photocrosslinked in HEK293 cells co-expressing HA-tagged Hsp90. UV light-induced HA-reactive bands at a size of ~160 kDa are indicative of the mutated position being in proximity to Hsp90. For more tested mutants see Extended Figure 3 and Extended Figure 4.

Several positions in FKBP51 were identified, which upon UV irradiation produced higher-molecular weight complexes corresponding to crosslinked FKBP51-Hsp90 heterodimers. During the screening for FKBP51→Hsp90 crosslinks, it was observed that the migration behavior in SDS-PAGE analysis can slightly vary. This included positions previously shown to be in tight contact with Hsp90 (FKBP51 M412) (Lee et al., 2021) as well as positions poised to interact with the unresolved linker proceeding the C-terminal MEEVD motif of Hsp90 (Hsp90^{MEEVD}). Furthermore, crosslinks in FKBP51^{FK1} were identified and provide a refined picture of the FKBP51-Hsp90 interaction that is beyond the interaction in the TPR domain. The crosslinks were mapped on the structure of Hsp90-FKBP51 complex (Lee et al., 2021), which allows an assignment of the crosslinks to the respected binding sites on Hsp90 (see Figure 23).

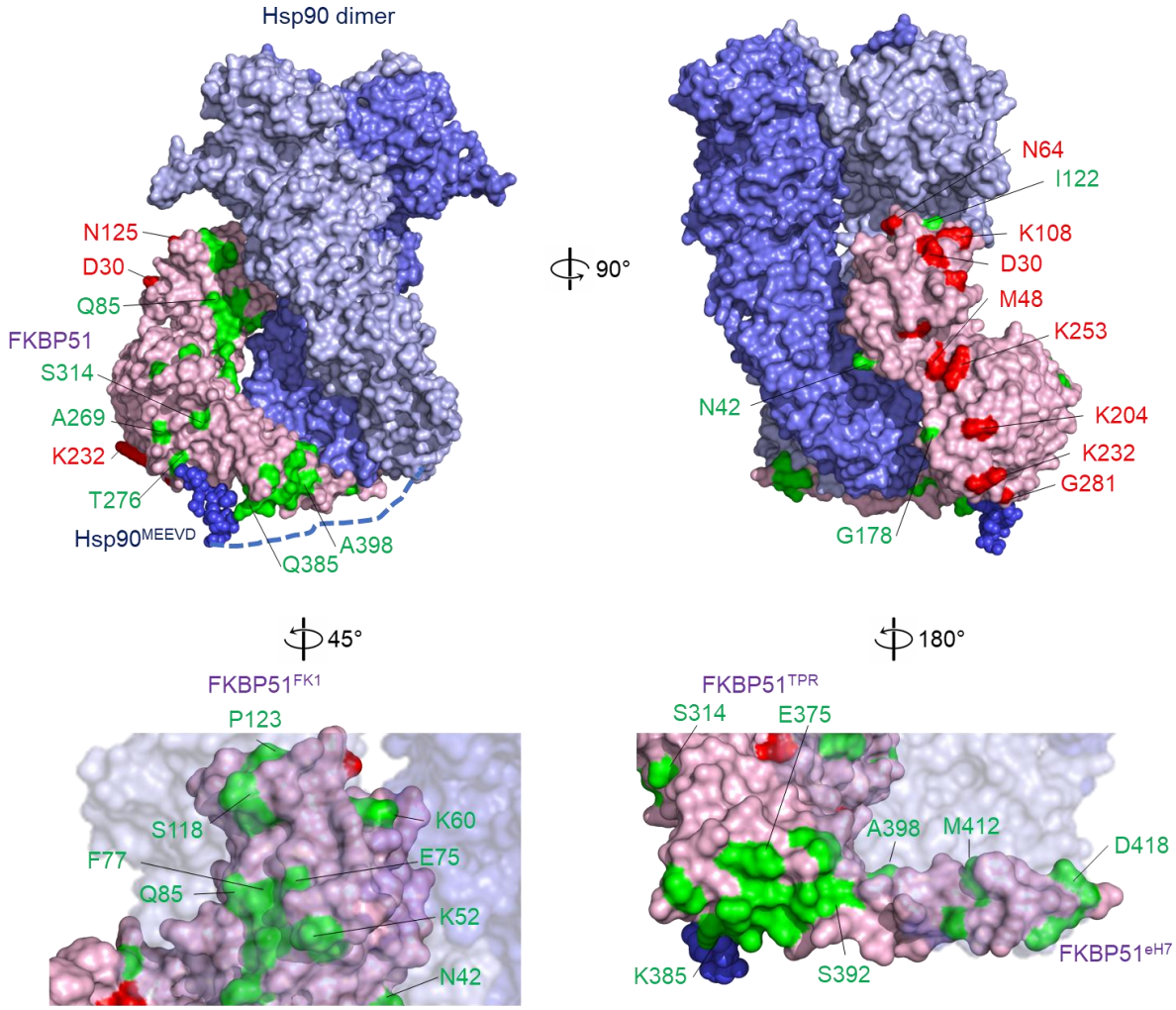

Figure 23: In-cell photocrosslinking confirms the interaction between FKBP51^{FK1} and Hsp90^{MD} & FKBP51^{TPR} and Hsp90^{CTD}. Hsp90-photoreactions and not photoreactive positions (highlighted in green and red) of FKBP51 (pale pink) identified by Western blotting as in Figure 22 were mapped on the structure of the Hsp90-FKBP51 complex (PDB: 7J7I, p23 omitted for clarity). Hsp90 dimers are shown in blue, the C-terminal MEEVD peptide of Hsp90 is depicted as blue spheres, and the unresolved linker between the MEEVD motif and one of the C-terminal domains of the Hsp90 dimers is indicated by a dotted blue line. Close-up view of crosslinks between positions of the FKBP51^{FK1} with Hsp90^{MD} and FKBP51^{TPR} with Hsp90^{CTD}.

The mapping shows a large interactions interface between the FK1 domain of FKBP51 and the middle domain of Hsp90, with multiple contact sites spread over one site of the FK1 domain facing Hsp90. They are in close proximity of the Hsp90 client binding site. No crosslink was detected on the opposite side of FKBP51, indicating the presence of a well ordered and reasonably populated FKBP51-Hsp90 complex inside human cells. FKBP51^{TPR} as well as the eH7 of FKBP51 interact with the C-terminal domain of Hsp90. Almost all test position in eH7 interact with Hsp90, proving evidence that this domain is highly important for the interaction, yet

flexible enough to allow incorporation of the bulky unnatural amino acid. FKBP51^{TPR} interacts at multiple sites with the MEEVD motif of Hsp90 as well as with the unsolved linker (dotted blue line). This only became apparent when the Hsp90^{MEEVD} motive was overlayed in the model, which was not present in the published version. The Hsp90^{MEEVD} motif was repeatedly described as the major interaction site with various TPR domain-containing proteins (Chen et al., 1998; Scheufler et al., 2000). The crosslinks strongly support a model were both the FK1 domain and the TPR domain are in contact with Hsp90. Potentially, the observed interaction represents a Hsp90-FKBP51 species where no client is bound and, in this state, the FK1 domain has space to bind the middle domain of Hsp90. This will be discussed in 3.1.7.3.

The found photocrosslinks fit the recent cryoEM structure of the FKBP51-Hsp90 complex, which show a multidomain interaction interface (Lee et al., 2021). Lee et al. performed additionally *in vitro* crosslinking experiments using the same unnatural amino acid pBpa and confirmed crosslinking of FKBP51^{FK1} (FKBP51 D72, N74, and E75) with Hsp90. The exact interaction sites were studied in HEK cells in this work (see Figure 23). One of the keys finding by Lee et al. is the binding motif of the extended C-terminal helix (FKBP51^{eH7}) to a groove at the interface of the two C-terminal domains of Hsp90 (Hsp90^{CTD}). The formation of this cleft was suggested to be coupled to the closed state of Hsp90. The interaction of FKBP51^{eH7}-Hsp90^{CTD} further suggests a preference for a $(Hsp90)_2$(FKBP51) stoichiometry and it beautifully explains earlier work by David Smith and colleagues, which indicated an important but incompletely understood role of the H7e for binding to Hsp90 (Cheung-Flynn et al., 2003).

Interestingly, the identified FKBP51 M412 as key interaction is weakened by the presented data (see Figure 22 and Figure 23), as the incorporation of the unnatural amino acid at this position produces a strong crosslink to Hsp90. No position was found to abrogate the interaction between FKBP51 and Hsp90 completely, despite the incorporation of a bulky, unnatural amino acid which points to a model in which not a single residue is responsible for the interaction, but rather a large, multidomain interaction interface. Nevertheless, a double mutant FKBP51 (K352A, R356A, described as TPR dead mutants (Cheung-Flynn et al., 2003)), which is proposed to be unable to interact with Hsp90, were amber suppressed and showed that the interaction is significantly imparted by these mutations (see Figure 24).

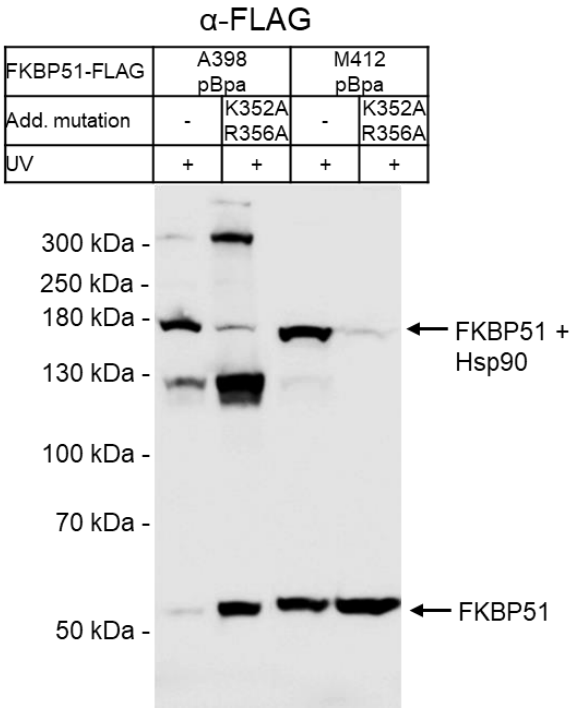

Figure 24: FKBP51→Hsp90 crosslink is sensitive to TPR-compromising mutations. Western blots of FKBP51 A398Bpa and FKBP51 M412pBpa expressed and photocrosslinked in HEK293 cells. UV light-induced FLAG-reactive bands at a size of ~160 kDa is sensitive to mutations in FKBP51 region important for Hsp90^{MEEVD} binding.

The Western blot shows that the crosslink to Hsp90 is significantly reduced in the TPR dead mutants. Both mutants are situated at the binding interface of FKBP51 to the MEEVD motif, again underlining the significance of the interact site. Potentially, the binding of FKBP51 to the Hsp90^{MEEVD} motif is crucial for recruitment of the protein to Hsp90. After the recruitment the interaction interface seems to be not depended on one single residue.

The Hsp90-FKBP51 interaction interface was also analyzed in NMR studies together with chemical crosslinking by Oroz *et al.* (Oroz et al., 2018). This study showed that FKBP51 can interact with Hsp90 in the open conformation in a head-to-head orientation at higher concentrations. This could be driven by the Hsp90^{MEEVD}-FKBP51^{TPR} interaction alone, which would allow for a $(Hsp90)_2(FKBP51)_2$ stoichiometry as observed by Oroz *et al*. The chemical crosslinking experiments followed by MS analysis allowed pin-pointing the interaction sites by identifying lysine residues that were crosslinked together. This is a great advantage over the incorporation of unnatural amino acids by amber suppression. However, initial experiment to pin-point the exact crosslinking sites using the incorporation of pBpa were presented in 3.1.5. The observed chemical crosslinks are limited to lysine residues and are not presenting a detailed picture but rather a rough orientation. They are usually applied as a tool to find interaction partners in general (Nguyen et al., 2018).

Chemical crosslinks were observed in the FKBP51 FK1 domain to the N- and Middle Domain of Hsp90 as well as the FKBP51 TPR domain with the C-terminal domain of Hsp90 (Oroz et al., 2018). The crosslinks are only partially fitting the cryoEM structure by Lee *et al.* and might represent a more flexible and dynamic model. While these chemical crosslinks represent a suitable tool to gain orientational insights, a systematic in-cell mapping is achieved only by the large-scale incorporation of unnatural amino acid.

The FKBP51-Hsp90 crosslinks were used as a proof-of-concept. For a single residue resolution map the incorporation should be performed at a more systematic approach using all surfaced exposed amino acid residues. The structural insights gained by the cryoEM structure by Lee *et al*. are complementary with in-cell photocrosslinking, with the cryoEM structure being evolved from *in vitro* experiments whereas in-cell photocrosslinking investigates protein interactions in a quasi-natural environment.

3.1.7.2. FKBP51 directly interacts with the Hsp90 cochaperone p23

During the screening of the FKBP51 surface for interaction partner, a crosslink band of ~80 kDa was observed for at least six FKBP51 mutants. MS analysis followed by Western blot confirmation identified the unknown interaction partner as the Hsp90 cochaperone p23. p23 is an important cochaperone of the Hsp90 machinery. In contrast to other cochaperones such as FKBP51 and FKBP52, it is part of the essential core chaperone machinery needed for client activation (Biebl et al., 2020). It is highly conserved over all eukaryotic species (Biebl & Buchner, 2019). p23 binds the closed conformation of Hsp90 (Li et al., 2011) and leads to a reduction of the Hsp90 ATPase activity, thereby prolonging the client interaction (McLaughlin et al., 2006).

The crosslinking sites were mapped on the structure of FKBP51 and reveal a single interaction hotspot at the tip of the FK1 domain (see Figure 25).

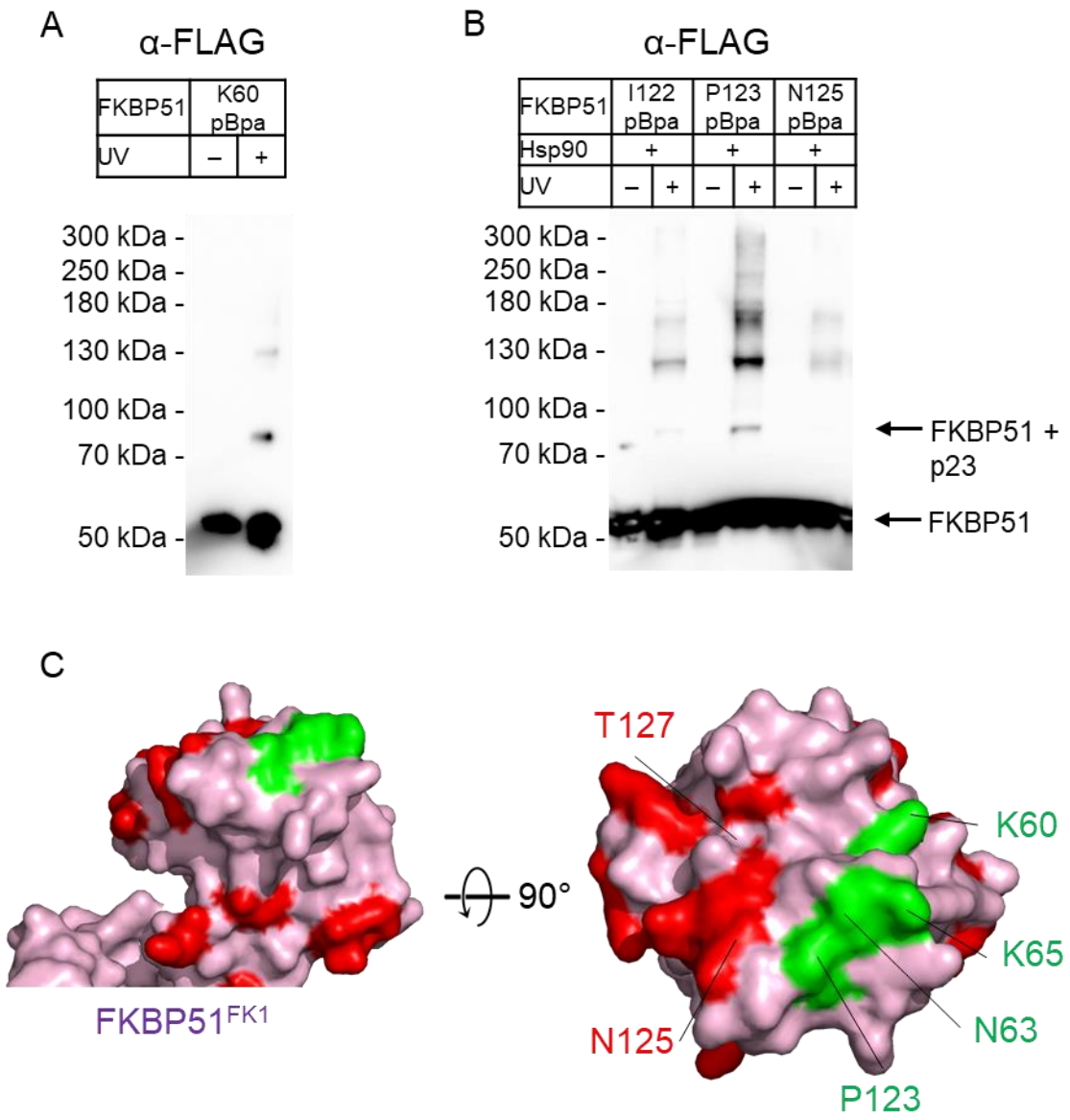

Figure 25: Photocrosslinking of the FKBP51 in mammalian cells confirms the interaction to the Hsp90 cochaperones p23. A + B, Western blots of exemplary FKBP51 pBpa mutants expressed and photocrosslinked in HEK293 cells (without p23 co-overexpression). UV light-induced FLAG-reactive bands at a size of 130 kDa are indicative of the mutated position being in proximity to p23. C, FKBP51→p23 crosslinks (green) and no crosslinks were mapped on the FKBP51 structure (PDB 5OMP, pale pink). For more tested mutants see Extended Figure 3 and Extended Figure 4.

The interaction site is cluster around the mutants FKBP51 K60, N63, and K65 as well as FKBP51 P123, N125, and T127 which are located close to the proline rich loop and form the top of the FK1 domain. Some of the interaction sites (K60 or P123) are also described as Hsp90 interaction sites (see Figure 23). It is most likely that the FKBP51→p23 interaction is Hsp90 depended, which explains the at least partially shared interaction sites. The photocrosslinker are somewhat

flexible and especially are at the rim of the interaction interface may be able to reach both proteins.

This is the first time a direct interaction between FKBP51 and p23 is described. Nevertheless, the observed preference of FKBP51 for p23-containing Hsp90 complexes is described repeatedly (Biebl & Buchner, 2019). For example, Ebong *et al*. found that only FKBP51 and not FKBP52 form a stable complex with p23, Hsp90 and the GR (Ebong et al., 2016). Additionally, Lee *et al.* solved the cryoEM structure the Hsp90-FKBP51-p23 (Lee et al., 2021). Interestingly, they positioned p23 at the opposing side of the Hsp90 dimer and proposed no direct interaction of FKBP51. It has to be mentioned that Lee *et al*. also observed a potential electron density for p23 at the same site as FKBP51 of the Hsp90 dimer. It could be speculated that p23 could bind at both sides. A stoichiometry 1:1 or 1:2 of the Hsp90-p23 complex has been reported (Karagöz et al., 2011; Sullivan et al., 2002), but the intracellular concentration of Hsp90 is much higher than of p23, so a stoichiometry of 1:1 is likely more physiologically relevant (Ghaemmaghami et al., 2003; Mayer & Le Breton, 2015). In the absence of clients, the observed orientations of FKBP51 and p23 have to be regarded with caution, potentially the orientation is dictated by the client.

A remodulation of the Hsp90-FKBP51-p23 structure which positions both cochaperones at the same side shows no clashes and strongly supports a direct interaction of FKBP51 and p23 observed by the in-cell photocrosslinking (see Figure 26).

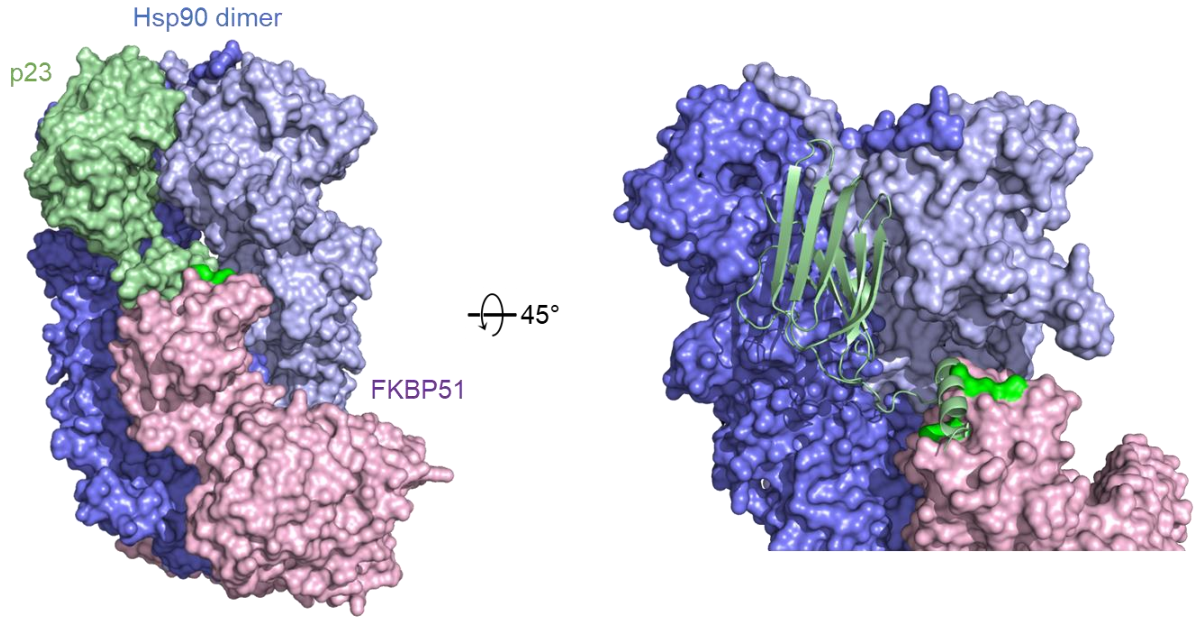

Figure 26: Photocrosslinking of FKBP51 in mammalian cells confirms the interaction to the Hsp90 cochaperones p23. FKBP51→p23 crosslinks are mapped on the structure of the Hsp90-FKBP51 complex (PDB: 7J7I, the position of p23 is flipped to the same side as FKBP51). Hsp90 dimers are shown in blue, FKBP51 in pale pink, and p23 (1-131) in green.

The top of the FK domain is likely to interact with the p23 tail (123-216, with p23 1-131 shown in Figure 26), while the p23 core domain (1-122) is interacting with the Hsp90 dimer. The flexible tail of p23 was recently studied in detail and reveals a coordinating function in client binding and maturation (Biebl et al., 2021). A helical motif in the C-terminal tail interacts and stabilizes the glucocorticoid receptor thereby preventing a premature release of the client from the chaperone complex (Biebl et al., 2021).

The detection of the p23 crosslinks raises the question, like for the Hsp90 crosslinks; whether the observed species is client bound or not. Here, a disadvantage of the in-cell photocrosslinking is exposed, that allows no direct distinction between different species. A potential approach would be the application of specific inhibitors as chemical tools to manipulate protein interaction which is discussed in Chapter 3.

Giving the importance of the GR a Hsp90 client and the role of FKBP51 in GR maturation, the next logical step is the detailed analysis of the FKBP51-GR interaction.

3.1.7.3. FKBP51 directly interacts with the glucocorticoid receptor

In initial crosslinking experiments, FKBP51 was shown to directly interact with the glucocorticoid receptor. As the GR is regulated by FKBP51 and disregulation of the GR is of high medical relevance, a better understanding of the interaction and regulation is crucial. To get a more detailed view on this interaction, several FKBP51 mutants, mostly positioned in the FK1 domain were tested and mapped on the FKBP51 structure. An anti-GR antibody was used to detect the endogenous GR and crosslinked products thereof.

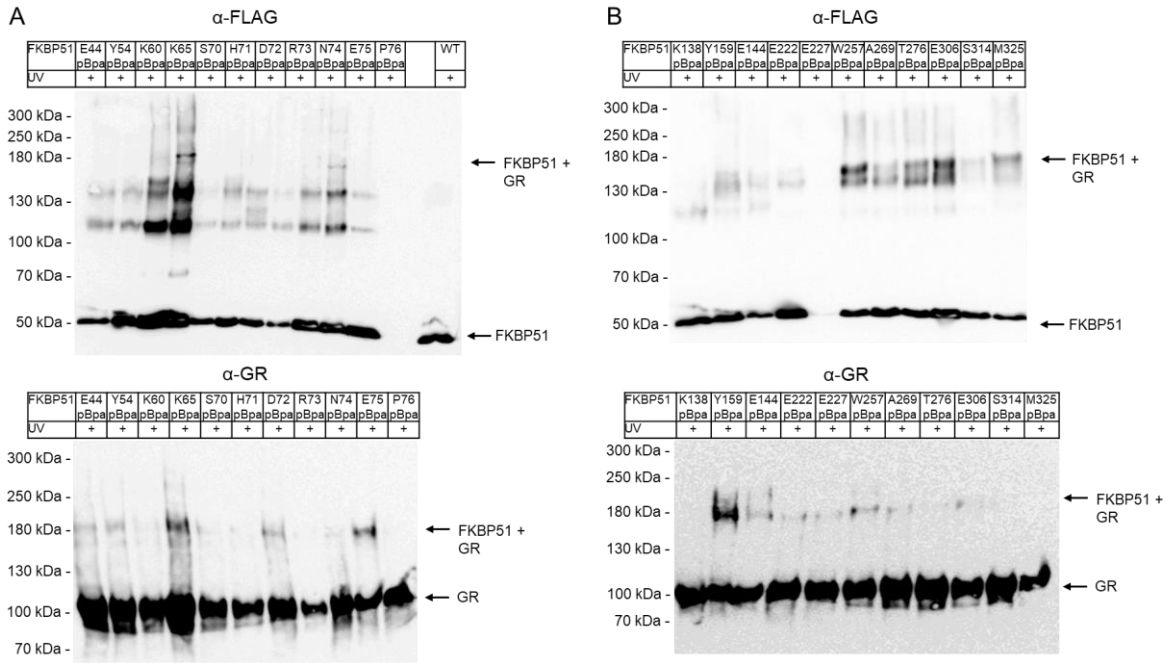

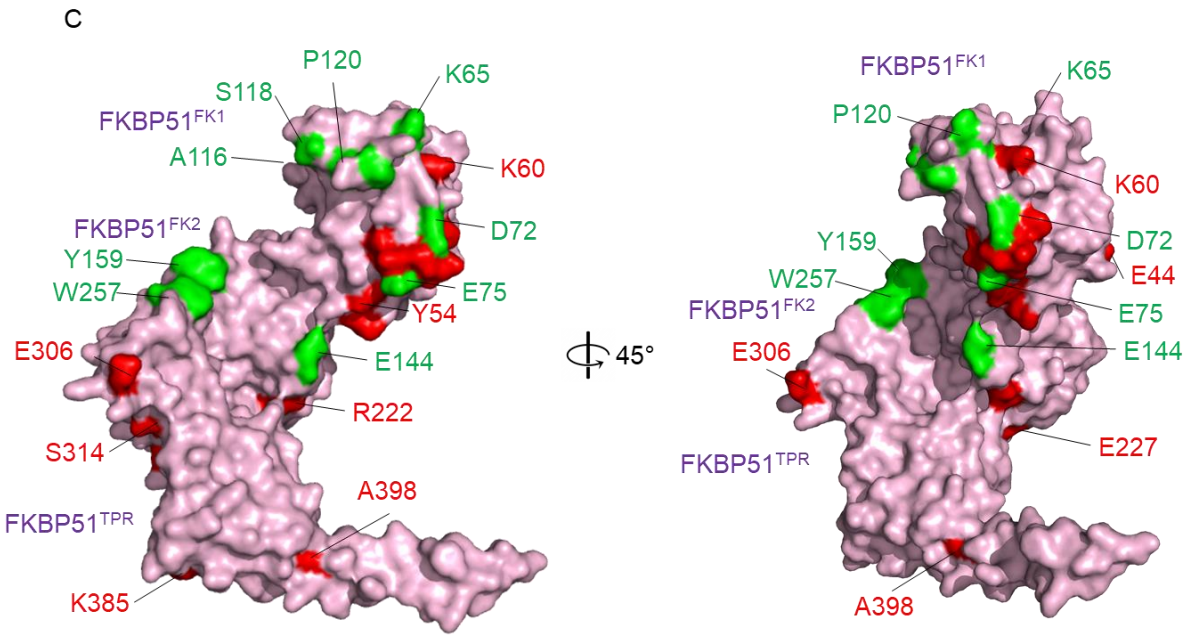

Figure 27: In-cell photocrosslinking of selected FKBP51 pBpa mutants reveals direct FKBP51-GR interaction. Western blots of exemplary FKBP51 pBpa mutants in the FK1 domain (A) and in the FK2 and TPR domain (B), expressed and photocrosslinked in HEK293 cells. UV light-induced FLAG- and GR-reactive bands at a size of ~180 kDa are indicative of the mutated position being in proximity to GR. C, GR-photoreactive positions (highlighted in green, with negative positions in red) were mapped on the structure of FKBP51 (PDB: 5OMP). For more mutants see Extended Figure 5.

The majority of the FKBP51→GR crosslinks are situated in the FK1 domain. Crosslinks are also observed in the FK2 domain and extended even down to the tip of the TPR domain.

Many crosslinks that were detected in the FK1 domain overlap with the FKBP51→Hsp90 crosslinks. Potentially, these observed $FKBP51^{FK1}$→Hsp90 crosslinks represent a Hsp90-FKBP51 species that is not client bound. These might occur after the client has been activated and released or as a species passing through the Hsp90 cycle without a client. As FKBP51 enters the late stage of the Hsp90 chaperone cycle, the client, e.g. GR is already bound. Therefore, the FK1 domain cannot interact, at least not to such a large extent, with Hsp90 but is rather possitioned on the client. It can be speculated, that during this binding the relative orientation of the FKBP51 domains have to be rearranged.

This is supported by a direct overlay depicted in Figure 28 with the Hsp90-p23-LBD^{GR} structure (Noddings et al., 2022) which shows massive clashes of GR^{LBD} with the FK1 domain as positioned in the Hsp90-FKBP51-p23 complex (Lee et al., 2021).

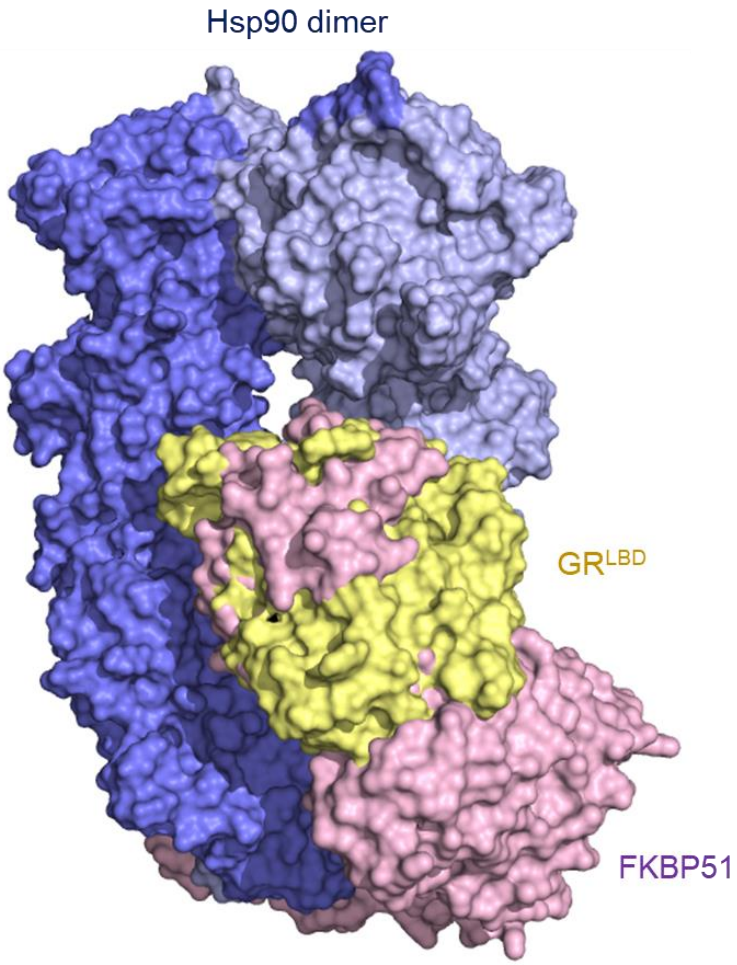

Figure 28: Overlay of the Hsp90-FKBP51-p23 structure (PDB-ID: 7L7I) with the Hsp90-p23-GR^{LBD} (PDB-ID: 7KRJ). FKBP51^{FK1} (pale pink) collides with GR^{LBD} (yellow).

The FK1 and FK2 domains of FKBP51 and perhaps also the Hsp90 clients have to undergo substantial movements to accommodate each other in ternary complexes.

In the mapping experiments, the endogenous GR is detected and used to validate the interaction to FKBP51. To facilitate the detection of the GR, a HA-tagged GR was overexpressed in a similar fashion as the HA-tagged Hsp90. The Western blot analysis of an experiment is shown that establishes the overexpression of HA tagged GR with amber suppression of FKBP51 (see Figure 29).

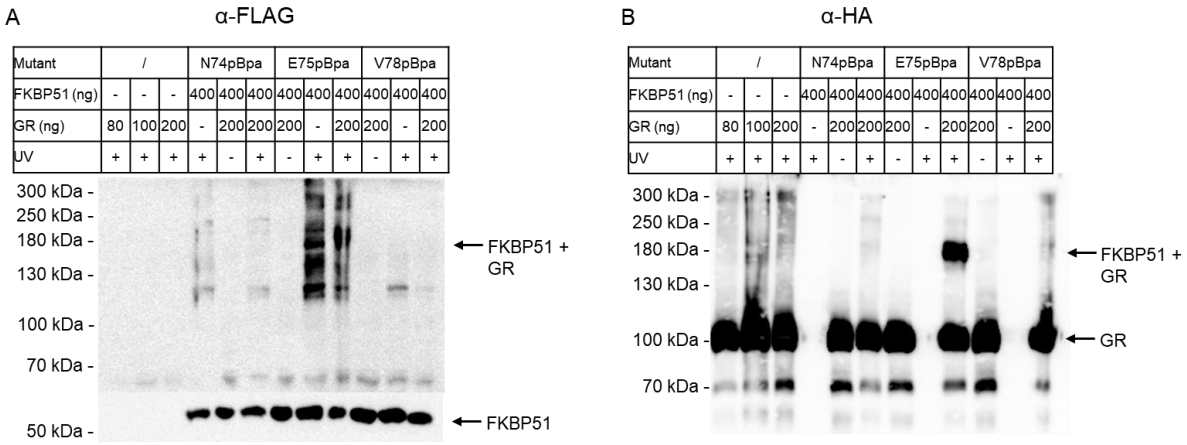

Figure 29: Amber-suppressed FKBP51 also crosslinks HA-tagged GR. Western blots of exemplary FKBP51 pBpa mutants were expressed and photocrosslinked in HEK293 cells. UV light-induced FLAG- and HA-reactive bands at a size of ~180 kDa are indicative of the mutated position being in proximity to GR.

The Western blot analysis shows a shift to a high molecular species depending on both the presence of the amber suppressed FKBP51 mutant and UV irradiation. Amber suppression is not impaired by the overexpression of HA-tagged GR as the level of FKBP51 does not vary significantly. The FKBP51 E75pBpa mutant shows a strong crosslink at the molecular weight of ~180 kDa. Even though, the overexpression of HA-tagged GR might disturb the quasi-natural environment by increasing the intracellular concentration of the GR, this is heavily outweighed by the much easier and specific two-way detection of the interaction by both anti-FLAG and anti-HA antibody in the Western blot analysis. Additionally, this opens the possibility of a high-throughput detection method of crosslinks, e.g., by ELISA.

After the establishment and optimization of the incorporation of the photocrosslinkable unnatural amino acid pBpa, initial screening experiments found a direct interaction of FKBP51 to Hsp90, the Hsp90 cochaperone p23, and the Hsp90 client GR which is regulated by FKBP51. This revealed for all three partner a preliminary interaction map. For the FKBP51-GR interaction map, the orientation of the GR in the interaction and the potential interaction sites on the GR remain enigmatic. Again, it was demonstrated that large-scale in cell photocrosslinking is a suitable tool to study protein interaction in great detail. Beyond the initial screening, the whole FKBP51 surface library was screened by Sarah Engel to map the FKBP51→GR interaction (Baischew & Engel, 2023). This beautifully revealed a large and continues interaction interface at single residue resolution. It provided much needed in-cell details of the interaction and regulation of GR by immunophilins.

3.2. Chapter 2: In detail study of the GR-FKBP51 interaction

In this chapter, the Golden Gate cloning approach was optimized from a one-tube-one-mutant approach to a 96 well format and streamlined to allow a whole surface library cloning in one week. This was applied exemplary to generate a surface library of the full-length glucocorticoid receptor. An ELISA for a fast and reliable detection of crosslinks was developed to facilitate mapping interaction interfaces. The previously detected direct interaction partner of FKBP51, the GR, was mapped for FKBP51 interaction in a high-throughput fashion. The goal was to gain details about the domain involved in the interaction as well as to reveal two interaction hotspots on the ligand binding domain of the GR. Additionally, the direct interaction of the GR and the Hsp90 cochaperone p23 was investigated.

3.2.1. High-throughput cloning approach of the GR TAG library

In a method developing step, the transfer of the cloning strategy from a one-mutant-one-reaction approach to a 96 well format was tested. To make the library generation process more efficient, a work schedule was developed to produce 48 mutants per run, which is shown in Figure 30.

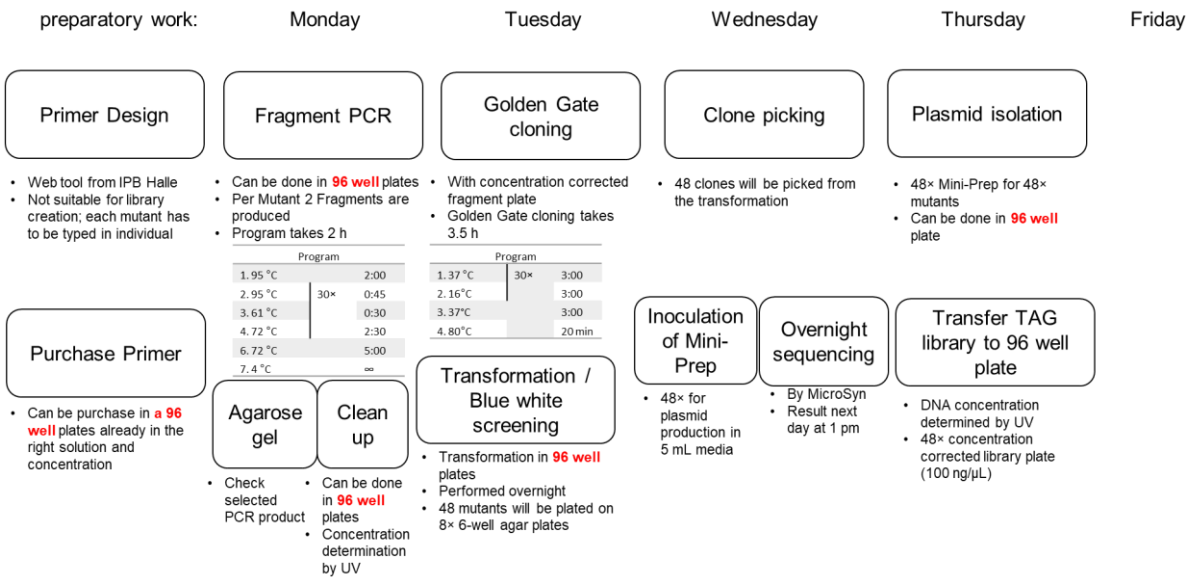

Figure 30: Schematic overview of the TAG library generation in a 96 well format. Steps that can be performed in a 96 well format are highlighted in red. The bottle neck is the plating of the transformation mixture on agar plates, which is the only step not adaptable to 96 well and which has to be performed manually.

The workflow fully begins by ordering the specific mutant primers for Golden Mutagenesis at the required concentration in 96 well plates. This allows for easy transfer into a 96 well PCR plate using a multichannel pipette. To produce 96 mutants per week, it requires 192 PCR performed in two 96 well PCR plates, since two PCR reactions are required for one mutant. The following PCR purification was performed using a PCR Clean up kit for 96 well plates. The Golden Gate reaction and the following transformation were also carried out in the 96 well format. Transformed *E. coli* were plated out in 6 well plates. This is a labor-intensive step. After clone picking and sequencing of each mutant, the plasmid DNA was isolated using a Miniprep 96 well kit. The efficiency of mutant generation after the first run of sequencing using one clone per mutant was about 80%. The plasmid DNA was eluted in 96 well plates, resulting in easier handling for the transfection protocol for amber suppression in HEK293 cells. The GR TAG library containing 215 mutants was created using this protocol. The establishing of the high-throughput cloning via Golden Gate cloning was heavily supported by Malin Wilfinger.

With the GR library at hand, the next step was the screening for GR→FKBP51 crosslinks, (I) to determine the domains involved in the FKBP51 interaction and (II) to find interaction hotspots of the GR-FKBP51 interaction. Both are important, to gain structural insights into the interaction at single residue resolution to investigate the inhibitory effect of FKBP51 on the GR.

3.2.2. ELISA as a tool to investigate the GR-FKBP51 interaction

3.2.2.1. Establishing ELISA for a high-throughput crosslinking screening

The analysis of crosslinks by Western blot is cumbersome and time consuming. The idea was to develop an enzyme-linked immunosorbent assay (ELISA), that enables a fast and reliable pin-pointing of direct interactions. Generally, an ELISA is used for detection and quantification of specific antigens or antibodies in a sample (Lequin, 2005). From the beginning, the goal was to establish a system that is broadly applicable and not limited to one particular protein-protein interaction. Therefore, a system was envisioned with three key components, (I) the immobilization of the protein of interest, (II) the detection of sufficient amber suppression, and (III) the detection of the crosslinked adduct. To make the ELISA generally applicable for abroad range of protein-protein interaction, the ELISA relies on well-established, high affinity protein tags to be independent of primary antibodies. Therefore, a three-tag system was developed for a good detection and a strong capture of the protein to the ELISA plate (see Figure 31). First, the bait-protein carrying the TAG amber codon is cloned with a tandem affinity tag, a twin Strep FLAG tag (Gloeckner et al., 2009). The twin Strep tag allows binding to a Streptactin coated ELISA plates. Proteins not containing this tag are washed away during washing steps. The FLAG tag is an octapeptide and allows detection by a horseradish peroxidase (HRP)-coupled anti-FLAG antibody (Gloeckner et al., 2009). Therefore, the FLAG signal serves as amber suppression control and shows if the amber suppression was successful. To investigate whether the bait-protein has formed a crosslink with an interacting partner, the interacting prey-protein is cloned with an HA tag. The use of HRP-coupled antibodies against the HA tag enables detection of crosslinks after UV irradiation. Therefore, irradiated cells and matched non-irradiated control cells are lysed, an aliquot of each lysate was absorbed on two separate Streptactin-coated 96 well plates. The HRP catalyzes the conversion of the substrate 3,3',5,5'-tetramethylbenzidine (TMB) and produce a measurable color change, that correlates with analyte levels. The absorption at 450 nm is measured and plotted to distinguish between successful and unsuccessful amber suppression for the anti-FLAG treated samples, and between crosslink and no crosslink in the anti-HA treated samples.

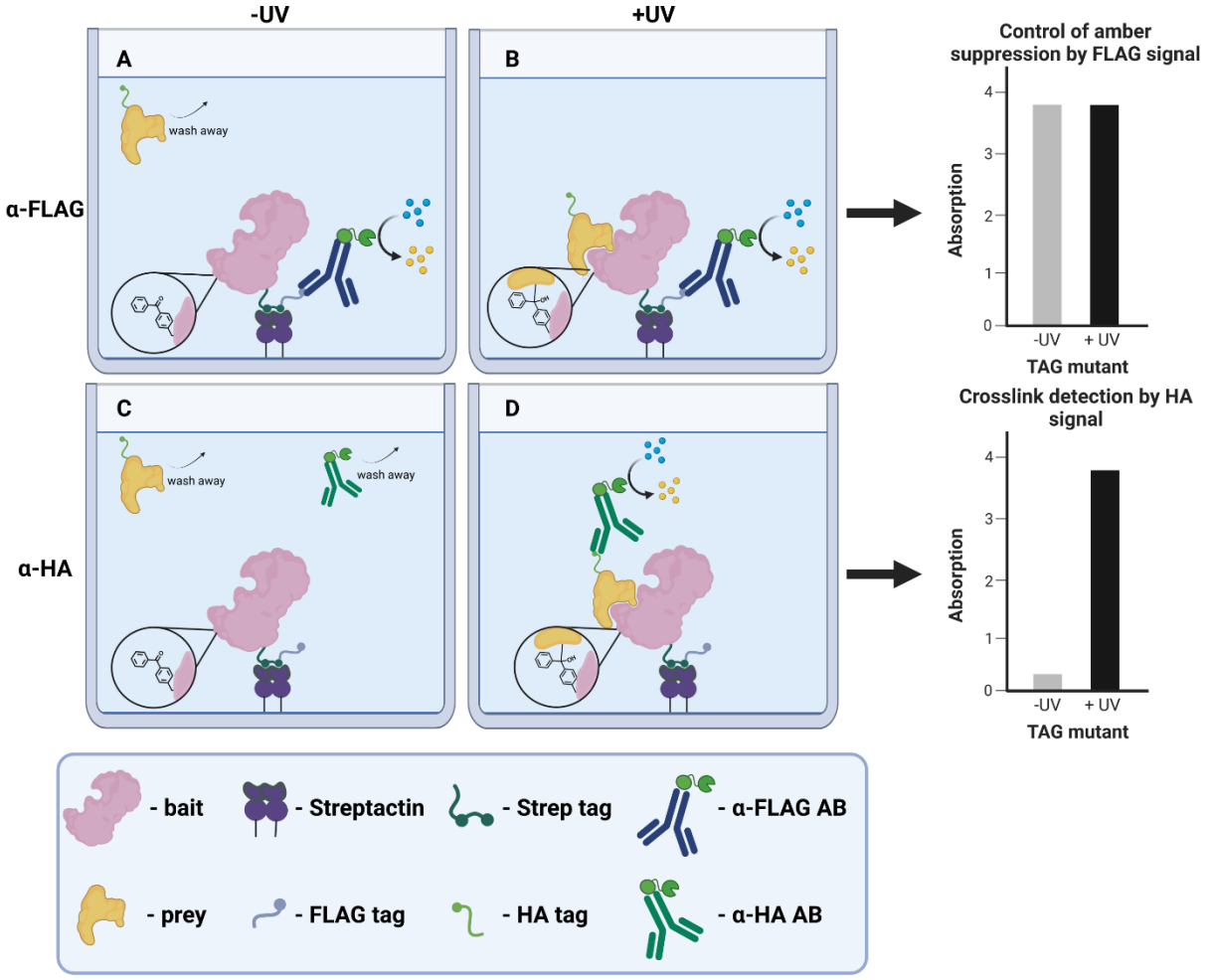

Figure 31: Detection of crosslinks by ELISA: The protein of interest (light pink) contains a twin Strep FLAG tag. The twin Strep tag allows binding to the Streptactin (purple) coated 96 well plate. HRP-coupled anti-FLAG antibodies (dark blue) are used to control whether amber suppression has worked (A and B). HRP-coupled anti-HA antibodies (green) are used to detect crosslinks. This should be possible after UV-irradiation (D) since the unnatural amino acid pBpa forms a covalent bond to the HA tagged interacting partner (yellow). Without UV-irradiation the interacting partner and in consequence the anti-HA antibody are washed away and only a background signal can be detected (C).

Different ELISA conditions were tested extensively for optimal results to enable fast and reliable detection of photocrosslinks. The testing included coating material and conditions, plate blocking, cell lysate incubation and conditions, antibody concentration and buffer conditions for detection amber suppressed proteins and crosslinked proteins. The systematic optimization was supported by Jan-Philip Kahl.

The ELISA for screening crosslinks was established and tested for the FKBP51 library. Therefore, the FKBP51 library was cloned into a eukaryotic expression vector with a C-terminal twin Strep FLAG tag. To evaluate the sensitivity of the ELISA and the necessary sample volume, a dilution

series of cell lysate from one large scale experiment (10 cm cell culture plate) was carried out for either amber suppressed FKBP51 E75pBpa or overexpressed FKBP51 WT. The FLAG signal is detected to evaluate the success of the amber suppression or overexpression, respectively. FKBP51 E75pBpa was used as a model mutant, that showed a strong FKBP51→GR crosslink.

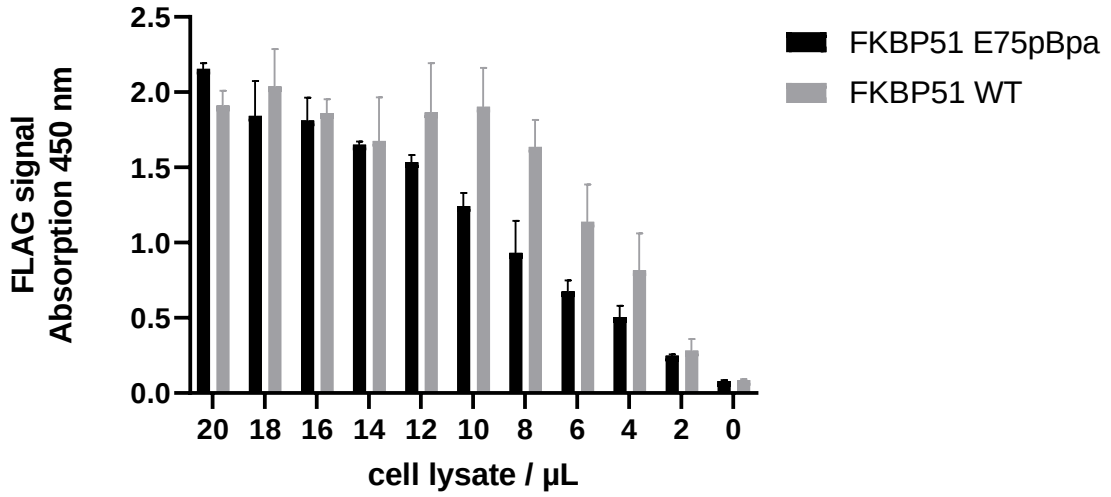

Figure 32: ELISA is sensitive for slight concentration changes of FKBP51. FLAG signal of both FKBP51 WT and FKBP51 E75pBpa. Different volumes of HEK 293 cell lysate from a 10 cm amber suppression experiment were incubated on the ELISA plate. Error bars for technical duplicates are shown.

For both dilution series, steps of 2 μL are detectable and for FKBP51 WT, a plateau starting from a sample volume of 10 μL can be seen. Furthermore, the absorbance of a total sample volume of 2 μL is still three times higher for both dilution series than the PBS reference (0 μL). The data shows that the ELISA is indeed capable of detecting amber suppressed FKBP51 E75pBpa and sensitive enough to detect small differences in protein concentration. In the next step, the sensitivity of the HA signal was tested for the FKBP51 E75pBpa→GR crosslink.

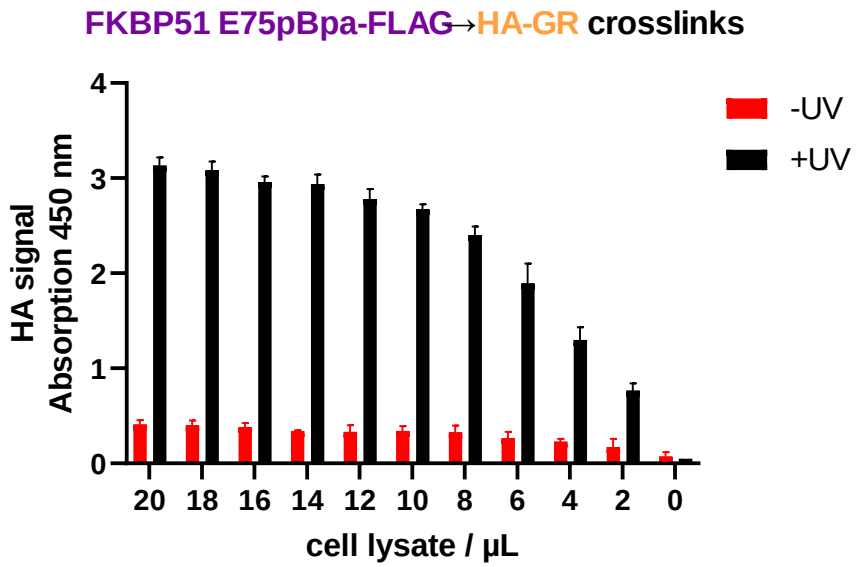

Figure 33: ELISA is sensitive for slight concentration changes in crosslinked GR. HA signal of FKBP51 E75pBpa. Different volumes of HEK 293 cell lysate from a 10 cm amber suppression experiment were incubated on the ELISA plate. Error bars for technical duplicates are shown.

The analysis of the ELISA shows the strong detection of the FKBP51→GR crosslink in all samples except for the negative control (0 μL). The dilution series with the UV treated samples show a plateau for sample volumes starting from 20–14 μL cell lysate. For lower concentrations, steps of 2 μL are detectable and a sample volume of 2 μL still leads to a difference in HA signal between the UV-irradiated and untreated samples. The signal of the untreated samples remains approximately constant.

For a reliable detection throughout different experiments, a value or threshold has to be defined for which the HA signal of a UV-irradiated sample is accounted as a crosslink or not. Two approaches were tested, (I) the subtraction of the HA signal of untreated sample from the UV-irradiated sample or (II) the ratio of the HA signal of UV-irradiated divided by the untreated sample (see Figure 34). More complex calculations were not considered for data traceability e.g., taking the amber suppression control into the calculation to account for outliers.

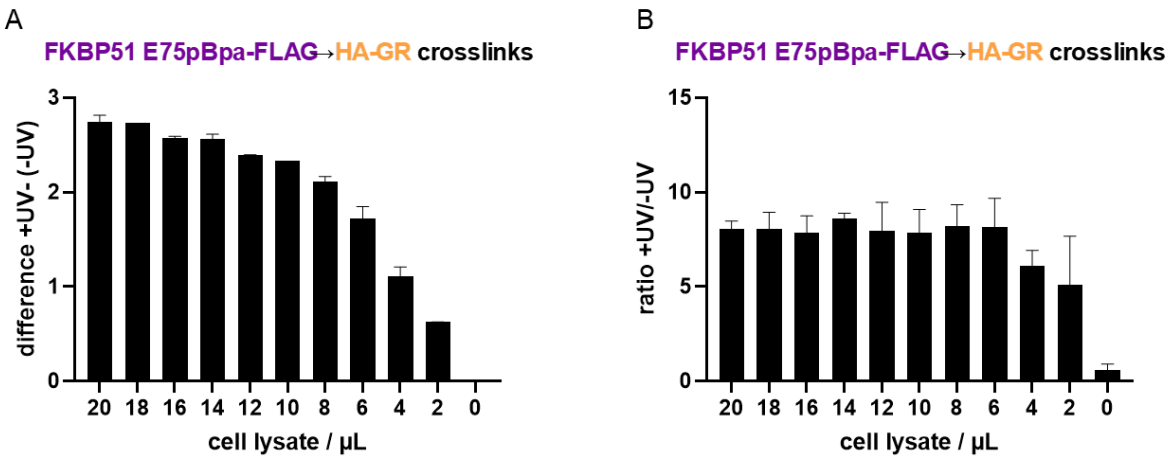

Figure 34: Different options for crosslink visualization. A, Subtraction of the untreated sample from the UV-irradiated. B, ratio of the UV-irradiated sample over the untreated sample. Different volumes of HEK 293 cell lysate from a 10 cm amber suppression experiment were incubated on the ELISA plate. Error bars for technical duplicates are shown.

The subtraction of the HA signal is an adjusted HA signal of the UV-irradiated sample and gives continuously decreasing values for the dilution series. Here, it might be harder to define a crosslink threshold. The ratio of the HA signal is not continuously decreasing and gives a constant value across the dilution series, until a cell lysate volume of 4 μL. Even for the lowest tested cell lysate volume the ratio is more than 4-fold higher than the control, which should be 1.

Both approaches were further tested in an exemplary FKBP51→GR crosslink screening experiment, with GR-photoreactive FKBP51 position already confirmed in Western blot analysis, to validate the ELISA screening and evaluation. Therefore, different FKBP51 mutants were amber suppressed and tested for GR crosslinks. The result of the ELISA screening is shown in Figure 35.

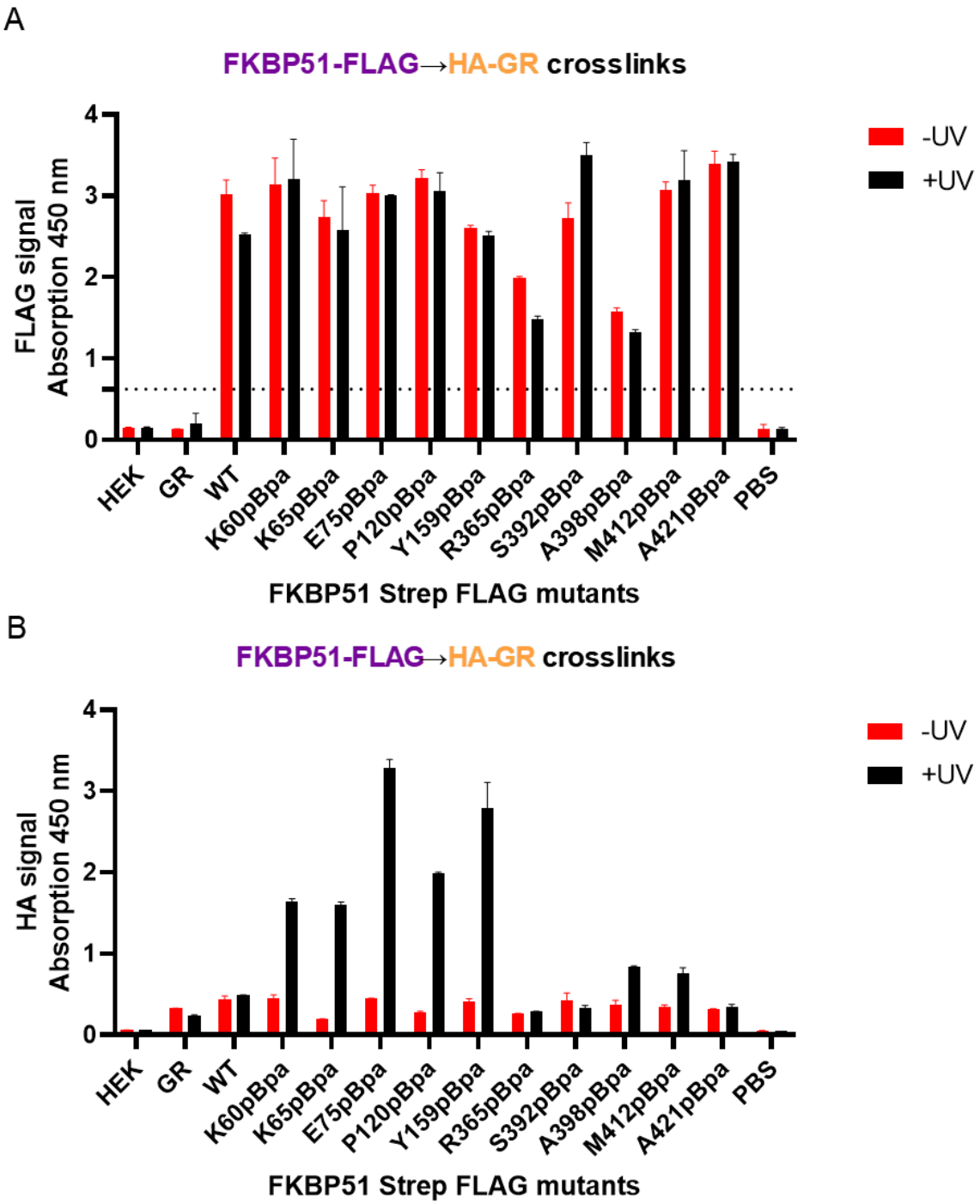

Figure 35: Pilot ELISA screening for FKBP51→GR crosslinks. ELISA data for FKBP51 pBpa mutants expressed and photocrosslinked in HEK293 cells co-overexpressing HA-tagged GR in 12 well plates. Irradiated cells and matched non-irradiated control cells are lysed, lysates are absorbed to two Streptactin-coated 96 well plates. Then after washing one plate is coated with HRP-coupled anti-FLAG for amber suppression control (A) and the other plate with anti-HA antibody to detect GR→FKBP51 crosslinks (B). The depicted values represent means of $n=3$ biological replicates and error bars with standard deviation. Mock (HEK), non FKBP51 (GR)- or $FKBP51^{WT}$ (WT)-transfected HEK293 cells and no cell lysate (PBS) were included as background controls. Dotted line in the FLAG signal indicated amber suppression ratio signal/WT <25%, which would be excluded from further analyses.

The control ELISA showed adequate amber suppression in all samples except the negative controls. A FLAG signal <25% of the FKBP51 WT is count as successful amber suppression and included for further analysis. The ELISA confirmed FKBP51→GR for FKBP51 K60pBpa, K65pBpa, E75pBpa, P120pBpa, and Y159pBpa (see Figure 27). None of the FKBP51^{TPR} mutant showed a crosslink to GR (see Figure 27). Nevertheless, a slightly elevated +UV HA signal was detected for FKBP51 A398pBpa and M412pBpa, which both show strong crosslinks to Hsp90 (Figure 22). It can be speculated that this FKBP51→Hsp90 crosslink stabilizes the GR client bound Hsp90-FKBP51 complex.

Again, the two approaches were tested for data representation of the photocrosslinker residue: (I) The subtraction of the HA signal of untreated sample from the UV-irradiated sample or (II) the ratio of the HA signal of UV-irradiated divided by the untreated sample.

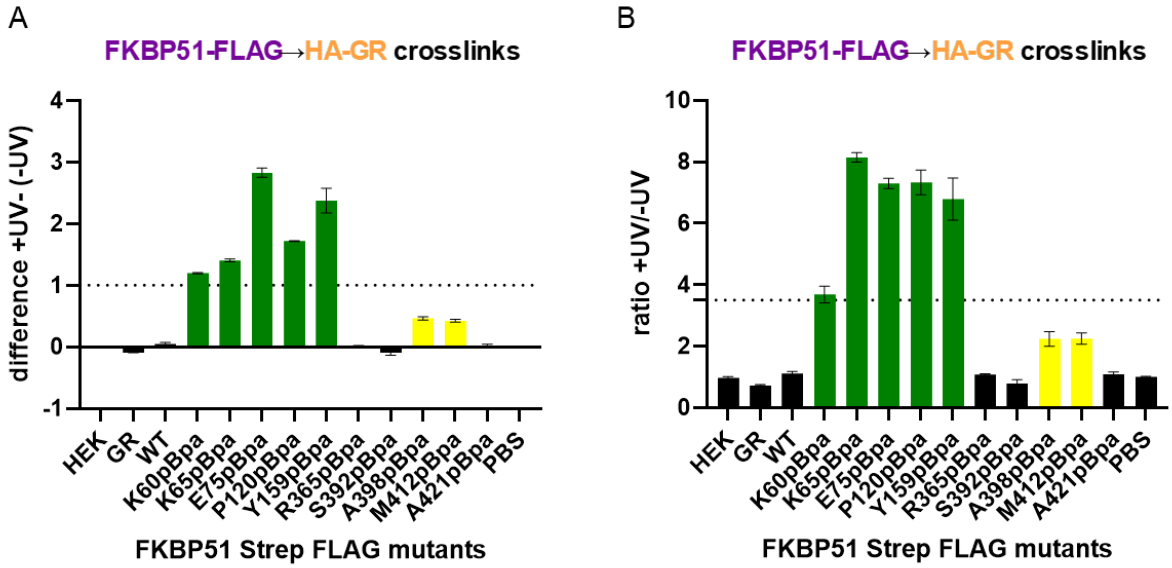

Figure 36: Pilot ELISA screening for FKBP51→GR crosslinks. A, depicted values represent difference of the signal of irradiated and untreated samples of Figure 35. HA ratios >1.0 are indicative of the mutated position being in proximity to GR. B, depicted values represent signal ratios of UV-irradiated vs untreated samples of Figure 35. HA ratios >3.5 are indicative of the mutated position being in proximity to GR. Yellow bar represent an unusually high signal for positions known to crosslink to Hsp90 but not to GR. Each bar represents data from biological replicates ($n=3$).

The subtraction of the HA signal detects all confirmed FKBP51→GR crosslinks. The values of the crosslinked position vary, with 3 out of 5 having a value between 1 and 2, while 2 out of 5 have a value above 2. The threshold of 1 was selected to include all crosslinks. This confirms the result from the previous test, that shows a stronger variation of the values for the subtraction of the untreated sample from the UV-irradiated sample. The ratio of the HA signal detects all confirmed FKBP51→GR crosslinks. Out of the 5 values 4 are in the same range from 7–8 and

the value of FKBP51 K60pBpa is 3.6. The threshold was set to 3.5 to include all crosslinks and is therefore 3.5-fold over the control sample. This confirms the result from the previous test, that shows less variation for the ratio of the UV-irradiated sample to untreated sample. Both approaches have their advantages, for example the subtraction seems to give rise to more detailed information. Indeed, FKBP51 E75pBpa and FKBP51 Y159pBpa were found to be particular strong crosslinks and were selected as model positions. This could be used for determination of crosslink strength, which would give a detailed interaction map. The ratio gives a more constant and smooth value which facilitates an initial screening. Nevertheless, one has to be aware of the fact, that both might lead to false-negative result, especially for mutants that show low amber suppression, which translates in a weaker HA-signal after crosslinking.

For a fast and reliable detection of crosslinks, a standard protocol was established for 96 well plates for a high-throughput screening (see Figure 37). This was supported by Malin Wilfinger. An overview of the necessary steps is schematically shown. The ELISA of screening for interaction was established and in the next step, the GR library was tested for FKBP51 interactions.

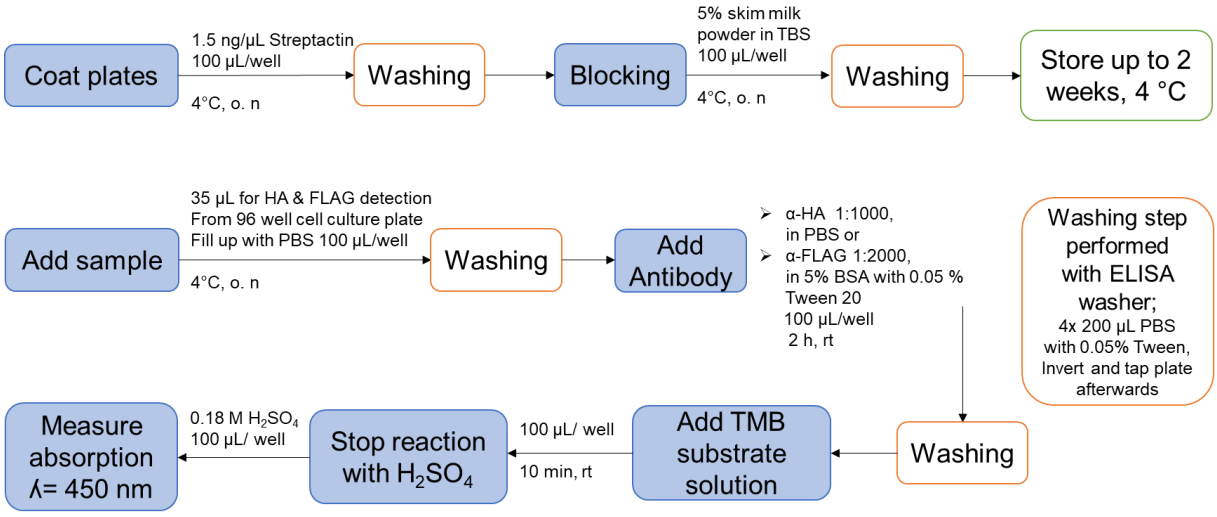

Figure 37: Overview of ELISA workflow.

3.2.2.2. Screening the GR for FKBP51 interactions

To further refine the orientation of GR in the Hsp90-GR-FKBP51 complex, a TAG mutant library (215 mutants) was generated and screened covering the putative surface of full-length GR, including 42 surface-exposed amino acid positions in the GR ligand binding domain (GR^{LBD}), 24 residues in the DNA-binding domain, and 149 residues in the structurally uncharacterized N-terminal part of GR.

First, the amber suppression of GR was validated to ensure the site-specific incorporation of the unnatural amino acid. Both N-terminal twin Strep FLAG-tagged mutants and C-terminal twin Strep FLAG-tagged mutants of GR were cloned and tested. The latter has the advantage that only the amber suppressed species will be detected. If the TAG stop codon is not amber suppressed and the unnatural amino acid not incorporated, the twin Strep FLAG tag is not expressed. Hence, no signal would be detected, in both Western blot analysis and ELISA. Also, the lack of the Strep motif would result in no immobilization on the ELISA plates. However, the C-terminal domain of the GR, the Ligand Binding Domain is conformational sensitive and potential hinders a sufficient expression, which is important for a fast and reliable interaction screening. Different N- and C-terminal SF (Strep-FLAG)-GR mutants were used to test whether the amber suppression works and to estimate the expression level. In order to choose the best conditions for further experiments, different amounts of HEK293 cells were seeded into 12 well plates and transfected with different concentrations of plasmid DNA, carrying the GR mutants and pBpa synthetase. Both constructs were tested and validated in a Western blot analysis shown in Figure 38.

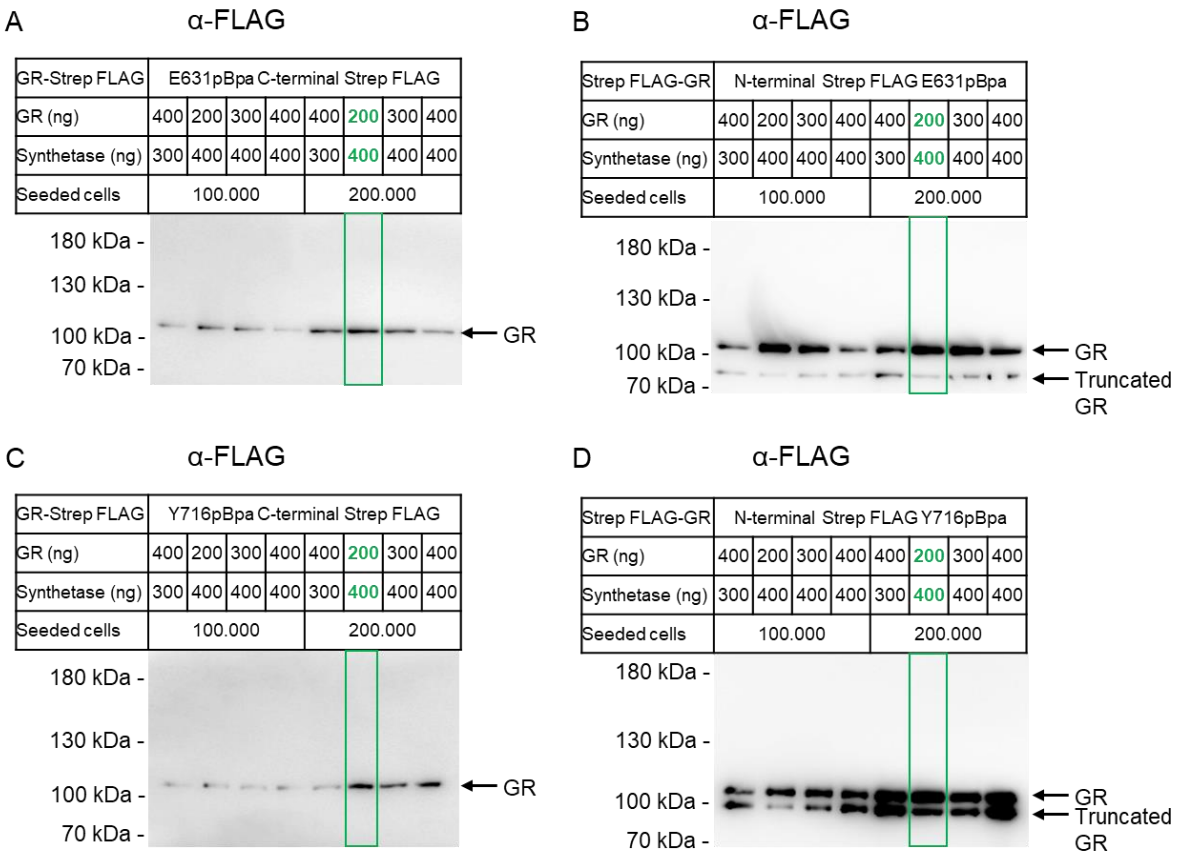

Figure 38: Method optimization for amber suppression of full-length GR. A + C, Western blot of selected full-length C-terminal Strep FLAG tagged GR pBpa mutants expressed in HEK293 cells in 12 well plates. B + D, Western blot of selected full-length N-terminal Strep FLAG tagged GR pBpa mutants expressed in HEK293 cells in 12 well plates. DNA amount is given for a transfection mix for one well on a 12 well plate. The best condition is highlighted in green.

All samples show a band with the expected molecular weight of 110 kDa. In addition, samples of the N-terminal version produced a weaker band <110 kDa. This band represents a truncated version of the protein, that is not amber suppressed. This leads to the detection of incompletely expressed proteins, which carries no unnatural amino acid. The N-terminal tagged version produced stronger bands than the C-terminal version and samples with 200,000 seeded cells a stronger band than samples with 100,000 cells. The strongest bands were seen for two conditions: GR: 200 ng, pBpa synthetase: 400 ng, and GR: 300 ng, pBpa: 400 ng, yet GR:200 ng, Syn:400 ng appeared to produce the lowest level of the truncated version. This condition was chosen for further experiments.

Next, the whole full-length GR library was screened for FKBP51 crosslinks. This is exemplary shown in Figure 39 for GR mutants in the N-terminal domain and in the GR^{LBD}, with both the HA signal ratio of UV-irradiated sample and untreated sample for the crosslinking detection and the FLAG signal for amber suppression control.

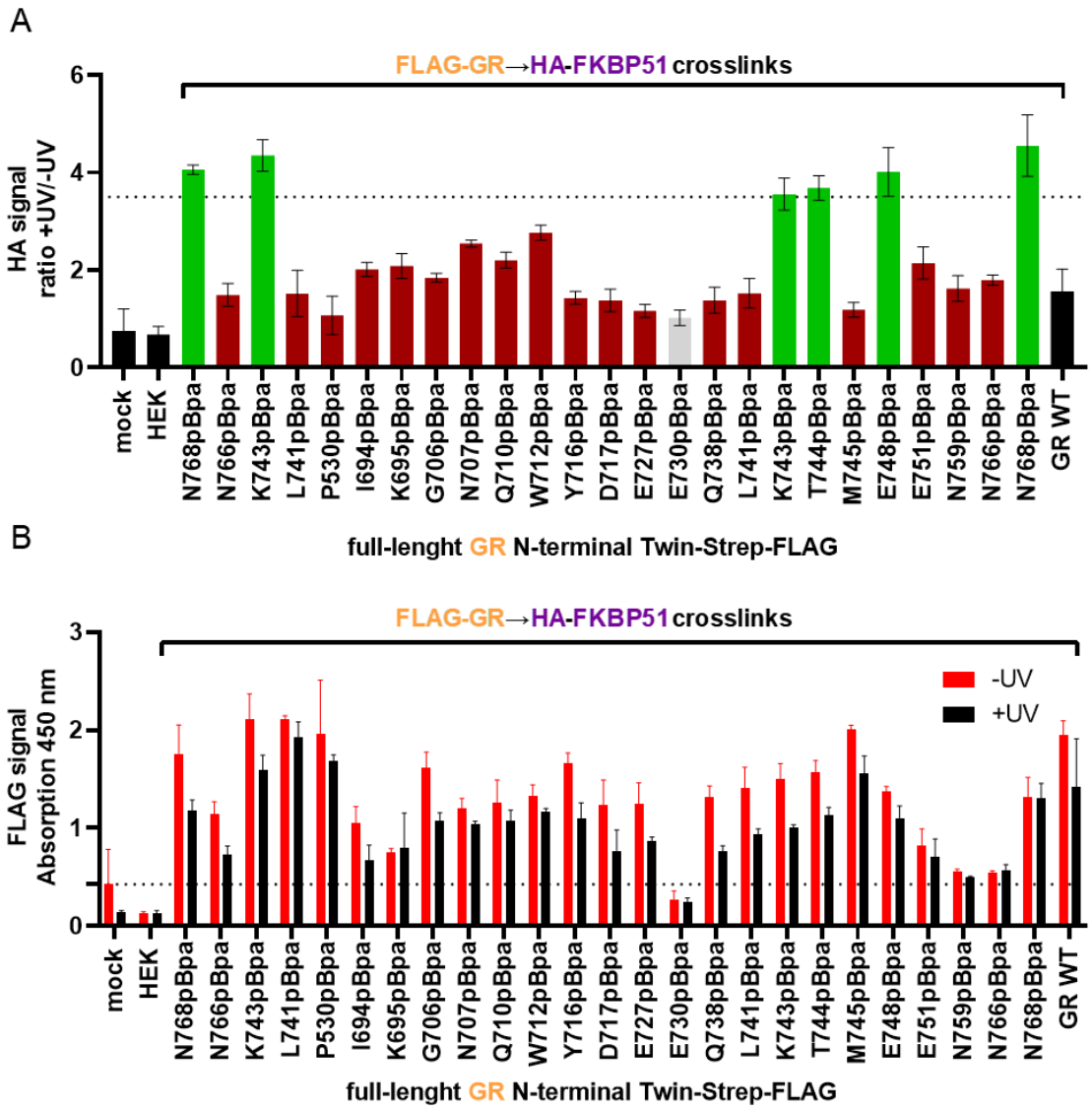

Figure 39: Large scale GR→FKBP51 crosslinking screening by ELISA. A, ELISA data for selected full-length N-terminal Twin-Strep-FLAG GR pBpa mutants expressed and photocrosslinked in HEK293 cells co-overexpressing HA-tagged FKBP51. Irradiated cells and matched non-irradiated control cells are lysed, lysates are absorbed to Streptactin-coated 96 well plates, washed, and coated with HRP-coupled anti-HA antibodies to detect GR→FKBP51 crosslinks. The depicted values represent signal ratios of irradiated vs non-irradiated samples. HA ratios >3.5 are indicative of the mutated position being in proximity to FKBP51. Crosslinks detected by ELISA are highlighted in green and positions below the threshold are shown in red (A). Mock, non- or $GR^{wildtype}$-transfected HEK293 cells were included as background controls (black bars). An aliquot of each lysate was absorbed to separate Streptactin-coated 96 well plates, washed, and coated with HRP-coupled anti-FLAG antibodies to control for adequate GR expression levels (B). Grey sample (A) indicated amber suppression ratio signal/WT <25% (B), which were excluded from further analyses. Each bar represents data from biological replicates ($n=3$). For more mutants see **Extended Figure 6**.

In the example ELISA shown, six mutants display a HA signal ratio higher than 3.5 and are counted as potential GR→FKBP51 crosslinks. In fact, several FKBP51-reactive crosslinks were identified in the GR^{LBD}, while none of the tested position in the N-terminal parts reached a HA signal ration higher than 3.5, confirming the GR^{LBD} as the relevant interaction domain for FKBP51 in cells. Within the GR^{LBD}, one interaction hotspot centered around helix α12 (e.g., K743, T744, E755, and N768), which is important for ligand and coactivator and therefore GR activation. The detected GR→FKBP51 crosslinks were further confirmed by Western blot analysis shown in Figure 40.

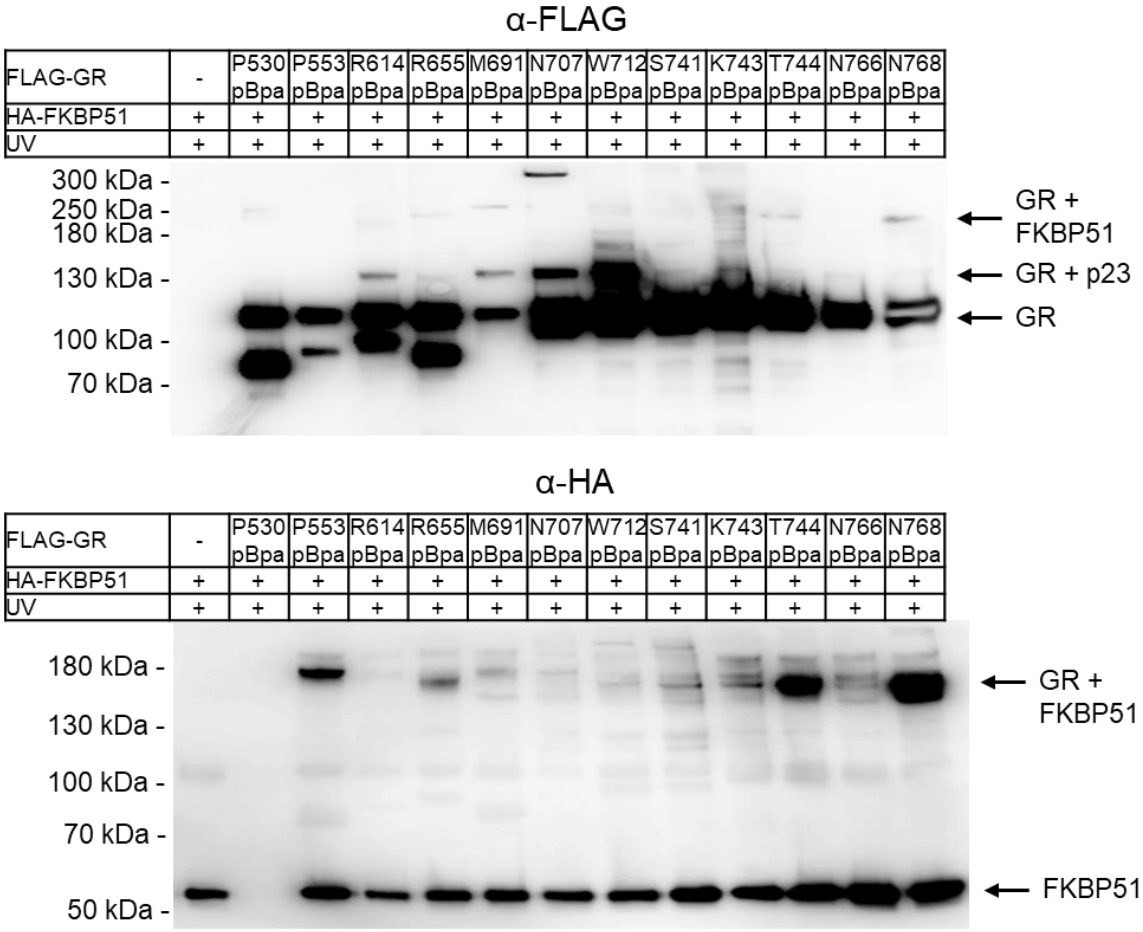

Figure 40: Large scale photocrosslinking of the full-length GR in mammalian cells confirms the interaction of the GR ligand binding domain and cochaperones FKBP51
Western blots of exemplary full-length GR pBpa mutants expressed and photocrosslinked in HEK293 cells co-overexpressing HA-tagged FKBP51. UV light-induced HA-reactive bands at a size of ~180 kDa are indicative of the mutated position being in proximity to FKBP51.

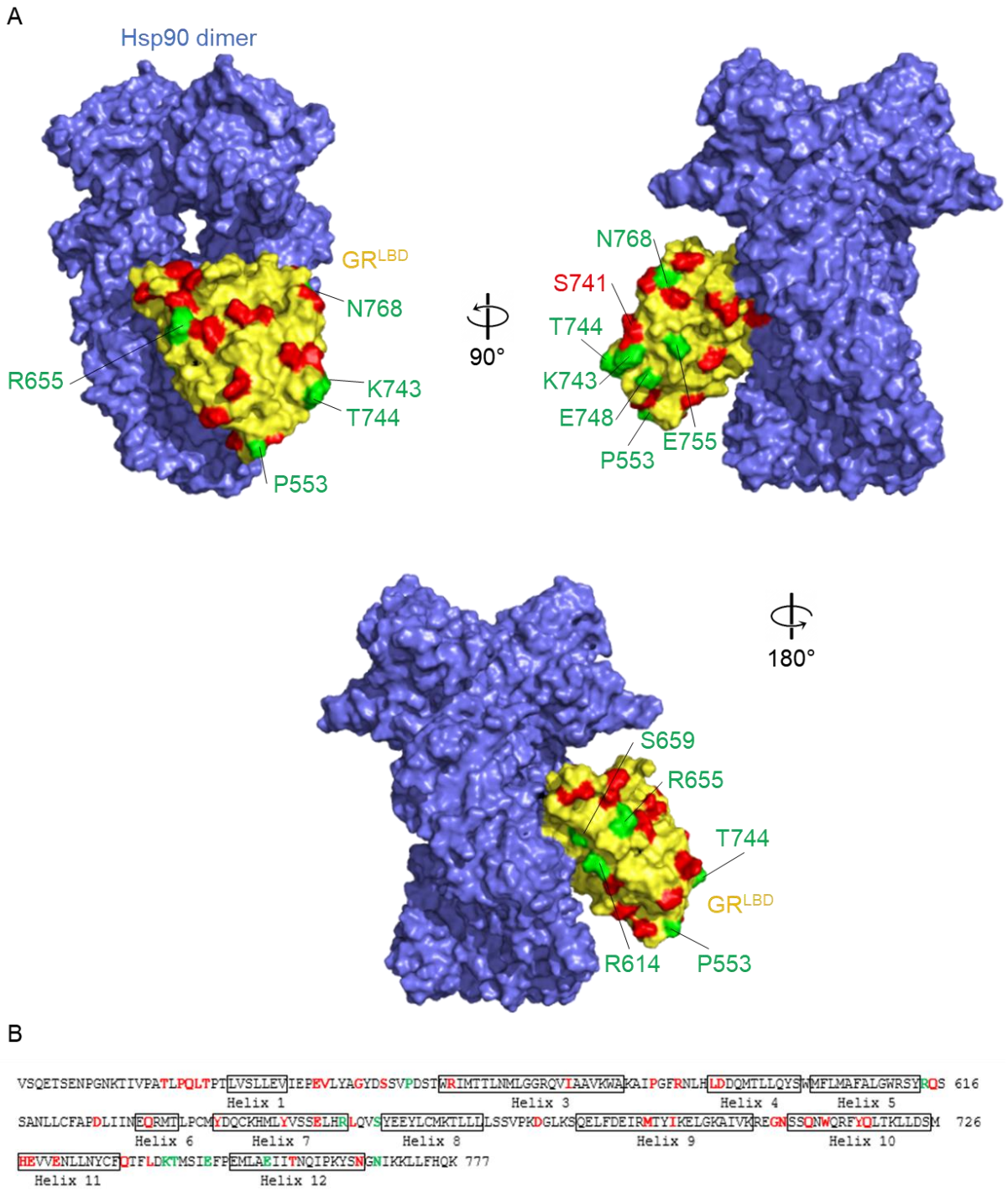

Figure 41: Large scale photocrosslinking of the full-length GR in mammalian cells confirms the interaction of the GR ligand binding domain and cochaperones FKBP51. A, GR→FKBP51 crosslinks were mapped on the structure of the Hsp90-GR complex (PDB: 7KRJ, p23 omitted for clarity) with crosslinks highlighted in green and inactive position indicated in red. B, Crosslinks or inactive positions are mapped to the sequence of GR^{LBD} (523–777), with indication of secondary structure.

Mapping the crosslinks on the structure of the GR^{LBD}-Hsp90 complex (Noddings et al., 2022) revealed another crosslinking hotspot on the other side of the GR^{LBD} (e.g., R614, R655, and S659), which are located at the tip of helix α5 and in the α7-α8 loop (see Figure 42). A broad overlay of FKBP51 in the Hsp90 client-bound complex envisions the putative ternary complex.

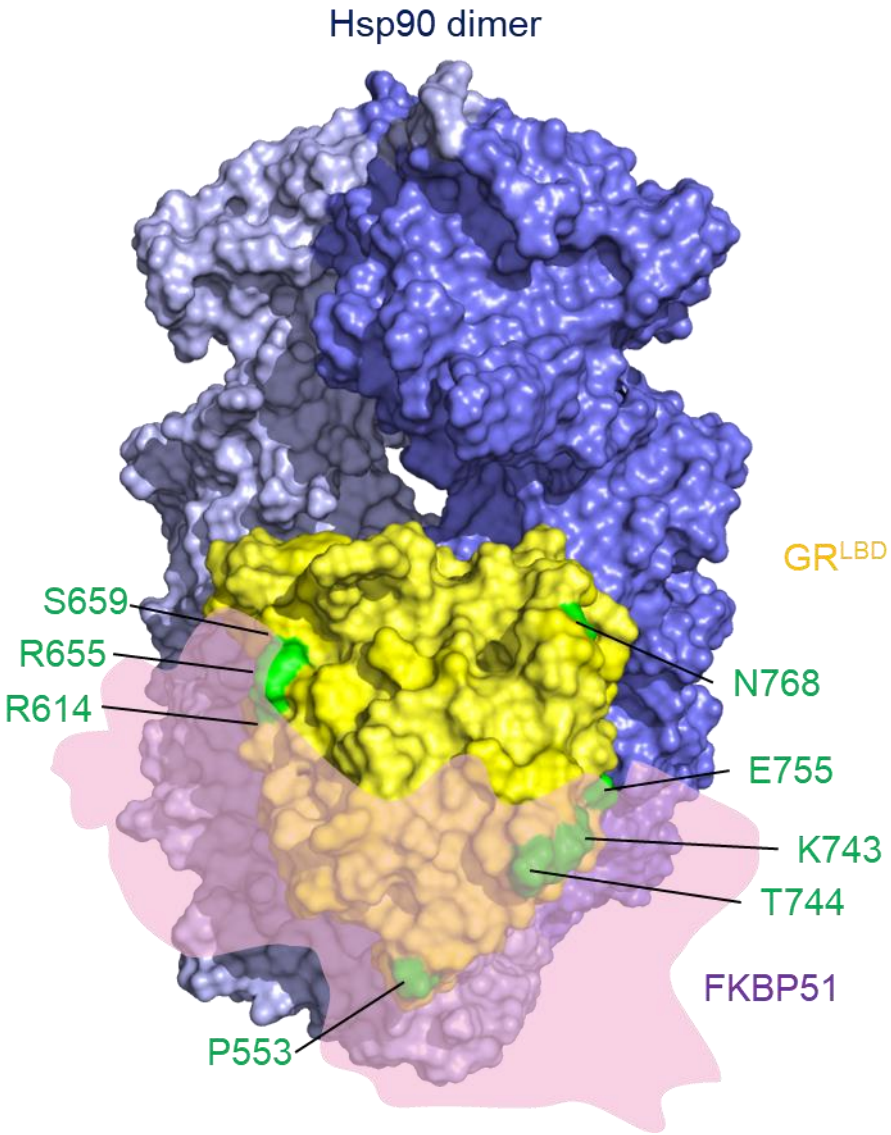

Figure 42: Structure of the Hsp90/FKBP51/GR complex. GR→FKBP51 crosslinks were mapped on the structure of the Hsp90-GR complex (PDB: 7KRJ, p23 omitted for clarity) with crosslinks highlighted in green. The broad position of Hsp90-bound FKBP51, estimated from PDB-ID: 7L7I, is indicated as a transparent light pink shape.

The full set of GR→FKBP51 crosslinks reveals a complex, where FKBP51 wraps around the GR^{LBD}, specifically from helix α12 around helix α3 and the α1-α3 loop to reach the tip of helix α5 and the α7-α8 loop. These findings, especially for N768 as the strongest GR→FKBP51 crosslink observed, require the GR^{LBD} to rearrange compared to the orientation observed in the

structure of the Hsp90-GR complex. Potentially, the GR^{LBD} has to rotate clockwise (viewed from Figure 42) to satisfy all crosslinks observed. The $FKBP51^{FK1}$ and $FKBP51^{FK2}$ domain have to undergo slight rearrangements to closely fit into the ternary complex. The suggested orientation of the $FKBP51^{FK1}$ interactions with the tip of helix α5 and in the α7-α8 loop of the GR^{LBD} was confirmed by pharmacological studies using $FKBP51^{FK1}$ ligand. This is discussed in detail in 3.3.2.

Also, the suggested orientation is remarkable consistent with a cryoEM structure of the Hsp90-FKBP51 complex with the dexamethasone-bound GR recently obtained by the Agard group after *in-vitro* reconstitution of the complex from purified protein (Noddings et al., 2023). The structure shows intensive contacts of all three FKBP domains with GR^{LBD} and the rotation of GR^{LBD} compared to the p23-Hsp90-GR^{LBD} complex (Noddings et al., 2022).

Additionally, a recent cryoEM structure of the Hsp90-AhR-p23 complex with bound XAP2 gives insight into a structurally related ternary complex (see Figure 43) (Gruszczyk et al., 2022; Wen et al., 2023). The Aryl hydrocarbon receptor (AhR) is a ligand-activated transcription factor (Gasiewicz et al., 2014), similar to the GR. As another Hsp90 client protein, AhR may also be remodeled and mature through the chaperone cycle of Hsp90. In the absence of ligand, AhR forms a multiprotein complex in the cytosol, including chaperone Hsp90, cochaperone p23, and the AhR interacting protein XAP2 (Meyer & Perdew, 1999). XAP2 is a TPR domain-containing protein and has one FKBP-like activity domain (Meyer & Perdew, 1999). Therefore, XAP2 can be viewed as a structurally related, truncated version of FKBP51 missing one FK domain. After ligand binding, AhR is conformationally changed to expose the N-terminal nuclear localization signal (NLS), triggering translocation into the nucleus.

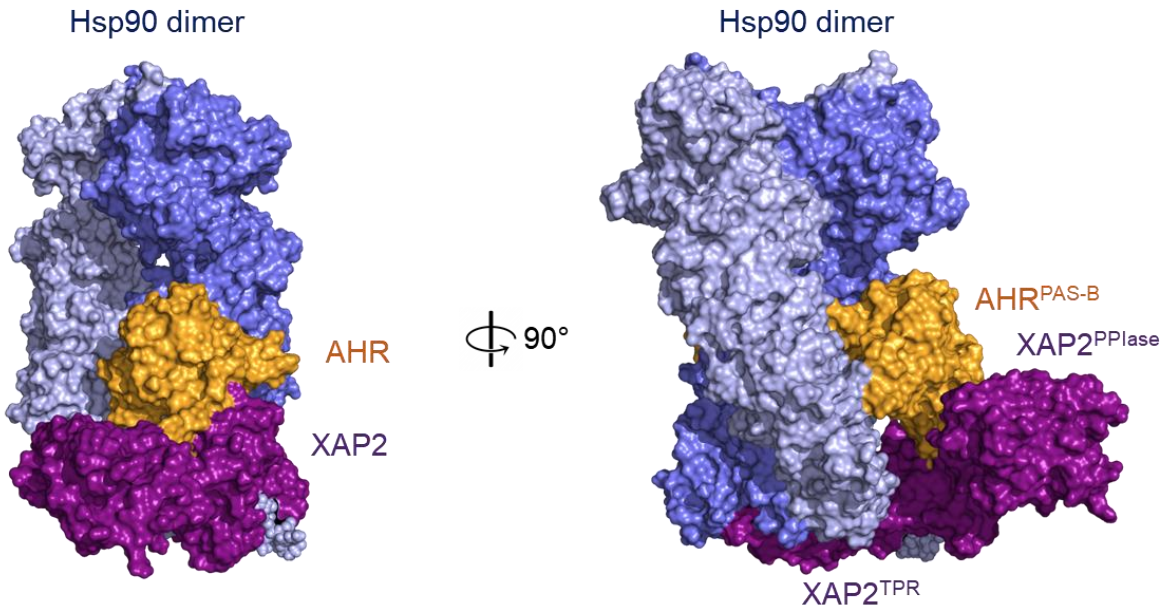

Figure 43: Structure of the Hsp90-AHR-XAP2 complex to envision Hsp90-GR-FKBP51 complex. Hsp90 dimer (light blue and blue), the AHR (orange), and XAP2 (deep purple) from PDB: 7ZUB.

The structure of the Hsp90-AHR-XAP2 can be used to at least partially envision the binding of FKBP51 to the Hsp90-bound GR, with the FKBP51^{FK2} binding around the GR. Wen *et al.* report that XAP2 seems to be highly dynamic with a local resolution of 5 Å in the C-terminus or even lower at its N-terminal FKBP-like domain (Wen et al., 2023). As strong GR→FKBP51 crosslinks in the tip of helix α5 and the α7-α8 loop and FKBP51→GR crosslink in the FKBP51^{FK1} were observed, FKBP51^{FK1} seems to add another layer of contacts to the Hsp90-GR-FKBP51 interaction, not possible for the Hsp90-AHR-XAP2 complex.

Interestingly, Wen *et al.* show the Hsp90-AHR-XAP2-p23 structure with two p23 molecules bound to the Hsp90 N-terminal domain, with p23 having no preferred occupation on one side of the Hsp90 dimer. Further, they observe no direct interaction of p23 to the AHR, while the recent Hsp90-GR-p23 complex proves a direct interaction of GR and p23 (Noddings et al., 2022). This leads to the speculation, that some clients like the GR dictated the orientation of p23 by a large interaction interface, while for others the Hsp90-p23 interaction is more dynamic.

3.2.3. Exploration of GR-p23 contacts

With the GR single point mutant library in hand, crosslinks of GR with the Hsp90 cochaperone p23, known to be essential for GR maturation, were also explored (Biebl & Buchner, 2019).

Western blot analysis revealed GR→p23 crosslinks based on the molecular weight and were confirmed by a p23-specific antibody. The crosslinks were mapped on the Hsp90-GR^{LBD}-p23 complex for better visualization in Figure 44.

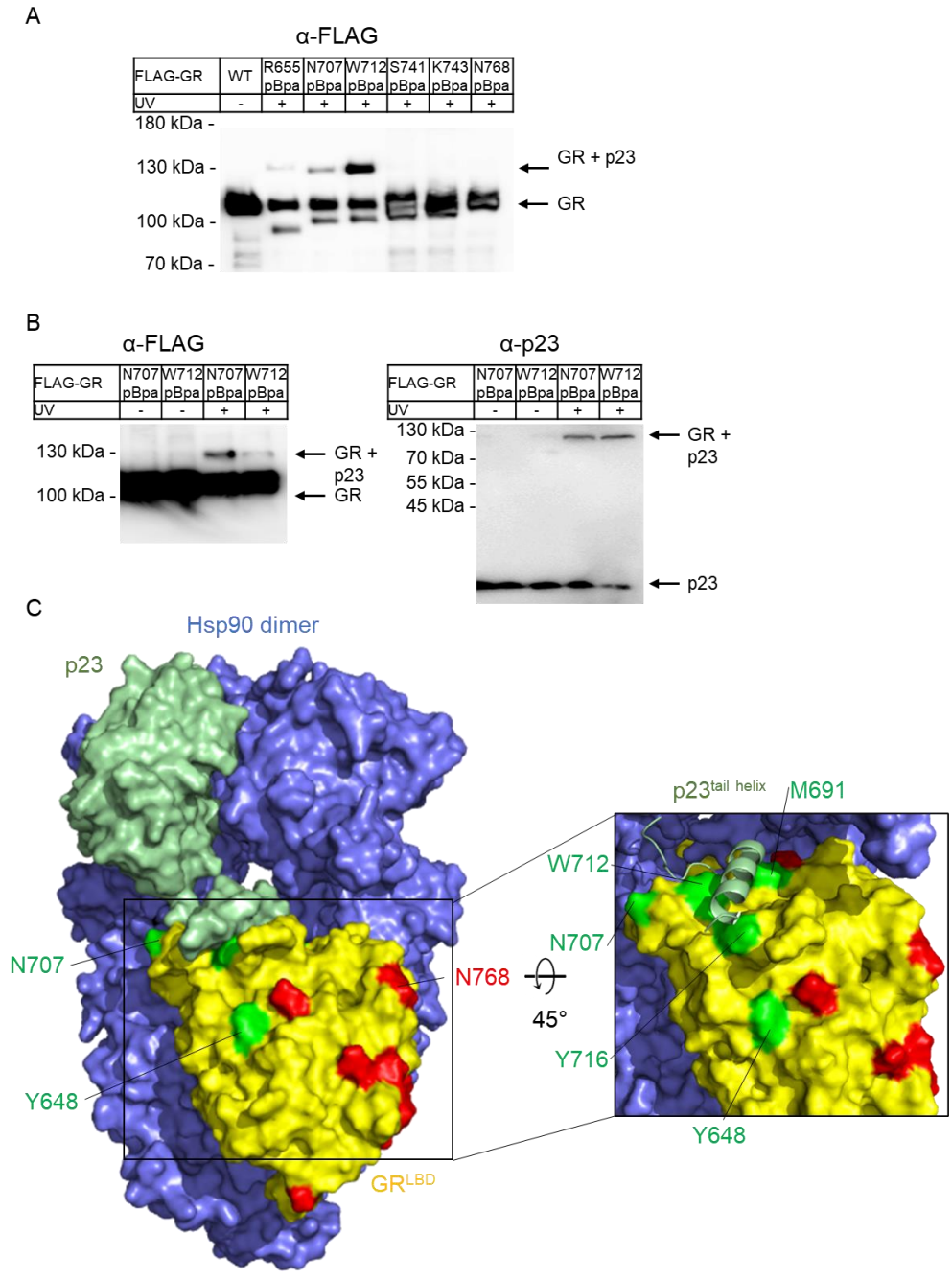

Figure 44: Photocrosslinking of the full-length GR in mammalian cells confirms the interaction of the GR ligand binding domain and Hsp90 cochaperone p23. A + B, Western blots of exemplary full-length GR pBpa mutants expressed and photocrosslinked in HEK293 cells. UV light-induced FLAG-reactive bands and p23-reactive bands at a size of 130 kDa are indicative of the mutated position being in proximity to p23. C, GR→p23 crosslinks were mapped on the structure of the Hsp90-GR-p23 complex (PDB: 7KRJ) with crosslinks highlighted in green and inactive position indicated in red. In the close-up view the p23tail helix (p23 120–130) is shown as cartoon.

Numerous GR→p23 crosslinks were observed that clustered on the GR e.g., at positions Y648, R655, M691, I694, N707, W712, and Y716. This pattern fits remarkably well to a recent cryoEM structure of the p23-Hsp90-GR^{LBD} complex (Noddings et al., 2022). Some GR→FKBP51 crosslinks (R614, R655 and S659) are suspiciously close or even identical to GR→p23 interaction sites. This suggests that FKBP51 may compensate for some of the GR-p23 contacts lost due to the GR rearrangement postulated above. The detection of GR→p23 crosslinks again raises the question whether the detected interaction occurs in a FKBP51-bound complex or possibly even in a Hsp90-independent manner. This cannot be easily answered, using the so far presented experiments. One potential approach is the combination of photocrosslinking behavior to pharmacological intervention, thereby forcing a certain protein into a distinct state by an agonist/antagonist or by interfering with interaction using protein inhibitors.

To summarize, a mutant library of the full-length GR was created in a high-throughput manner using an optimized Golden Gate mutagenesis protocol in a 96 well format. The GR library was amber suppressed to investigate the full-length GR-FKBP51 interaction in a quasi-natural environment, in mammalian cells at single residues resolution. The cumbersome crosslinking analysis by Western blot was supplemented by a self-developed ELISA for a fast and reliable investigation of the interaction interface. The ELISA in combination with Western blot analysis revealed the direct interaction between the GR^{LBD} and FKBP51. This proved, for the first time, the long speculated, direct interaction of the GR^{LBD} and FKBP51. The crosslink analysis allowed to suggest a model where the $FKBP51^{FK1}$ and $FKBP51^{FK2}$ wrap around the GR^{LBD}. Potentially, the GR^{LBD} has to undergo a slight rotation to accommodate FKBP51 binding. Further, GR→p23 crosslinks were observed, that allowed a study of the interaction interface. Together, selected GR→FKBP51 and GR→p23 crosslinks can be further used as proximity senor to investigate the interactions in greater detail.

3.3. Chapter 3: Pharmacological studies reveals the architecture of the FKBP51-Hsp90-apoGR complex

In the third chapter, the results of pharmacological interventions on the Hsp90-FKBP51-(GR) complex were monitored by photocrosslinking. The combination of ligand treatment and photocrosslinking was established using FKBP51 and rapamycin, a system independent of the GR maturation. Hsp90 inhibitor treatment confirmed the Hsp90-dependent interaction of FKBP51 and GR. Moreover, the tested FKBP51 E75pBpa→GR crosslink was interrupted by the FKBP51 inhibitor SAFit2, however not all GR→FKBP51 crosslinks were diminished after treatment. GR activation by the synthetic agonist dexamethasone disrupts GR→FKBP51, GR→p23, and GR→Hsp90 crosslinks. This demonstrated the observed interactions were predominantly formed by a ligand-unbound apoGR. Furthermore, the combination of ELISA and pharmacological studies allows dexamethasone titration to determine different stimulation thresholds for GR-complex with either FKBP51 and FKBP52.

3.3.1. FKBP51 and rapamycin

A unique advantage of amber suppression is the analysis in a quasi-natural environment. Crosslinking in combination with pharmacological intervention leads to the possibility to derive a dynamic and accurate model of molecular processes in living cells. Therefore, crosslinking behavior of FKBP51 was observed after treatment with the immunosuppressive drugs FK506 or rapamycin. Both are structurally related and are common ligands for FKBP-domain containing proteins. They do not bind exclusively to FKBP12 but rather bind with high affinity to most members of the FKBP family, including FKBP51^{FK1}, resulting in the inhibition of their peptidyl-prolyl cis-trans isomerase activity (Kozany et al., 2009). FK506 and rapamycin induce the non-physiological interaction with calcineurin or serine-threonine protein kinase mammalian target of rapamycin (mTOR), respectively (Van Duyne et al., 1991a; Van Duyne et al., 1991b). The association is mediated by a molecular glue mechanism by which FKBPs first bind rapamycin and only thereby forming a interaction interface for mTOR^{FRB} (Geiger et al., 2022). The crosslinking behavior of selected FKBP51 mutants was tested after ligand treatment by Western blot analysis (see Figure 45). The selected mutants are all situated around the ligand binding site of FKBP51. This work was supported by Monika Gnatzy and Karola Bahrami.

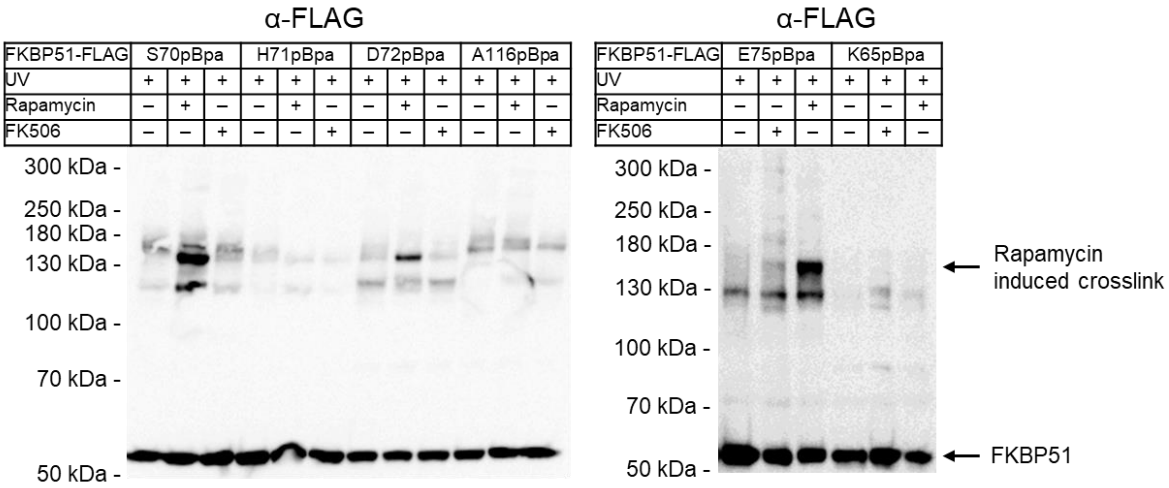

Figure 45: Rapamycin induced FKBP51 crosslink. Western blots of FKBP51 pBpa mutants expressed and photocrosslinked in HEK293 cells after 1 h treatment with 1 μM rapamycin or FK506.

For at least 3 mutants, FKBP51 S70pBpa, FKBP51 D72pBpa, and FKBP51 E75pBpa a rapamycin induced crosslink at a molecular weight of ~160 kDa was detected. No FK506 induced crosslinks were observed for the investigated FKBP51 mutants. A more detailed analysis of the interaction time frame was conducted and evaluated the influence on different rapamycin treatment times on the induction of crosslinks.

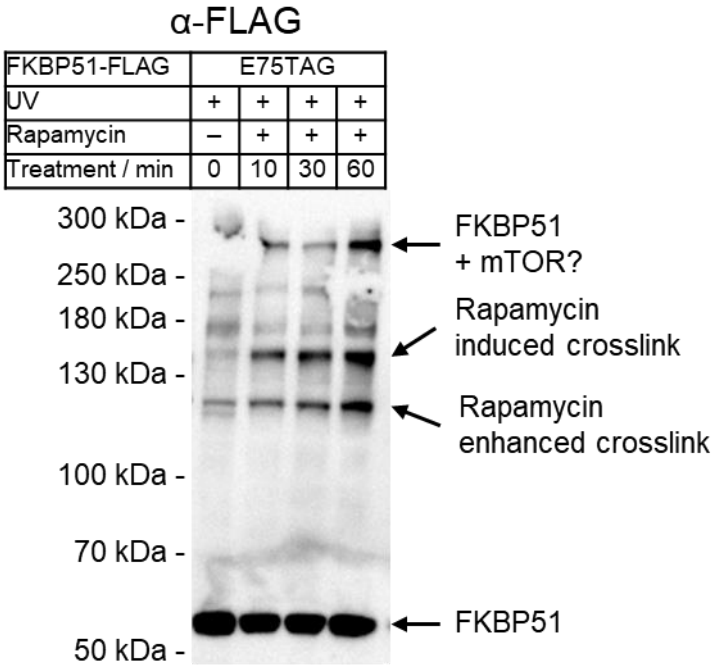

Figure 46: Rapamycin induced FKBP51 crosslinks are fast occurring. Western blots of FKBP51 E75pBpa mutant expressed and photocrosslinked in HEK293 cells after different treatment times with 1 μM rapamycin.

The Western blot shows that a treatment time of 10 min is sufficient to induce a rapamycin dependent change in crosslinking behavior, yet it seems that the crosslinks are stronger in the longer treated sample. Moreover, the higher resolution of the Western blot in comparison to Figure 45 reveals that the crosslinks are potentially not induced by rapamycin treatment, but rather rapamycin only enhances previously existing crosslinks for this FKBP51 mutant. This is a limitation of the Western blot analysis that does not allow a differentiation of occurring bands at the same molecular weight. It is speculated that the binding to a ligand limits the flexibility of FKBP51^{FK1} thereby enhancing crosslinking yields. This was not investigated further. Potentially, a rapamycin induced band is visible above 250 kDa, that could correspond to a FKBP51-rapamycin-mTOR complex. Nevertheless, the intracellular concentration of mTOR might be not high enough for a detection or the majority of mTOR was bound to a FKBP12-rapamycin complex that is not detected.

In a next step, the ability of rapamycin to act as a molecular glue to recruit the FKBP protein-rapamycin binding (FRB) domain, of mTOR to FKBP51 was further investigated by specific overexpression of mTOR^{FRB}. This will greatly enhance detection. Therefore, FKBP51 S70pBpa and FKBP51 E75pBpa were amber suppressed in the presence of mTOR^{FRB}. Both mutants showed a rapamycin induced change in crosslinking behavior. This FKBP51-rapamycin-mTOR^{FRB} crosslink was tested for different FRB concentration and analyzed by Western blot.

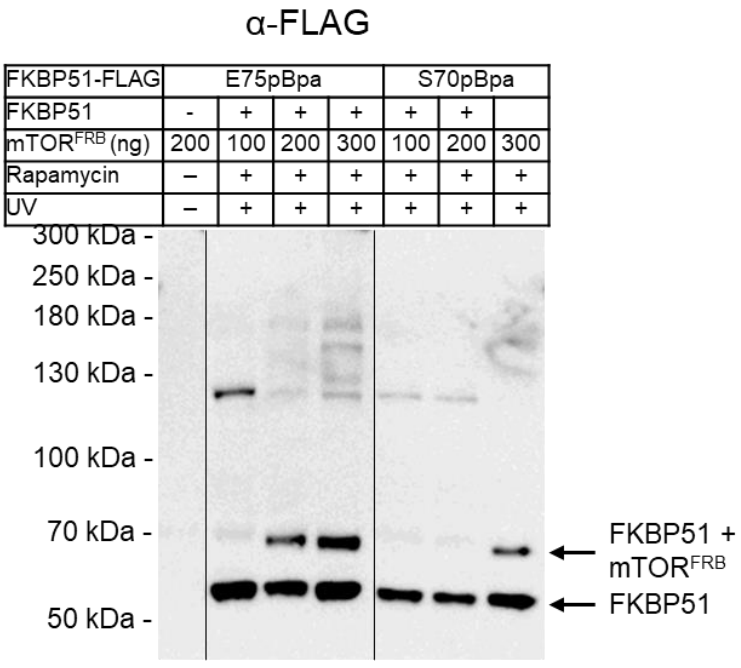

Figure 47: Rapamycin triggers association of mTOR^{FRB} to FKBP51. Western blots of FKBP51 E75pBpa and FKBP51 S70pBpa mutant expressed and photocrosslinked in HEK293 cells after treatment with 1 μM rapamycin for 1 h. Transfection conditions were tested in a 12 well format with different concentration of plasmid DNA of mTOR^{FRB}. The black line indicates different parts of the same Western blot were combined.

The Western blot analysis shows a mTOR^{FRB} concentration dependent appearance of a band at ~70 kDa in the presents of rapamycin. For both mutants, a band that corresponds to a FKBP51-rapamycin-mTOR^{FRB} crosslink is visible for the highest tested plasmid DNA concentration of mTOR^{FRB}. Interestingly, the FKBP51-rapamycin→mTOR^{FRB} clearly competes with a rapamycin induced crosslink at ~130 kDa. Both crosslinks were mapped on the structure of the FKBP51^{FK1}-rapamycin-mTOR^{FRB} complex for visualization.

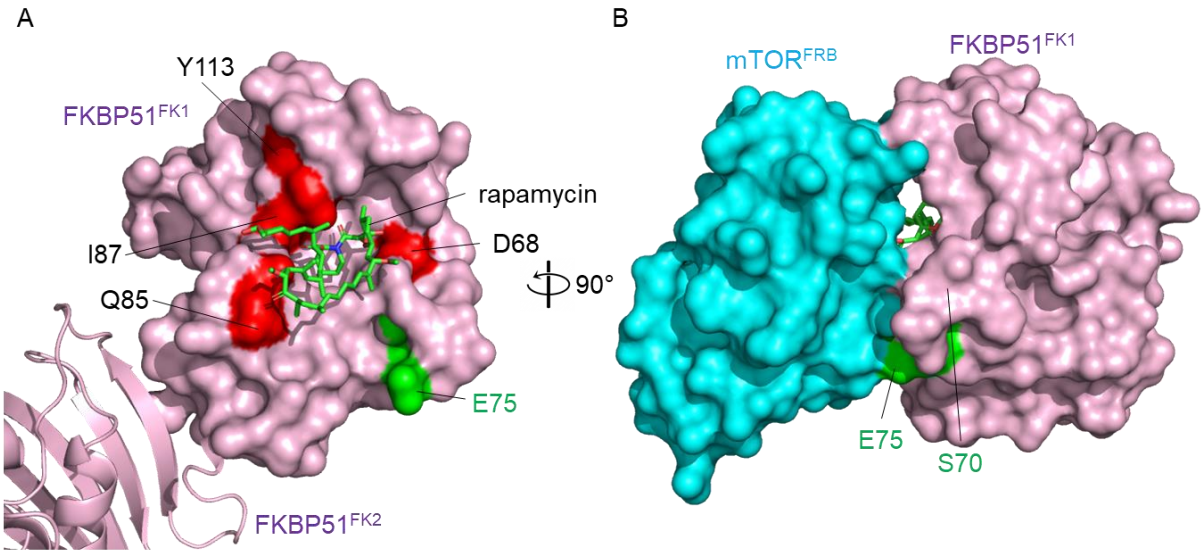

Figure 48: Structure of FKBP51^{FK1}-rapamycin and FKBP51^{FK1}-rapamycin→mTOR^{FRB}. A, FKBP51^{FK1} bound to rapamycin (PDB: 4DRI) highlighted in light pink with crosslinks highlighted in green and residues important for ligand binding highlighted in black. For orientation FKBP51^{FK2} (PBD: 5OMP) was superimposed. B, FKBP51^{FK1} bound to rapamycin (PDB: 4DRI) highlighted in light pink with crosslinks highlighted in green and mTOR^{FRB} highlighted in cyan.

The molecular glue mechanism of rapamycin can be monitored by photocrosslinking, with mutants that incorporate pBpa at a position in the vicinity of the binding pocket of FKBP51^{FK1}. This could serve as a potential chemical tool to investigate novel molecular glues and targets thereof.

Recently, a similar approach was presented in a proof-of-concept study using a photocrosslinker rapamycin analog termed photo-rapamycin for photoaffinity labeling *in vitro* (Flaxman et al., 2019). In combination with mass spectrometry, they created a binding site hotspot map of the ternary complex FKBP12-photo-rapamycin-mTOR^{FRB}. Flaxman *et al.* used distance constraint between the conjugated residues and the photoreactive moiety for molecular modeling and proposed a flexibility of the cyclohexyl ring of rapamycin in solution resulting in two distinct conformation the FKBP12-photo-rapamycin-mTOR^{FRB} (Flaxman et al., 2019).

The combination of ligand treatment and photocrosslinking, to stimulate a distinct behavior of proteins and to create an intracellular snapshot, was further applied to the FKBP51-GR interaction.

3.3.2. The FKBP51 inhibitor SAFit2 reveals a multi-layered interaction of GR and FKBP51

The molecular basis for the differential effects of FKBP51 and FKBP52 on GR is still unknown. Several studies pointed towards a key role of the FK1 domains (Riggs et al., 2003, 2007; Wochnik et al., 2005), in particular for the proline-rich loop around L/P119 overhanging the FK506-binding site (Riggs et al., 2007). However, studies on the role of the FK506-binding site itself have remained controversial (Smith & Toft, 2008). To investigate the role of the FK506-binding site for FKBP-Hsp90-GR complex assembly, FKBP51 E75pBpa, a representative GR-photoreactive position in FKBP51 was tested for sensitivity towards the FKBP51 ligand SAFit2 (Gaali et al., 2015).

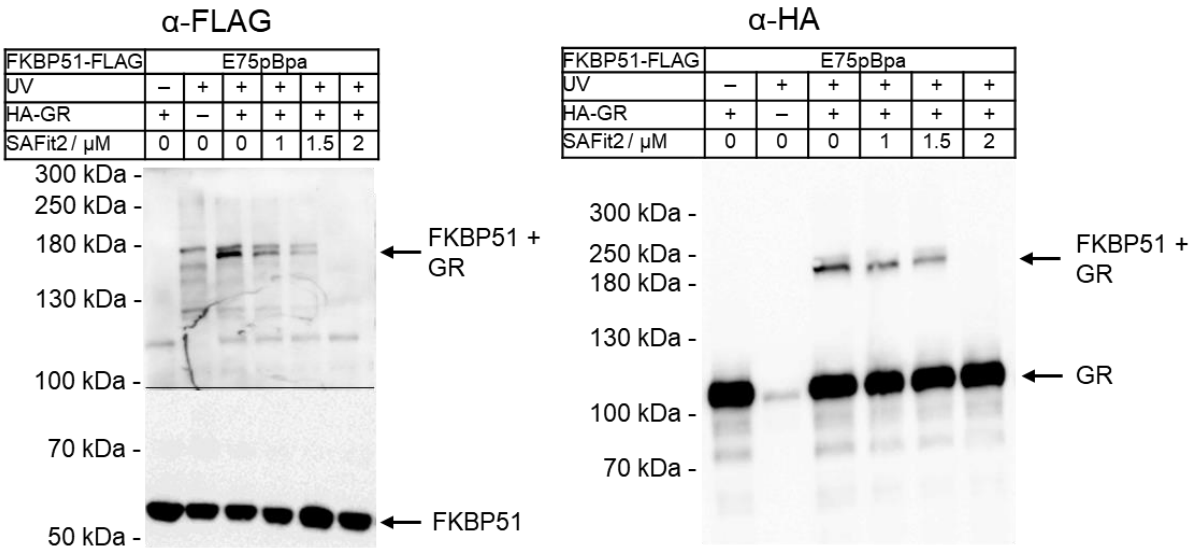

Figure 49: FKBP51 inhibitor disrupts FKBP51→GR crosslink. SAFit2 treatment for 1 h before UV-irradiation and cell lysis shows a dose-dependent disruption of FKBP51 E75pBpa→GR crosslink. The black line indicates different parts of the same Western blot were combined.

The Western blot analysis shows that the FKBP51 E75pBpa-GR crosslink was blunted after SAFit2 treatment in a dose-dependent manner. Further positions were tested for SAFit2 sensitivity by Sarah Engel. For numerous positions in FKBP51^{FK1}, this revealed a disruption of FKBP51→GR upon SAFit2 treatment. Strikingly, however, none of the investigated positions in the FK2 or TPR domains of FKBP51 were affected (all tested by Sarah Engel). Importantly,

SAFit2 disrupted crosslinks in FKBP51^{FK1} at concentrations consistent with their potency to occupy intracellular FKBP51 (Gnatzy et al., 2021). This identifies the FK2 and TPR domains as the major drivers for the assembly of FKBP51-Hsp90-GR complexes in cells, while many of the FK1 contacts are dispensable.

In the next logical step, representative FKBP51-photoreactive positions in GR were probed for SAFit2 sensitivity. This included positions in both identified GR^{LBD} interaction hotspots, which were tested and analyzed (see Figure 50).

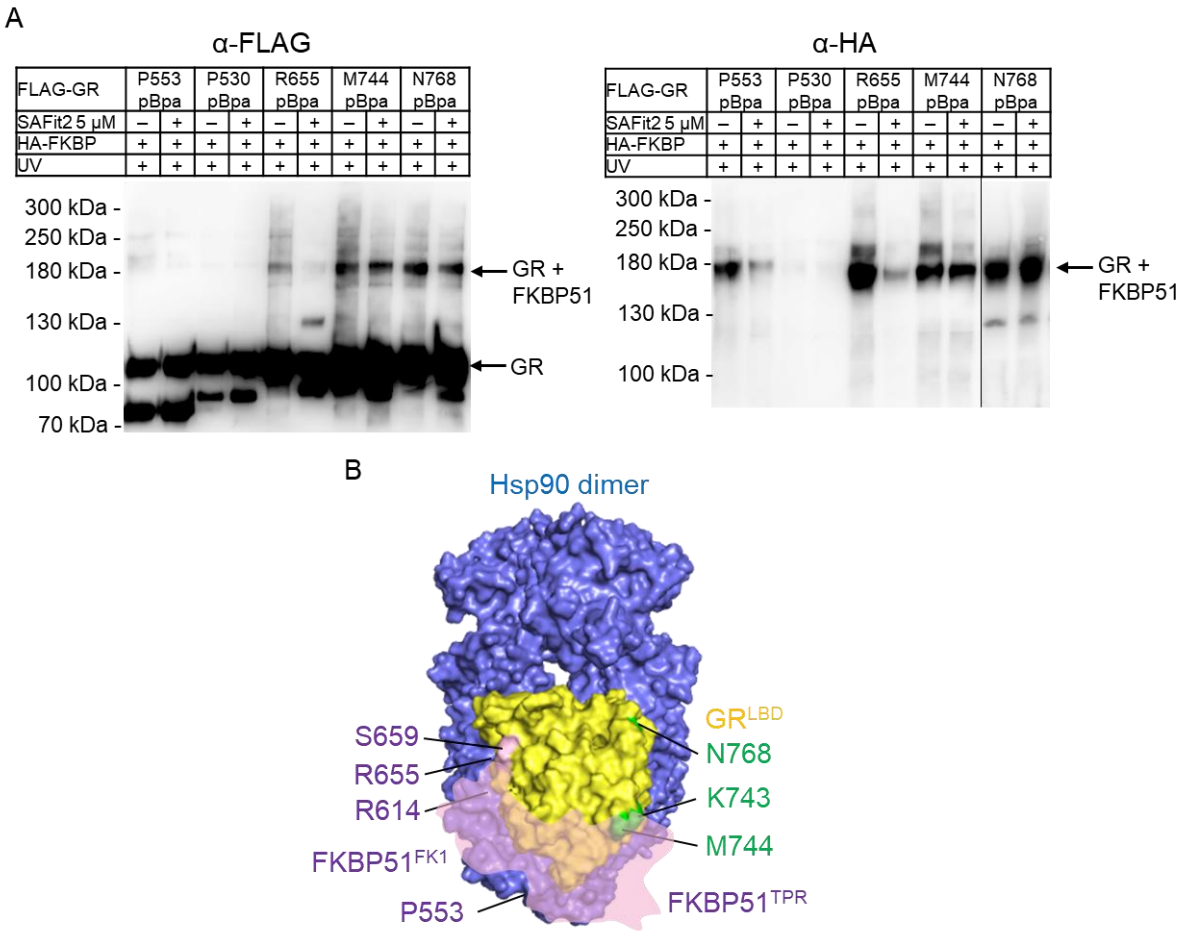

Figure 50: Inhibition of FKBP51 only partially disrupts GR-FKBP51 interactions. SAFit2-sensitivity or resistance of exemplary GR pBpa mutants, detected by Western blots after expression and photocrosslinked in HEK293 cells with co-overexpressing HA-tagged FKBP51. B, GR→FKBP51 crosslinks tested for SAFit2 sensitivity were mapped to the structure of the GR-Hsp90 complex (PDB: 7KRJ, p23 omitted for clarity). SAFit2-sensitive GR→FKBP51 crosslinks are shown in pink, SAFit2-insensitive GR→FKBP51 crosslinks (i.e., persisting in the presence of SAFit2) are shown in green. The black line indicates the same sample was applied on a different Western blot.

The Western blot analysis shows GR positions clustering around R614, R655 and S659 were found to be SAFit2-sensitive as well as P553, which is situated in the α1-α3 loop. Crosslinks clustered around helix α12 were not affected (e.g., M744 and N768). Together with the ligand sensitivity findings for FKBP51, this suggests that residues around GR helix α12 form an interface with the FK2 and/or TPR domain of FKBP51, while the region around the tip of α5 and the α7-α8 loop of GR contact FKBP51^{FK1}. This is consistent with the potential rotation postulated for GR above.

3.3.3. FKBP51 and p23 interact with apoGR in a Hsp90-dependent manner

To further define the functional characteristics of the FKBP51- and p23-GR-Hsp90 complexes in cells, a selected set of crosslinking positions was used as intracellular proximity sensors. First, FKBP51→GR crosslinks were investigated for Hsp90 dependency by treatment with the Hsp90 inhibitor Geldanamycin (Czar et al., 1997). Geldanamycin inhibits the inherent ATPase activity of Hsp90, which is essential for its function, leading to a collapse of Hsp90 complexes (Roe et al., 1999).

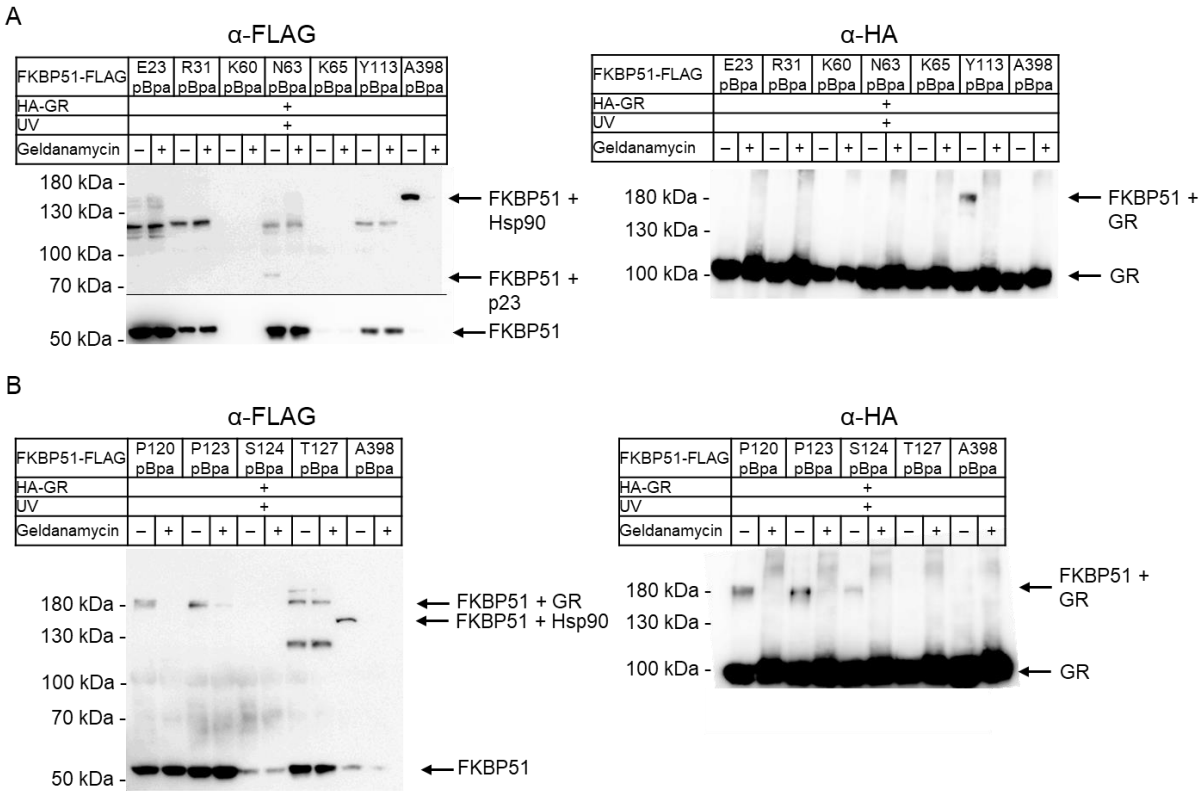

Figure 51: FKBP51-GR interaction is Hsp90-dependent. A + B, Hsp90 inhibitor (Geldanamycin) treatment (5 μM, 1 h) disrupts FKBP51→GR, FKBP51→p23, and FKBP51→Hsp90 crosslinks, suggesting a Hsp90-dependent interaction. Black line indicates a different exposure time of the same Western blot.

The Western blot analysis shows the abrogation of FKBP51→GR in all cases e.g., FKBP51 Y113pBpa, P120pBpa, P123pBpa and S124pBpa, strongly indicating that the observed intracellular FKBP51-Hsp90-GR complex is depended on a functional Hsp90 machinery. The dominant FKBP51 A398pBpa→Hsp90 crosslink is completely disrupted upon treatment with a Hsp90-inhibitor, thereby further validating the suitability of photocrosslinking in combination with pharmacological intervention. Also, the FKBP51 N63pBpa→p23 crosslink is sensitive to geldanamycin treatment and confirms the Hsp90-dependency of the FKBP51-p23 interaction. Overall, the ligand sensitivity, as well as the crosslinks alone can be seen as an indirect confirmation, that the site-specific incorporation of the unnatural amino does not interfere with the binding affinity of the mutated species.

Second, it was tested whether GR→Hsp90 crosslinks are sensitive to Hsp90 inhibitor treatment. GR M691pBpa was used as a proximity sensor of the GR-Hsp90 interaction. Western blot analysis was applied to monitor changes in the crosslinking behavior (see Figure 52).

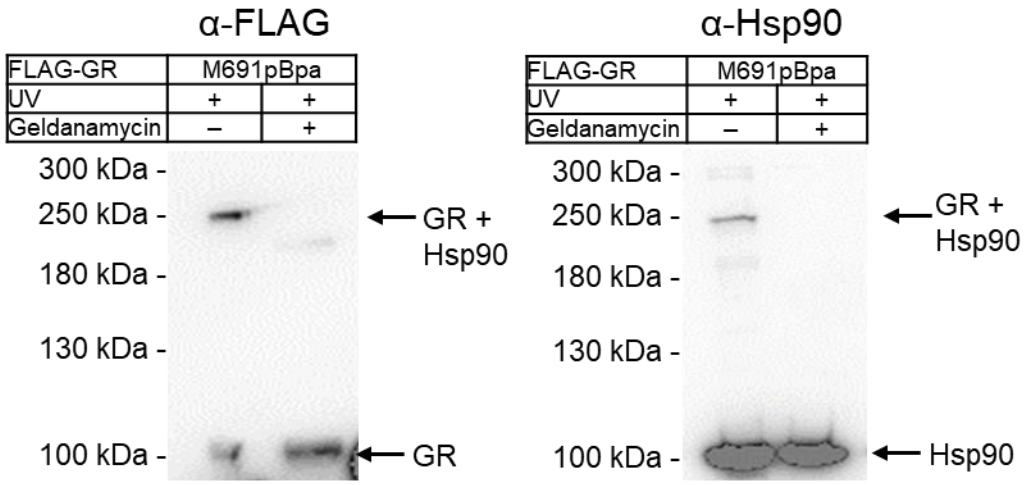

Figure 52: GR-Hsp90 interaction is sensitive to Hsp90 inhibitor. Hsp90 inhibitor (geldanamycin) treatment (5 μM, 1 h) disrupts GR→Hsp90 crosslink.

The Western blot shows a complete disruption of the GR-Hsp90 interaction confirming the geldanamycin-induced alteration in GR-Hsp90 complex composition. Geldanamycin treatment is associated with a rapid (15–30 min), noncompetitive loss of dexamethasone-binding activity of the GR in mammalian cells. (Whitesell & Cook, 1996). This underpins the requirement of a functional Hsp90 machinery to maintain both the hormone-binding activity.

Next, the effect of GR activation was explored on GR→FKBP51 crosslinks. GR K743pBpa and N768pBpa were selected and treated prior to UV-irradiation, with either dexamethasone, mifepristone or geldanamycin (see Figure 53). Given the important role of helix α12 of GR in complexing FKBP51 (see Figure 42), cells were treated with the GR antagonist mifepristone

(RU486), which is known to induce a GR conformation with a rearranged helix α12 (Kauppi et al., 2003).

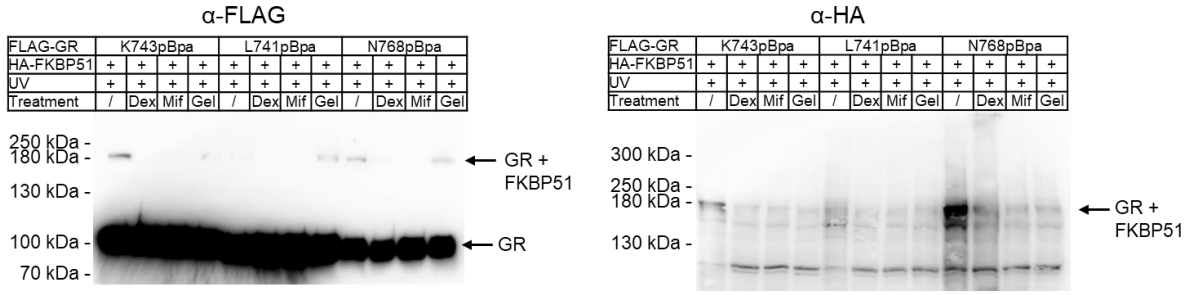

Figure 53: FKBP51 interacts with the apoGR in a Hsp90-dependent manner. GR agonist (dexamethasone, Dex, 5 μM), GR antagonist (mifepristone, Mif, 5 μM) and Hsp90 inhibitor (geldanamycin, Gel, 5 μM) treatment for 1 h disrupts GR→FKBP51 crosslinks.

Stimulation with the GR agonist dexamethasone induced rapid dissociation of the GR-FKBP51 complex. Like dexamethasone, mifepristone completely disrupted all GR→FKBP51 crosslinks, indicating that the specific conformation of helix α12 is not important for dissociation of the FKBP-GR complexes in cells. The Western blot analysis also confirms the Hsp90-dependent interaction of GR-FKBP51, as for the FKBP51→GR crosslinks (see Figure 51), GR→FKBP51 crosslinks are sensitive to Hsp90 inhibition.

The availability of intracellular GR activation-sensitive sensors allows to investigate the potency of GR agonists for GR activation in a subcomplex-resolved manner in cells. A dexamethasone titration experiment was performed using two representative GR mutants which crosslink to FKBP51 and are situated in the structurally import α12 helix, GR K743pBpa and GR N768 pBpa. The ELISA was used as a read-out, presented in Figure 54.

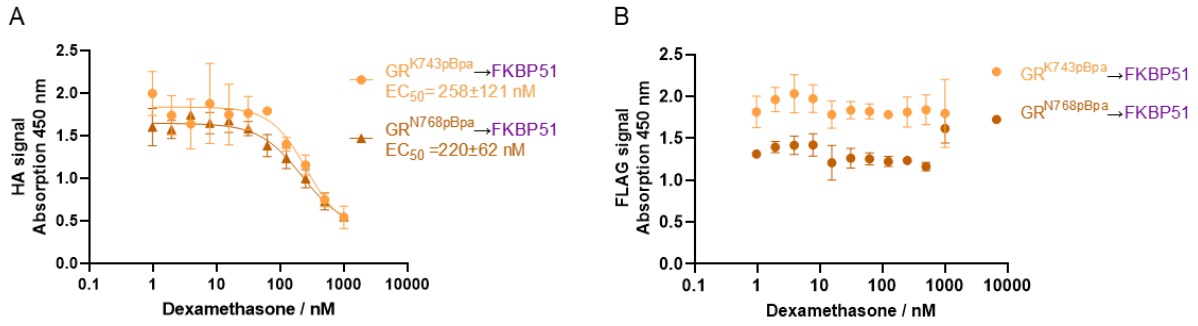

Figure 54: ELISA enables in-cell detection of dose-dependent disruption of the GR-FKBP51 interaction. A, Dexamethasone dose-dependently disrupted the GR→FKBP51 crosslink in cells as determined by ELISA after cellular stimulation for 30 min, in-cell photocrosslinking and cell lysis. B, Amber suppression control of A, mean ± s.d are shown. (n = 3 biological replicates).

Using GR pBpa mutants co-expressed with FKBP51 and ELISA as a readout, dexamethasone titration revealed an apparent EC_{50} for GR activation of GR K743pBpa→FKBP51= 258±121 nM and GR N768pBpa→FKBP51= 220±62 nM when starting from a GR complex containing FKBP51.

The ELISA setup was also used to quantify the sensitivity of FKBP→GR crosslinks to GR activation, performed separately for FKBP51 and FKBP52 using the same photocrosslinking positions for FKBP51 and FKBP52.

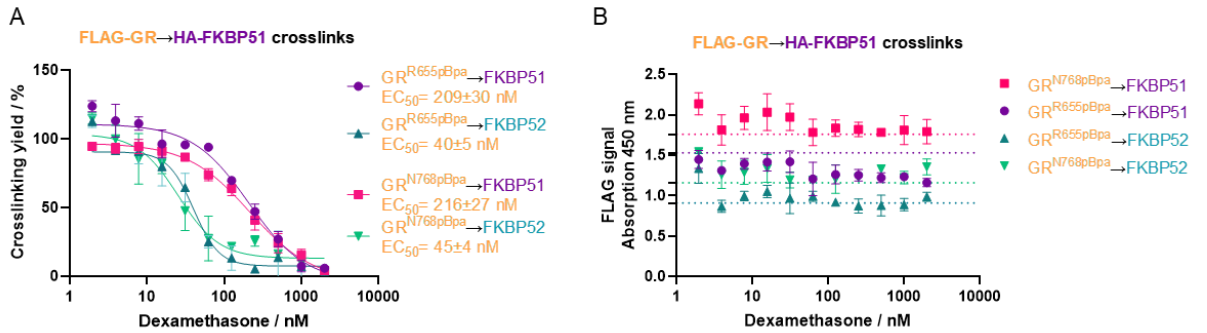

Figure 55: Both large immunophilins interact with the apoGR. A, Dexamethasone disrupts GR→FKBP52 complexes more potently compared to GR→FKBP51 complexes, as determined by ELISA after cellular stimulation for 1 h, in-cell photocrosslinking and cell lysis. For better comparison, the crosslinking yield is shown (mean±s.d.) with 0 μM Dex=100% crosslinking yield and –UV= 0%, plot represents data from biological replicates (n=3) per concentration. B, Amber suppression control of A, mean±s.d. are shown (n=3 biological replicates). Dotted line represents the 0 nM concentration.

Using GR R655pBpa co-expressed with FKBP51 or FKBP52 and ELISA as a readout, Dex titration revealed an apparent EC_{50} for GR activation of 40±5 nM when starting from a GR complex containing FKBP52 and an apparent EC_{50} for GR activation of 209±30 nM when starting from a GR complex containing FKBP51. GR→FKBP52 crosslinks were found to be 5-fold more sensitive to GR activation compared to GR→FKBP51 crosslinks. This is true for both tested GR mutants which are situated on opposite interaction hotspots (see Figure 42). The values for GR→FKBP51 are in line with separated experiments presented above (see Figure 54). Nevertheless, the absolute potencies for GR activation depend on GR expression levels, activation time, and photocrosslinking position. The ELISA data show that GR activation is facilitated in the context of a FKBP52-Hsp90-GR complex compared to GR in a FKBP51-Hsp90-GR complex, in accordance with the well-documented GR-facilitating effect of FKBP52 and the GR-repressing effect of FKBP51 (Riggs et al., 2007). However, the disruption of apoGR-FKBP52 interaction upon GR activation was surprising since FKBP52 has been thought to enter GR-Hsp90 complex after GR activation, possibly by replacing FKBP51 (Davies et al., 2002). The

ELISA findings show that prior to activation, both FKBPs bind to GR in the apo form, in a pre-activation complex and provide a more detailed view on the late stage Hsp90 cycle.

Furthermore, the ligand-sensitivity for GR crosslinks to p23 as well as GR crosslinks to Hsp90 were investigated. The Western blot analysis is shown in Figure 56 for several GR^{LBD} pBpa mutants.

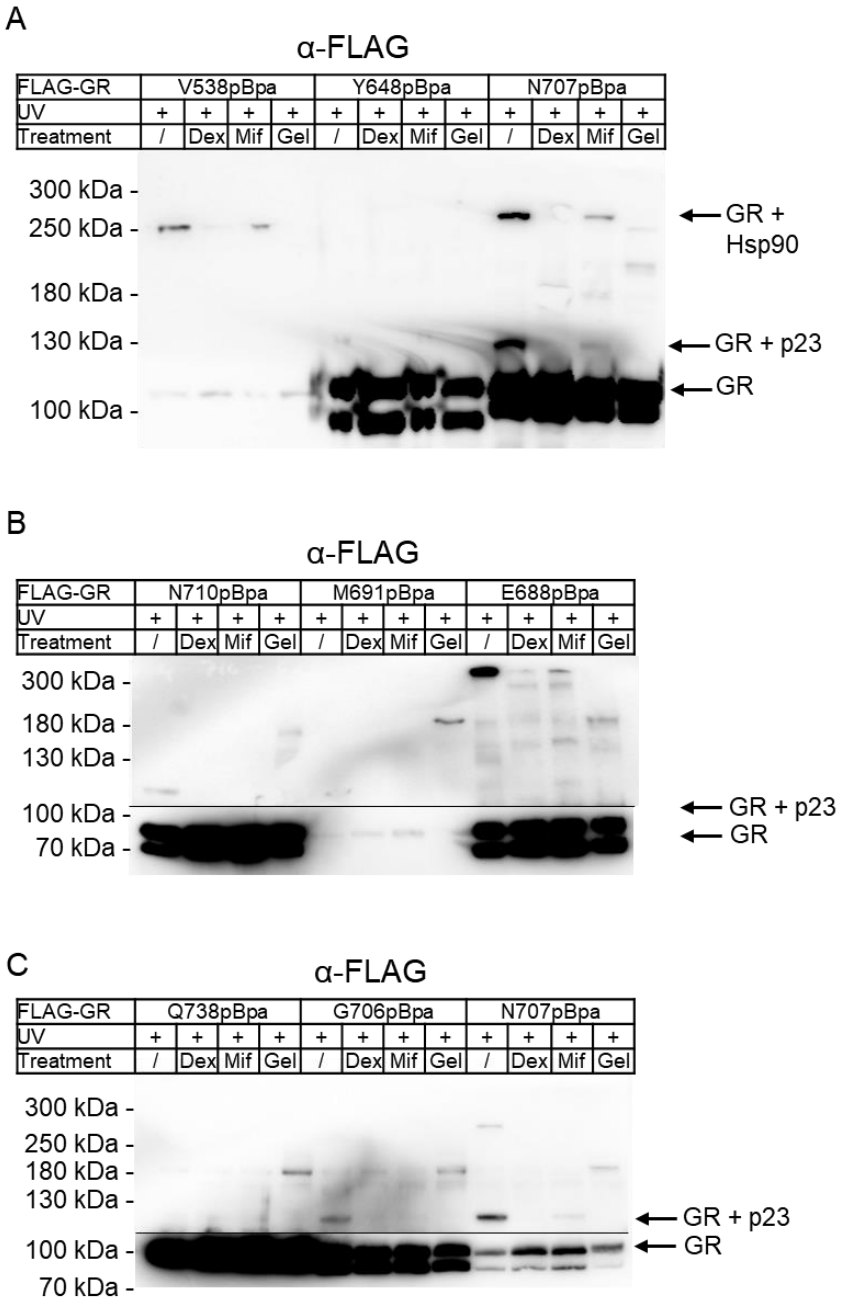

Figure 56: p23 interacts with the apoGR in a Hsp90-dependent manner. GR agonist (Dexamethasone, Dex, 5 μM) and Hsp90 inhibitor (Geldanamycin, Gel, 5 μM) treatment for 1 h disrupts GR→p23 crosslinks; GR antagonist (Mifepristone, Mif, 5 μM) treatment for 1 h partially disrupts GR→p23 crosslinks. Black line indicates a different exposure time of the same Western blot.

Stimulation with geldanamycin, dexamethasone or mifepristone disrupted or severely compromised all GR→p23 crosslinks (Figure 56), suggesting that p23 too preferentially bound apoGR in a Hsp90-dependent manner. Additionally, GR→Hsp90 crosslinks were also disrupted, suggesting a dissociation of ligand-bound, activated GR from the Hsp90 complex. Detected GR→Hsp90 crosslinks were either situated in pre-α1 helix (A523–T531) or α1 helix (L532–I539) or on the Hsp90 facing side of the GR^{LBD}. The GR activation studies provide substantial evidence efficient for a pre-activation complex of Hsp90-FKBP51/(FKBP52)-apoGR as well as Hsp90-apoGR-p23, which is visualized in Figure 57.

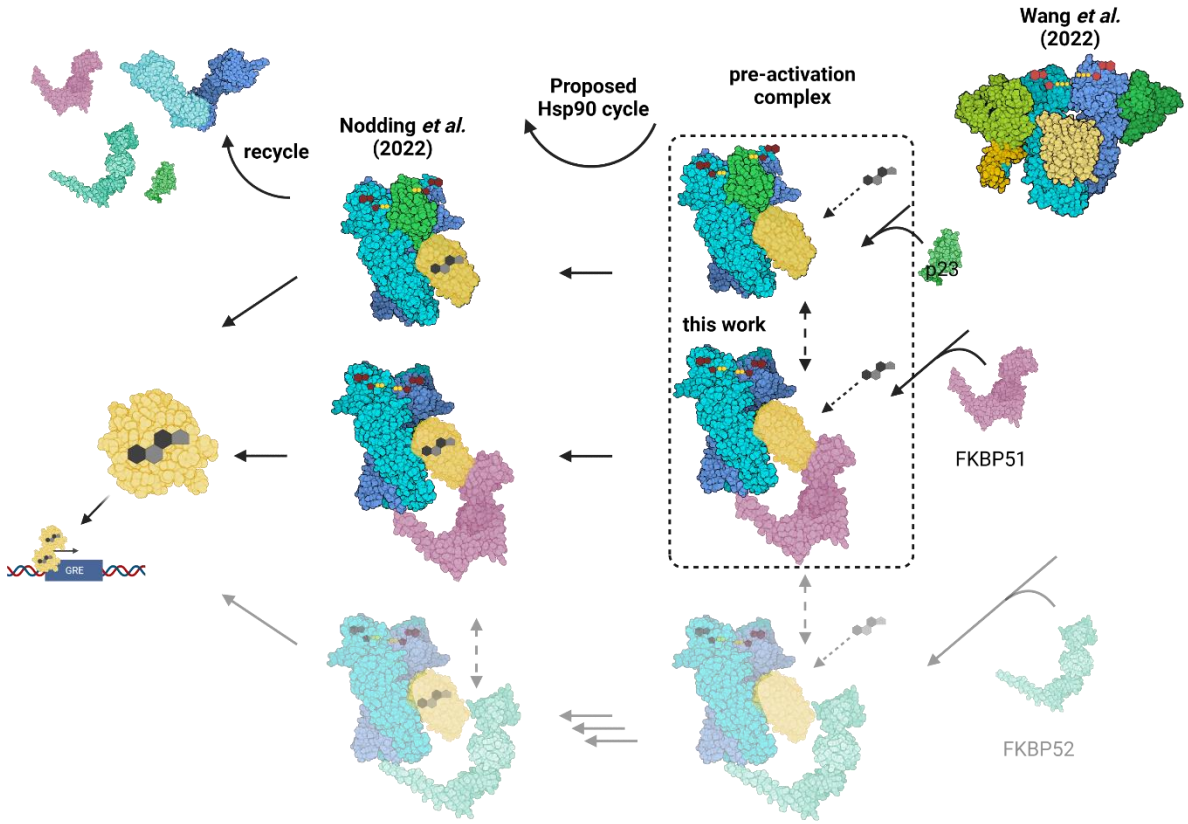

Figure 57: Cochaperones preferentially engage apoGR in pre-activation complexes in human cells. After Hop-mediated transfer from Hsp70 to Hsp90 (right), apoGR transitions further to FKBP51 or p23 containing pre-activation complexes, which represent the predominantly populated FKBP51/p23-GR species in cells. The pre-activation complexes can progress to Hsp90-cochaperone complexes containing activated GR (left) by GR ligand (grey-black) activation or recycle by disassembly of the heterocomplexes. FKBP52-GR species were not part of this work but are shown in transparent for completion, the faster activation of the GR-FKBP52 complex is indicated by 3 arrows (this work was performed by Sarah Engel).

The results of the GR activation studies using the incorporation of photoreactive unnatural amino acids as in-cell proximity-sensor, raises the question on the time point of the ligand binding event. It was suggested that during the transition from the Hsp70-present to the Hsp70-

absent complex with Hsp90, hormone could bind to the GR^{LBD} (Noddings et al., 2022; Wang et al., 2022). This is supported by the cryoEM structure of the Hsp90-p23-GR^{LBD} complex (see Figure 44) (Noddings et al., 2022), which contains bound ligand. This structure shows how remodeling of the GR allows pre-helix-1 (see Figure 3), previously held by Hsp70, to move into the lumen of the fully closed Hsp90 dimer. This rearrangement might allow α1 helix to associate with the GR^{LBD} thereby closing the hormone binding pocket (Prodromou & Bjorklund, 2022). This implies that the hormone has already bound to the GR. Within this complex the activation of the GR is facilitated by p23 binding. p23 stabilizes the closed conformation of Hsp90 and plays a role in stabilizing the dynamic α12 helix of the GR in its agonist-binding conformation (Prodromou & Bjorklund, 2022). The activated GR must be released from the complex, but the trigger remains enigmatic. However, Kirschke *et al*. showed that the activation of the GR is enhanced by the presence of p23 in a fully reconstituted chaperone system that contains Hsp90, Hsp70, Hsp40, HOP and the GR^{LBD} (Kirschke et al., 2014). This suggests that the action of p23 appears to occur prior to the GR–helix 1 rearrangement capping of hormone access to GR^{LBD}. This may indicate that release of the GR from the Hsp90 complex occurs as a direct result of hormone binding (Kirschke et al., 2014). The presented results provide strong evidence for a rapid dissociation of the GR from the pre-activation complex after hormone binding, which triggers translocation in to the nucleus.

In the last chapter, the results of pharmacological interventions on the Hsp90-FKBP51-GR complex were presented, which gave significant and exciting insights into the Hsp90-FKBP51-GR interaction. Selected mutants were used as a proximity sensor to detect the interaction in mammalian cells. The treatment with the Hsp90-inhibitror geldanamycin confirmed the Hsp90-dependent interaction of FKBP51 and GR. Further, the FKBP51-GR interaction was partially disrupted by SAFit2 treatment, a FKBP51 inhibitor. Surprisingly, not all GR→FKBP51 crosslinks were diminished after SAFit2 treatment proving strong evidence of a multilayer interaction of FKBP51 and GR. Lastly, stimulation with the GR ligand dexamethasone disrupts GR→FKBP51, GR→p23, and GR→Hsp90 crosslinks confirming the Hsp90-FKBP51-apoGR and Hsp90-p23-apoGR (ligand unbound state) to be the predominant species in mammalian cells. The combination of ELISA and ligand titration enabled the determination of intracellular EC_{50} values for dexamethasone with both large immunophilins. Interestingly, FKBP51 delays the activation of GR by dexamethasone 5-fold over FKBP52 giving additional insights into why FKBP51 inhibits the GR function.

4. Conclusion

This part is partially taken from: Baischew, A., Engel, S., Geiger, T. M., & Hausch, F. (2023). Large-scale in-cell photocrosslinking at single residue resolution reveals the molecular basis for glucocorticoid receptor regulation by immunophilins. *bioRxiv*, 2023-01.

Steroid hormone receptor functioning relies crucially on the Hsp90 chaperone machinery for loading and activation by hydrophobic steroids. The minimal chaperone machinery, best defined for GR, consists of five factors (Hsp90, Hsp70, Hsp40, Hop, and p23) (Kirschke et al., 2014). Two key intermediate states of the basic GR chaperoning cycle have recently been structurally elucidated by the Agard group (Noddings et al., 2022; Wang et al., 2022) (Figure 57), which represent early chaperoning and late activated states, respectively. Higher eukaryotes have evolved FKBP51 and FKBP52 as additional Hsp90 cochaperones to super-regulate steroid receptor signaling, with essential physiological roles in mammals (Biebl & Buchner, 2019). While FKBP52s main function seems to be to support optimal receptor activation (incl. subsequent transport to the nucleus (Silverstein et al., 1999; Wochnik et al., 2005)), FKBP51 is a GR repressor and key effector of an ultrashort negative feedback loop (Jääskeläinen et al., 2011). However, how and precisely when FKBPs interact with GR in the chaperone cycle has been matter of debate.

To gain a more detailed view on the late stage of GR maturation, large scale in-cell photocrosslinking was applied to investigate the Hsp90-FKBP51-complex-dependent modulation of the GR pathway in mammalian cells. Site-directed photocrosslinking is an elegant technique that enables analysis of protein interaction in living cells with high spatial resolution. It allows the covalent capture of protein interaction thereby serving as an in-cell snapshot of a highly dynamic system. By using photocrosslinking in intact cells, FKBP51 and GR were captured in their functionally relevant states, which have so far eluded any purification or reconstitution attempts. The studied system recapitulates the hallmarks of the FKBP-Hsp90-GR machinery, incl. Hsp90 dependence and facilitated GR activation by FKBP52 compared to FKBP51. The data reveal that in the absence of hormones FKBP51 as well as p23 predominantly reside in apoGR-Hsp90 containing complexes in human cells (Figure 57). These states can either progress towards activation by GR ligand stimulation or recycle through the Hsp90 machinery. Both of these processes are fast (<30min) and complete. GR activation assays showed that either pathway leads to complete disassembly of the entire complex, since none of the investigated interactions survived as long as hormone stimulation persists or reassembly, respectively, is blocked.

The findings presented do not exclude the existence of FKBP-Hsp90 complexes with activated, ligand-bound GR, which were previously suggested especially for FKBP52 (Davies et al., 2002, 2005). However, these complexes are likely short-lived in cells and quickly disassemble after the (co)-chaperone machinery has done its job to deliver activated GR.

Also, the results provide a picture for the overall architecture of the relevant FKBP51/p23-Hsp90-apoGR pre-activation complexes (Figure 57). The p23-Hsp90-apoGR complex resembles the maturation complex (Hsp90-dexamethasone-GR-p23) elucidated by cryoEM (Noddings et al., 2022). For FKBP-containing complexes, the GR has to rearrange, e.g., by rotation of the GR^{LBD}, which stays tethered to the client-binding channel of Hsp90 via pre-helix α1 of GR. This rotation will most likely abrogate p23-GR contacts observed in the absence of FKBP51 (Figure 44 and (Noddings et al., 2022)), which may be partially replaced by contacts with the tip of FKBP51. So far, it was not possible to elucidated the question whether FKBP51 and p23 occur in the same pre-activation complex. Nevertheless, *in vitro* studies suggest the existence of a Hsp90-GR-FKBP51-p23 complex (Ebong et al., 2016). FKBP51, FKBP52, and p23 are likely inter-exchangeable in the Hsp90-apoGR complex, either directly at preassembled Hsp90-apoGR complexes or via Hsp90/Hsp70/Hsp40/Hop-mediated dis- and reassembly.

Large scale GR→FKBP51 crosslink screening confirm the ligand binding domain of GR as the predominant interaction site for FKBP51, which is in line with prior studies (Riggs et al., 2003). The identified FKBP→GR interaction surface is largely consistent with the conformation of FKBP51 bound to Hsp90 in the absence of GR (Lee et al., 2021) and requires only minor rearrangements of the FK1 and FK2 domains. The GR has to reorient more profoundly compared to available structures (Noddings et al., 2022; Wang et al., 2022) to allow for the observed interaction surface. FKBP51 wraps around the GR^{LBD} from helix α12 to the α7-α8 loop, covering the α1-α3 loop, where mutations were previously shown enhance GR repression by FKBP51 (Cluning et al., 2013).

A key question is how FKBP51 and FKBP52 exert strikingly opposing effects on GR signaling in spite of high structural and sequence similarity. In line with their similarities, most of the GR-interacting interface is identical between FKBP51 and FKBP52 which was beautifully shown by Sarah Engel (Baischew & Engel et al., 2023). While the inter-domain arrangements of FKBP52 were shown to be flexible (Hähle et al., 2019), it is now clear that FKBP51 and FKBP52 adopt an almost identical conformation in complex with Hsp90-apoGR. Previous domain swapping analyses pointed to the FK1 domain as a major factor underlying the opposing effects of FKBP51 and FKBP52. Swapping L119 in FKBP51 for P119 as in FKBP52 was previously shown to impart GR-stimulating activity to FKBP51 (Riggs et al., 2007). Crystal structures previously showed the proline-rich loop to be flexible in FKBP51 (Gaali et al., 2015; Kumar et al., 2017; Sinars et al.,

2003) as well as in FKBP52 (Bracher et al., 2013; Gaali et al., 2015), and NMR studies suggested differential dynamics of this loop as well as the beta bulge on the opposite side of the FK506-binding pocket to account for the diverging effects of the large FKBPs for GR regulation (LeMaster et al., 2015).

The proposed binding modes for the FKBP51-Hsp90-apoGR pre-activation complexes are remarkable consistent with two structures for the related complexes containing dexamethasone-bound GR, recently obtained by the Agard group by cryoEM after *in vitro* reconstitution (Noddings et al., 2023). Shared features are the intensive contacts of all three FKBP domains with GR^{LBD}, the highly similar interaction pattern for FKBP51 and FKBP52, the rotation of GR^{LBD} compared to the p23-Hsp90-dexamethasone-GR^{LBD} complex, the stronger, well-defined docking of the FK2 and TPR domains to GR^{LBD} compared to a more dynamic, and partially displaceable FK1-GR^{LBD} interaction. The observed interdomain assembly seems to be a strong scaffold that can accommodate GR in pre- and post-activation states.

Systematic site-specific incorporation of photoreactive unnatural amino acids has been used before to probe interactions of small or peptide ligands with receptors in mammalian cells (Coin et al., 2013; Grunbeck et al., 2011; Rannversson et al., 2016; Rudolf et al., 2022) or between proteins in yeast, *E. coli* or *in vitro* (Kashiwagi et al., 2016; Wilkins et al., 2014). However, this is the first example, where the architecture of a multi-protein complex has been determined directly in intact mammalian cells. Notably, this enables determination of apoGR-containing complexes that so far have eluded any biochemical purification of reconstitution attempts. The streamlining of large-scale photocrosslinking screening allowed to reconstruct the overall architecture of metastable complexes that have eluded structural or tailored functional studies so far. Moreover, the use of proximity sensors enabled to trace the remodeling of complexes at much higher detail than previously possible in cells. Systematic surface mapping might be a general approach for low-resolution in-cell structural biology that is poised to interface with functional cellular studies. The ELISA read-out of photocrosslinking results further facilitated the investigation of the Hsp90-GR heterocomplex. The combination of ELISA and photocrosslinking has not been explored by other labs.

Taken together, this work exploits large scale in-cell incorporation of a photocrosslinker unnatural amino acid into FKBP51 to (I) expand the Hsp90-FKBP51 interaction interface beyond the $FKBP51^{TPR}$-$Hsp90^{CTD}$ interaction; (II) identify p23 as a direct Hsp90-dependent interaction partner; and (III) monitor ligand-induced heterodimerization of FKBP51 and $mTOR^{FRB}$. Further, the same technique was applied to the full-length GR to (I) identify the GR^{LBD} as the preferred interaction site to large FKBPs; (II) reveal the orientation of the FKBP51-GR interaction by SAFit2-induced partial disruption of the interaction; and (III) discover the pre-

activation complex of Hsp90-FKBP51/p23-apoGR as the predominate species in mammalian cells. The proposed interaction modes are likely extendable to other FKBP-regulated steroid hormone receptors such as progesterone, estrogen or androgen receptors, with important implications for breast and prostate cancers (Habara et al., 2022; Maeda et al., 2022).

5. References

Ali, M. M. U., Roe, S. M., Vaughan, C. K., Meyer, P., Panaretou, B., Piper, P. W., Prodromou, C., & Pearl, L. H. (2006). Crystal structure of an Hsp90–nucleotide–p23/Sba1 closed chaperone complex. *Nature*, *440*(7087), 1013–1017.

Bain, D. L., Heneghan, A. F., Connaghan-Jones, K. D., & Miura, M. T. (2007). Nuclear receptor structure: implications for function. *Annual Review of Physiology*, *69*(1), 201–220.

Baischew, A., Engel, S., Geiger, T. M., & Hausch, F. (2023). Large-scale in-cell photocrosslinking at single residue resolution reveals the molecular basis for glucocorticoid receptor regulation by immunophilins. *BioRxiv*, 2023.01.16.524346. https://doi.org/10.1101/2023.01.16.524346

Baischew, A., Engel, S., Geiger, T. M., Taubert, M. C., & Hausch, F. (2023). Structural and biochemical insights into FKBP51 as a Hsp90 cochaperone. *Journal of Cellular Biochemistry*, https://doi.org/10.1002/jcb.30384

Balsevich, G., Häusl, A. S., Meyer, C. W., Karamihalev, S., Feng, X., Pöhlmann, M. L., Dournes, C., Uribe-Marino, A., Santarelli, S., Labermaier, C., Hafner, K., Mao, T., Breitsamer, M., Theodoropoulou, M., Namendorf, C., Uhr, M., Paez-Pereda, M., Winter, G., Hausch, F., Schmidt, M. V. (2017). Stress-responsive FKBP51 regulates AKT2-AS160 signaling and metabolic function. *Nature Communications*, https://doi.org/10.1038/s41467-017-01783-y

Banaszynski, L. A., Liu, C. W., & Wandless, T. J. (2005). Characterization of the FKBP-Rapamycin-FRB ternary complex. *Journal of the American Chemical Society*, *127*(13), 4715–4721.

Banerjee, A., Periyasamy, S., Wolf, I. M., Hinds Jr, T. D., Yong, W., Shou, W., & Sanchez, E. R. (2008). Control of glucocorticoid and progesterone receptor subcellular localization by the ligand-binding domain is mediated by distinct interactions with tetratricopeptide repeat proteins. *Biochemistry*, *47*(39), 10471–10480.

Barent, R. L., Nair, S. C., Carr, D. C., Ruan, Y., Rimerman, R. A., Fulton, J., Zhang, Y., & Smith, D. F. (1998). Analysis of FKBP51/FKBP52 chimeras and mutants for Hsp90 binding and association with progesterone receptor complexes. *Molecular Endocrinology*, *12*(3), 342–354.

Barth, H. G., Jackson, C., & Boyes, B. E. (1994). Size exclusion chromatography. *Analytical Chemistry*, *66*(12), 595–620.

Baughman, G., Wiederrecht, G. J., Chang, F., Martin, M. M., & Bourgeois, S. (1997). Tissue distribution and abundance of human FKBP51, an FK506-binding protein that can mediate calcineurin inhibition. *Biochemical and Biophysical Research Communications*, *232*(2), 437–443.

Benzer, S., & Champe, S. P. (1962). A change from nonsense to sense in the genetic code. *Proceedings of the National Academy of Sciences*, *48*(7), 1114–1121.

Berggård, T., Linse, S., & James, P. (2007). Methods for the detection and analysis of protein–protein interactions. *Proteomics*, *7*(16), 2833–2842.

Biebl, M. M., & Buchner, J. (2019). Structure, function, and regulation of the Hsp90 machinery. *Cold Spring Harbor Perspectives in Biology*, *11*(9), a034017, https://doi.org/10.1101/cshperspect.a034017

Biebl, M. M., Lopez, A., Rehn, A., Freiburger, L., Lawatscheck, J., Blank, B., Sattler, M., & Buchner, J. (2021). Structural elements in the flexible tail of the cochaperone p23 coordinate client binding and progression of the Hsp90 chaperone cycle. *Nature Communications*, *12*(1). https://doi.org/10.1038/s41467-021-21063-0

Biebl, M. M., Riedl, M., & Buchner, J. (2020). Hsp90 Cochaperones form plastic genetic networks adapted to client maturation. *Cell Reports*, *32*(8), 108063.

Binder, E. B., Salyakina, D., Lichtner, P., Wochnik, G. M., Ising, M., Pütz, B., Papiol, S., Seaman, S., Lucae, S., & Kohli, M. A. (2004). Polymorphisms in FKBP5 are associated with increased recurrence of depressive episodes and rapid response to antidepressant treatment. *Nature Genetics*, *36*(12), 1319–1325.

Bracher, A., Kozany, C., Hähle, A., Wild, P., Zacharias, M., & Hausch, F. (2013). Crystal structures of the free and ligand-bound FK1–FK2 domain segment of FKBP52 reveal a flexible inter-domain hinge. *Journal of Molecular Biology*, *425*(22), 4134–4144.

Bracher, A., Kozany, C., Thost, A.-K., & Hausch, F. (2011). Structural characterization of the PPIase domain of FKBP51, a cochaperone of human Hsp90. *Acta Crystallographica Section D: Biological Crystallography*, *67*(6), 549–559.

Brillantes, A.-M. B., Ondrias, K., Scott, A., Kobrinsky, E., Ondriašová, E., Moschella, M. C., Jayaraman, T., Landers, M., Ehrlich, B. E., & Marks, A. R. (1994). Stabilization of calcium release channel (ryanodine receptor) function by FK506-binding protein. *Cell*, *77*(4), 513–523.

Brunner, J. (1993). New photolabeling and crosslinking methods. *Annual Review of Biochemistry*, *62*(1), 483–514.

Chen, M.-S., Silverstein, A. M., Pratt, W. B., & Chinkers, M. (1996). The tetratricopeptide repeat domain of protein phosphatase 5 mediates binding to glucocorticoid receptor heterocomplexes and acts as a dominant negative mutant. *Journal of Biological Chemistry*, *271*(50), 32315–32320.

Chen, S., Prapapanich, V., Rimerman, R. A., Honore, B., & Smith, D. F. (1996). Interactions of p60, a mediator of progesterone receptor assembly, with heat shock proteins hsp90 and hsp70. *Molecular Endocrinology*, *10*(6), 682–693.

Chen, S., Sullivan, W. P., Toft, D. O., & Smith, D. F. (1998). Differential interactions of p23 and the TPR-containing proteins Hop, Cyp40, FKBP52 and FKBP51 with Hsp90 mutants. *Cell Stress & Chaperones*, *3*(2), 118.

Cheung-Flynn, J., Roberts, P. J., Riggs, D. L., & Smith, D. F. (2003). C-terminal sequences outside the tetratricopeptide repeat domain of FKBP51 and FKBP52 cause differential binding to Hsp90. *Journal of Biological Chemistry*, https://doi.org/10.1074/jbc.M300955200

Chevallet, M., Luche, S., & Rabilloud, T. (2006). Silver staining of proteins in polyacrylamide gels. *Nature Protocols*, https://doi.org/10.1038/nprot.2006.288

Chin, J. W. (2017). Expanding and reprogramming the genetic code. *Nature*, *550*(7674), 53–60.

Chin, J. W., Cropp, T. A., Anderson, J. C., Mukherji, M., Zhang, Z., & Schultz, P. G. (2003). An expanded eukaryotic genetic code. *Science*, *301*(5635), 964–967.

Chou, C., Uprety, R., Davis, L., Chin, J. W., & Deiters, A. (2011). Genetically encoding an aliphatic diazirine for protein photocrosslinking. *Chemical Science*, https://doi.org/10.1039/c0sc00373e

Clark, L. J., Krieger, J., White, A. D., Bondarenko, V., Lei, S., Fang, F., Lee, J. Y., Doruker, P., Böttke, T., & Jean-Alphonse, F. (2020). Allosteric interactions in the parathyroid hormone GPCR–arrestin complex formation. *Nature Chemical Biology*, *16*(10), 1096–1104.

Cluning, C., Ward, B. K., Rea, S. L., Arulpragasam, A., Fuller, P. J., & Ratajczak, T. (2013). The helix 1-3 loop in the glucocorticoid receptor LBD is a regulatory element for FKBP cochaperones. *Molecular Endocrinology*, *27*(7), 1020–1035.

Coin, I. (2018). Application of non-canonical crosslinking amino acids to study protein–protein interactions in live cells. *Current Opinion in Chemical Biology*, https://doi.org/10.1016/j.cbpa.2018.07.019

Coin, I., Katritch, V., Sun, T., Xiang, Z., Siu, F. Y., Beyermann, M., Stevens, R. C., & Wang, L. (2013). Genetically encoded chemical probes in cells reveal the binding path of urocortin-I to CRF class B GPCR. *Cell*, *155*(6), 1258–1269.

Cox, J., & Mann, M. (2008). MaxQuant enables high peptide identification rates, individualized ppb-range mass accuracies and proteome-wide protein quantification. *Nature Biotechnology*, *26*(12), 1367–1372.

Czar, M. J., Galigniana, M. D., Silverstein, A. M., & Pratt, W. B. (1997). Geldanamycin, a heat shock protein 90-binding benzoquinone ansamycin, inhibits steroid-dependent translocation of the glucocorticoid receptor from the cytoplasm to the nucleus. *Biochemistry*, *36*(25), 7776–7785.

Davies, T. H., Ning, Y.-M., & Sánchez, E. R. (2002). A new first step in activation of steroid receptors: hormone-induced switching of FKBP51 and FKBP52 immunophilins. *Journal of Biological Chemistry*, *277*(7), 4597–4600.

Davies, T. H., Ning, Y.-M., & Sánchez, E. R. (2005). Differential control of glucocorticoid receptor hormone-binding function by tetratricopeptide repeat (TPR) proteins and the immunosuppressive ligand FK506. *Biochemistry*, *44*(6), 2030–2038.

Dehling, E., Volkmann, G., Matern, J. C. J., Dörner, W., Alfermann, J., Diecker, J., & Mootz, H. D. (2016). Mapping of the communication-mediating interface in nonribosomal peptide synthetases using a genetically encoded photocrosslinker supports an upside-down helix-hand motif. *Journal of Molecular Biology*, *428*(21), 4345–4360.

Denny, W. B., Valentine, D. L., Reynolds, P. D., Smith, D. F., & Scammell, J. G. (2000). Squirrel monkey immunophilin FKBP51 is a potent inhibitor of glucocorticoid receptor binding. *Endocrinology*, *141*(11), 4107–4113.

Dittmar, K. D., Demady, D. R., Stancato, L. F., Krishna, P., & Pratt, W. B. (1997). Folding of the Glucocorticoid Receptor by the Heat Shock Protein (hsp) 90-based Chaperone Machinery. *Journal of Biological Chemistry*. https://doi.org/10.1074/jbc.272.34.21213

Dunham, W. H., Mullin, M., & Gingras, A. (2012). Affinity-purification coupled to mass spectrometry: Basic principles and strategies. *Proteomics*, *12*(10), 1576–1590.

Ebong, I., Beilsten-Edmands, V., Patel, N. A., Morgner, N., & Robinson, C. V. (2016). The interchange of immunophilins leads to parallel pathways and different intermediates in the assembly of Hsp90 glucocorticoid receptor complexes. *Cell Discovery*, https://doi.org/10.1038/celldisc.2016.2

Ernst, R. J., Krogager, T. P., Maywood, E. S., Zanchi, R., Beránek, V., Elliott, T. S., Barry, N. P., Hastings, M. H., & Chin, J. W. (2016). Genetic code expansion in the mouse brain. *Nature Chemical Biology*, *12*(10), 776–778.

Felts, S. J., & Toft, D. O. (2003). p23, a simple protein with complex activities. *Cell Stress & Chaperones*, *8*(2), 108.

Flaxman, H. A., Chang, C.-F., Wu, H.-Y., Nakamoto, C. H., & Woo, C. M. (2019). A binding site hotspot map of the fkbp12–rapamycin–frb ternary complex by photoaffinity labeling and mass spectrometry-based proteomics. *Journal of the American Chemical Society*, *141*(30), 11759–11764.

Forne, I., Ludwigsen, J., Imhof, A., Becker, P. B., & Mueller-Planitz, F. (2012). Probing the conformation of the ISWI ATPase domain with genetically encoded photoreactive crosslinkers and mass spectrometry. *Molecular & Cellular Proteomics*, *11*(4).

Gaali, S., Kirschner, A., Cuboni, S., Hartmann, J., Kozany, C., Balsevich, G., Namendorf, C., Fernandez-Vizarra, P., Sippel, C., Zannas, A. S., Draenert, R., Binder, E. B., Almeida, O. F. X., Rühter, G., Uhr, M., Schmidt, M. V., Touma, C., Bracher, A., & Hausch, F. (2015). Selective inhibitors of the FK506-binding protein 51 by induced fit. *Nature Chemical Biology*, *11*(1), 33. https://doi.org/10.1038/nchembio.1699

Galat, A. (2008). Functional drift of sequence attributes in the FK506-binding proteins (FKBPs). *Journal of Chemical Information and Modeling*, *48*(5), 1118–1130.

Galigniana, M. D., Radanyi, C., Renoir, J. M., Housley, P. R., & Pratt, W. B. (2001). Evidence that the Peptidylprolyl Isomerase Domain of the hsp90-binding Immunophilin FKBP52 is Involved in Both Dynein Interaction and Glucocorticoid Receptor Movement to the Nucleus. *Journal of Biological Chemistry*, https://doi.org/10.1074/jbc.M010809200

Garen, A., & Siddiqi, O. (1962). Suppression of mutations in the alkaline phosphatase structural cistron of E. coli. *Proceedings of the National Academy of Sciences*, *48*(7), 1121–1127.

Gasiewicz, T. A., Singh, K. P., & Bennett, J. A. (2014). The Ah receptor in stem cell cycling, regulation, and quiescence. *Annals of the New York Academy of Sciences*, *1310*(1), 44–50.

Geiger, T. M., Schäfer, S. C., Dreizler, J. K., Walz, M., & Hausch, F. (2022). Clues to molecular glues. *Current Research in Chemical Biology*, *2*, 100018.

Ghaemmaghami, S., Huh, W.-K., Bower, K., Howson, R. W., Belle, A., Dephoure, N., O'Shea, E. K., & Weissman, J. S. (2003). Global analysis of protein expression in yeast. *Nature*, *425*(6959), 737–741.

Gloeckner, C. J., Boldt, K., & Ueffing, M. (2009). Strep/FLAG tandem affinity purification (SF-TAP) to study protein interactions. *Current Protocols in Protein Science*, https://doi.org/10.1002/0471140864.ps1920s57

Gnatzy, M. T., Geiger, T. M., Kühn, A., Gutfreund, N., Walz, M., Kolos, J. M., & Hausch, F. (2021). Development of NanoBRET-Binding Assays for FKBP-Ligand Profiling in Living Cells. *ChemBioChem*, *22*(13), 2257–2261.

Goodman, H. M., Abelson, J., Landy, A., Brenner, S., & Smith, J. D. (1968). Amber suppression: a nucleotide change in the anticodon of a tyrosine transfer RNA. *Nature*, *217*(5133), 1019–1024.

Götze, M., Pettelkau, J., Fritzsche, R., Ihling, C. H., Schäfer, M., & Sinz, A. (2014). Automated assignment of MS/MS cleavable cross-links in protein 3D-structure analysis. *Journal of the American Society for Mass Spectrometry*, *26*(1), 83–97.

Götze, M., Pettelkau, J., Schaks, S., Bosse, K., Ihling, C. H., Krauth, F., Fritzsche, R., Kühn, U., & Sinz, A. (2011). StavroX—a software for analyzing crosslinked products in protein interaction studies. *Journal of the American Society for Mass Spectrometry*, *23*(1), 76–87.

Greiss, S., & Chin, J. W. (2011). Expanding the genetic code of an animal. *Journal of the American Chemical Society*, *133*(36), 14196–14199.

Grossmann, C., Ruhs, S., Langenbruch, L., Mildenberger, S., Strätz, N., Schumann, K., & Gekle, M. (2012). Nuclear shuttling precedes dimerization in mineralocorticoid receptor signaling. *Chemistry & Biology*, *19*(6), 742–751.

Grunbeck, A., Huber, T., Sachdev, P., & Sakmar, T. P. (2011). Mapping the ligand-binding site on a G protein-coupled receptor (GPCR) using genetically encoded photocrosslinkers. *Biochemistry*, *50*(17), 3411–3413.

Gruszczyk, J., Grandvuillemin, L., Lai-Kee-Him, J., Paloni, M., Savva, C. G., Germain, P., Grimaldi, M., Boulahtouf, A., Kwong, H.-S., Bous, J., Ancelin, A., Bechara, C., Barducci, A., Balaguer, P., & Bourguet, W. (2022). Cryo-EM structure of the agonist-bound Hsp90-XAP2-AHR cytosolic complex. *Nature Communications*, *13*(1), 7010. https://doi.org/10.1038/s41467-022-34773-w

Habara, M., Sato, Y., Goshima, T., Sakurai, M., Imai, H., Shimizu, H., Katayama, Y., Hanaki, S., Masaki, T., & Morimoto, M. (2022). FKBP52 and FKBP51 differentially regulate the stability of estrogen receptor in breast cancer. *Proceedings of the National Academy of Sciences*, *119*(15), e2110256119.

Hähle, A., Merz, S., Meyners, C., & Hausch, F. (2019). The many faces of FKBP51. *Biomolecules*, *9*(1), 35.

Han, S., Yang, A., Lee, S., Lee, H. W., Park, C. B., & Park, H. S. (2017). Expanding the genetic code of Mus musculus. *Nature Communications*. https://doi.org/10.1038/ncomms14568

Hartmann, J., Wagner, K. V, Liebl, C., Scharf, S. H., Wang, X.-D., Wolf, M., Hausch, F., Rein, T., Schmidt, U., & Touma, C. (2012). The involvement of FK506-binding protein 51 (FKBP5) in the behavioral and neuroendocrine effects of chronic social defeat stress. *Neuropharmacology*, *62*(1), 332–339.

He, D., Xie, X., Yang, F., Zhang, H., Su, H., Ge, Y., Song, H., & Chen, P. R. (2017). Quantitative and comparative profiling of protease substrates through a genetically encoded multifunctional photocrosslinker. *Angewandte Chemie International Edition*, *56*(46), 14521–14525.

Hemsley, A., Arnheim, N., Toney, M. D., Cortopassi, G., & Galas, D. J. (1989). A simple method for site-directed mutagenesis using the polymerase chain reaction. *Nucleic Acids Research*, *17*(16), 6545–6551.

Iacobucci, C., Götze, M., Piotrowski, C., Arlt, C., Rehkamp, A., Ihling, C., Hage, C., & Sinz, A. (2018). Carboxyl-photo-reactive MS-cleavable cross-linkers: unveiling a hidden aspect of diazirine-based reagents. *Analytical Chemistry*, *90*(4), 2805–2809.

Jääskeläinen, T., Makkonen, H., & Palvimo, J. J. (2011). Steroid up-regulation of FKBP51 and its role in hormone signaling. *Current Opinion in Pharmacology*, *11*(4), 326–331.

Jakob, U., Lilie, H., Meyer, I., & Buchner, J. (1995). Transient interaction of Hsp90 with early unfolding intermediates of citrate synthase: Implications for heat shock in vivo. *Journal of Biological Chemistry*, https://doi.org/10.1074/jbc.270.13.7288

Jayaraman, T., Brillantes, A. M., Timerman, A. P., Fleischer, S., Erdjument-Bromage, H., Tempst, P., & Marks, A. R. (1992). FK506 binding protein associated with the calcium release channel (ryanodine receptor). *Journal of Biological Chemistry*, *267*(14), 9474–9477.

Joiner, C. M., Breen, M. E., Clayton, J., & Mapp, A. K. (2017). A Bifunctional Amino Acid Enables Both Covalent Chemical Capture and Isolation of in Vivo Protein–Protein Interactions. *ChemBioChem*, https://doi.org/10.1002/cbic.201600578

Jumper, C. C., Bomgarden, R., Rogers, J., Etienne, C., & Schriemer, D. C. (2012). High-resolution mapping of carbene-based protein footprints. *Analytical Chemistry*, *84*(10), 4411–4418.

Kage, R., Leeman, S. E., Krause, J. E., Costello, C. E., & Boyd, N. D. (1996). Identification of methionine as the site of covalent attachment of a p-benzoyl-phenylalanine-containing analogue of substance P on the substance P (NK-1) receptor. *Journal of Biological Chemistry*, *271*(42), 25797–25800.

Karagöz, G. E., Duarte, A. M. S., Ippel, H., Uetrecht, C., Sinnige, T., van Rosmalen, M., Hausmann, J., Heck, A. J. R., Boelens, R., & Rüdiger, S. G. D. (2011). N-terminal domain of human Hsp90 triggers binding to the cochaperone p23. *Proceedings of the National Academy of Sciences*, *108*(2), 580–585.

Kashiwagi, K., Takahashi, M., Nishimoto, M., Hiyama, T. B., Higo, T., Umehara, T., Sakamoto, K., Ito, T., & Yokoyama, S. (2016). Crystal structure of eukaryotic translation initiation factor 2B. *Nature*, *531*(7592), 122–125.

Kauppi, B., Jakob, C., Färnegårdh, M., Yang, J., Ahola, H., Alarcon, M., Calles, K., Engström, O., Harlan, J., & Muchmore, S. (2003). The three-dimensional structures of antagonistic and agonistic forms of the glucocorticoid receptor ligand-binding domain: RU-486 induces a transconformation that leads to active antagonism. *Journal of Biological Chemistry*, *278*(25), 22748–22754.

Kirschke, E., Goswami, D., Southworth, D., Griffin, P. R., & Agard, D. A. (2014). Glucocorticoid receptor function regulated by coordinated action of the Hsp90 and Hsp70 chaperone cycles. *Cell*. https://doi.org/10.1016/j.cell.2014.04.038

Kozany, C., März, A., Kress, C., & Hausch, F. (2009). Fluorescent probes to characterise FK506-binding proteins. *ChemBioChem*, *10*(8), 1402–1410.

Krukenberg, K. A., Förster, F., Rice, L. M., Sali, A., & Agard, D. A. (2008). Multiple Conformations of E. coli Hsp90 in Solution: Insights into the Conformational Dynamics of Hsp90. *Structure*. https://doi.org/10.1016/j.str.2008.01.021

Krukenberg, K. A., Street, T. O., Lavery, L. A., & Agard, D. A. (2011). Conformational dynamics of the molecular chaperone Hsp90. *Quarterly Reviews of Biophysics*, *44*(2), 229–255.

Kumar, R., Moche, M., Winblad, B., & Pavlov, P. F. (2017). Combined x-ray crystallography and computational modeling approach to investigate the Hsp90 C-terminal peptide binding to FKBP51. *Scientific Reports*, *7*(1), 14288.

Lässle, M., Blatch, G. L., Kundra, V., Takatori, T., & Zetter, B. R. (1997). Stress-inducible, murine protein mSTI1: Characterization of binding domains for heat shock proteins and in vitro phosphorylation by different kinases. *Journal of Biological Chemistry*, *272*(3), 1876–1884.

Lee, K., Thwin, A. C., Nadel, C. M., Tse, E., Gates, S. N., Gestwicki, J. E., & Southworth, D. R. (2021). The structure of an Hsp90-immunophilin complex reveals cochaperone recognition of the client maturation state. *Molecular Cell*, *81*(17), 3496–3508.

LeMaster, D. M., Mustafi, S. M., Brecher, M., Zhang, J., Héroux, A., Li, H., & Hernández, G. (2015). Coupling of conformational transitions in the N-terminal domain of the 51-kDa FK506-binding protein (FKBP51) near its site of interaction with the steroid receptor proteins. *Journal of Biological Chemistry*, *290*(25), 15746–15757.

Lequin, R. M. (2005). Enzyme immunoassay (EIA)/enzyme-linked immunosorbent assay (ELISA). *Clinical Chemistry*, *51*(12), 2415–2418.

Li, J., Richter, K., & Buchner, J. (2011). Mixed Hsp90–cochaperone complexes are important for the progression of the reaction cycle. *Nature Structural & Molecular Biology*, *18*(1), 61–66.

Lin, S., He, D., Long, T., Zhang, S., Meng, R., & Chen, P. R. (2014). Genetically encoded cleavable protein photo-cross-linker. *Journal of the American Chemical Society*, *136*(34), 11860–11863.

Liu, C. C., & Schultz, P. G. (2010). Adding new chemistries to the genetic code. *Annual Review of Biochemistry*, *79*, 413–444.

Long, X., Lin, Y., Ortiz-Vega, S., Busch, S., & Avruch, J. (2007). The Rheb switch 2 segment is critical for signaling to target of rapamycin complex 1. *Journal of Biological Chemistry*, *282*(25), 18542–18551.

Lorenz, O. R., Freiburger, L., Rutz, D. A., Krause, M., Zierer, B. K., Alvira, S., Cuéllar, J., Valpuesta, J., Madl, T., Sattler, M., & Buchner, J. (2014). Modulation of the Hsp90 chaperone cycle by a stringent client protein. *Molecular Cell*, https://doi.org/10.1016/j.molcel.2014.02.003

Maeda, K., Habara, M., Kawaguchi, M., Matsumoto, H., Hanaki, S., Masaki, T., Sato, Y., Matsuyama, H., Kunieda, K., & Nakagawa, H. (2022). FKBP51 and FKBP52 regulate androgen receptor dimerization and proliferation in prostate cancer cells. *Molecular Oncology*, *16*(4), 940–956.

Maiarù, M., Tochiki, K. K., Cox, M. B., Annan, L. V., Bell, C. G., Feng, X., Hausch, F., & Géranton, S. M. (2016). The stress regulator FKBP51 drives chronic pain by modulating spinal glucocorticoid signaling. *Science Translational Medicine*, https://doi.org/10.1126/scitranslmed.aab3376

Mayer, M. P., & Le Breton, L. (2015). Hsp90: breaking the symmetry. *Molecular Cell*, *58*(1), 8–20.

McLaughlin, S. H., Sobott, F., Yao, Z., Zhang, W., Nielsen, P. R., Grossmann, J. G., Laue, E. D., Robinson, C. V, & Jackson, S. E. (2006). The cochaperone p23 arrests the Hsp90 ATPase cycle to trap client proteins. *Journal of Molecular Biology*, *356*(3), 746–758.

Meyer, B. K., & Perdew, G. H. (1999). Characterization of the AhR− hsp90− XAP2 core complex and the role of the immunophilin-related protein XAP2 in AhR stabilization. *Biochemistry*, *38*(28), 8907–8917.

Miyata, Y., Chambraud, B., Radanyi, C., Leclerc, J., Lebeau, M.-C., Renoir, J.-M., Shirai, R., Catelli, M.-G., Yahara, I., & Baulieu, E.-E. (1997). Phosphorylation of the immunosuppressant FK506-binding protein FKBP52 by casein kinase II: regulation of HSP90-binding activity of FKBP52. *Proceedings of the National Academy of Sciences*, *94*(26), 14500–14505.

Morishima, Y., Kanelakis, K. C., Murphy, P. J. M., Lowe, E. R., Jenkins, G. J., Osawa, Y., Sunahara, R. K., & Pratt, W. B. (2003). The hsp90 cochaperone p23 is the limiting component of the multiprotein hsp90/hsp70-based chaperone system in vivo where it acts to stabilize the client protein· hsp90 complex. *Journal of Biological Chemistry*, *278*(49), 48754–48763.

Morishima, Y., Murphy, P. J. M., Li, D. P., Sanchez, E. R., & Pratt, W. B. (2000). Stepwise assembly of a glucocorticoid receptor·hsp90 heterocomplex resolves two sequential ATP-dependent events involving first hsp70 and then hsp90 in opening of the steroid binding pocket. *Journal of Biological Chemistry*, https://doi.org/10.1074/jbc.M000434200

Müller, D. R., Schindler, P., Towbin, H., Wirth, U., Voshol, H., Hoving, S., & Steinmetz, M. O. (2001). Isotope-tagged cross-linking reagents. A new tool in mass spectrometric protein interaction analysis. *Analytical Chemistry*, https://doi.org/10.1021/ac001379a

Nair, S. C., Rimerman, R. A., Toran, E. J., Chen, S., Prapapanich, V., Butts, R. N., & Smith, D. F. (1997). Molecular cloning of human FKBP51 and comparisons of immunophilin interactions with Hsp90 and progesterone receptor. *Molecular and Cellular Biology*, *17*(2), 594–603.

Nathan, D. F., & Lindquist, S. (1995). Mutational analysis of Hsp90 function: interactions with a steroid receptor and a protein kinase. *Molecular and Cellular Biology*, *15*(7), 3917–3925.

Nguyen, T. A., Cigler, M., & Lang, K. (2018). Expanding the Genetic Code to Study Protein–Protein Interactions. *Angewandte Chemie - International Edition*, *57*(44), 14350–14361.

Ni, L., Yang, C.-S., Gioeli, D., Frierson, H., Toft, D. O., & Paschal, B. M. (2010). FKBP51 promotes assembly of the Hsp90 chaperone complex and regulates androgen receptor signaling in prostate cancer cells. *Molecular and Cellular Biology*, *30*(5), 1243–1253.

Noddings, C. M., Johnson, J. L., & Agard, D. A. (2023). Cryo-EM reveals how Hsp90 and FKBP immunophilins co-regulate the Glucocorticoid Receptor. *BioRxiv*, 2023.01.10.523504. https://doi.org/10.1101/2023.01.10.523504

Noddings, C. M., Wang, R. Y.-R., Johnson, J. L., & Agard, D. A. (2022). Structure of Hsp90–p23–GR reveals the Hsp90 client-remodelling mechanism. *Nature*, *601*(7893), 465–469.

O'Leary III, J. C., Dharia, S., Blair, L. J., Brady, S., Johnson, A. G., Peters, M., Cheung-Flynn, J., Cox, M. B., de Erausquin, G., & Weeber, E. J. (2011). A new anti-depressive strategy for the elderly: ablation of FKBP5/FKBP51. *PloS One*, *6*(9), e24840.

Oroz, J., Chang, B. J., Wysoczanski, P., Lee, C. T., Pérez-Lara, Á., Chakraborty, P., Hofele, R. V., Baker, J. D., Blair, L. J., Biernat, J., Urlaub, H., Mandelkow, E., Dickey, C. A., & Zweckstetter, M. (2018). Structure and pro-toxic mechanism of the human Hsp90/PPIase/Tau complex. *Nature Communications*, https://doi.org/10.1038/s41467-018-06880-0

Owens-Grillo, J. K., Hoffmann, K., Hutchison, K. A., Yem, A. W., Deibel, M. R., Handschumacher, R. E., & Pratt, W. B. (1995). The Cyclosporin A-binding Immunophilin CyP-40 and the FK506-binding Immunophilin hsp56 Bind to a Common Site on hsp90 and Exist in Independent Cytosolic Heterocomplexes with the Untransformed Glucocorticoid Receptor. *Journal of Biological Chemistry*, *270*(35), 20479–20484.

Periyasamy, S., Hinds, T., Shemshedini, L., Shou, W., & Sanchez, E. R. (2010). FKBP51 and Cyp40 are positive regulators of androgen-dependent prostate cancer cell growth and the targets of FK506 and cyclosporin A. *Oncogene*, *29*(11), 1691–1701.

Pettelkau, J., Ihling, C. H., Frohberg, P., Van Werven, L., Jahn, O., & Sinz, A. (2014). Reliable identification of cross-linked products in protein interaction studies by 13C-labeled p-benzoylphenylalanine. *Journal of the American Society for Mass Spectrometry*, https://doi.org/10.1007/s13361-014-0944-6

Picard, D., Khursheed, B., Garabedian, M. J., Fortin, M. G., Lindquist, S., & Yamamoto, K. R. (1990). Reduced levels of hsp90 compromise steroid receptor action in vivo. *Nature*, https://doi.org/10.1038/348166a0

Piotrowski, C., & Sinz, A. (2018). Structural investigation of proteins and protein complexes by chemical cross-linking/mass spectrometry. *Integrative Structural Biology with Hybrid Methods*, 101–121.

Pratt, W B, Morishima, Y., Murphy, M., & Harrell, M. (2006). Chaperoning of glucocorticoid receptors. In *Molecular Chaperones in Health and Disease* (pp. 111–138). Springer.

Pratt, William B, & Toft, D. O. (1997). Steroid receptor interactions with heat shock protein and immunophilin chaperones. *Endocrine Reviews*, *18*(3), 306–360.

Prodromou, C., & Bjorklund, D. M. (2022). Advances towards Understanding the Mechanism of Action of the Hsp90 Complex. *Biomolecules*, *12*(5), 600.

Prodromou, C., Panaretou, B., Chohan, S., Siligardi, G., O'Brien, R., Ladbury, J. E., Roe, S. M., Piper, P. W., & Pearl, L. H. (2000). The ATPase cycle of Hsp90 drives a molecular 'clamp'via transient dimerization of the N-terminal domains. *The EMBO Journal*, *19*(16), 4383–4392.

Püllmann, P., Ulpinnis, C., Marillonnet, S., Gruetzner, R., Neumann, S., & Weissenborn, M. J. (2019). Golden Mutagenesis: An efficient multi-site-saturation mutagenesis approach by Golden Gate cloning with automated primer design. *Scientific Reports*, https://doi.org/10.1038/s41598-019-47376-1

Rannversson, H., Andersen, J., Sørensen, L., Bang-Andersen, B., Park, M., Huber, T., Sakmar, T. P., & Strømgaard, K. (2016). Genetically encoded photocrosslinkers locate the high-affinity binding site of antidepressant drugs in the human serotonin transporter. *Nature Communications*, *7*(1), 1–9.

Ratajczak, T., & Carrello, A. (1996). Cyclophilin 40 (CyP-40), Mapping of Its hsp90 Binding Domain and Evidence That FKBP52 Competes with CyP-40 for hsp90 Binding (∗). *Journal of Biological Chemistry*, *271*(6), 2961–2965.

Reynolds, P. D., Ruan, Y., Smith, D. F., & Scammell, J. G. (1999). Glucocorticoid resistance in the squirrel monkey is associated with overexpression of the immunophilin FKBP51. *The Journal of Clinical Endocrinology & Metabolism*, *84*(2), 663–669.

Riggs, D. L., Cox, M. B., Tardif, H. L., Hessling, M., Buchner, J., & Smith, D. F. (2007). Noncatalytic role of the FKBP52 peptidyl-prolyl isomerase domain in the regulation of steroid hormone signaling. *Molecular and Cellular Biology*, *27*(24), 8658–8669.

Riggs, D. L., Roberts, P. J., Chirillo, S. C., Cheung-Flynn, J., Prapapanich, V., Ratajczak, T., Gaber, R., Picard, D., & Smith, D. F. (2003). The Hsp90-binding peptidylprolyl isomerase FKBP52 potentiates glucocorticoid signaling in vivo. *The EMBO Journal*, *22*(5), 1158–1167.

Roe, S. M., Prodromou, C., O'Brien, R., Ladbury, J. E., Piper, P. W., & Pearl, L. H. (1999). Structural Basis for Inhibition of the Hsp90 Molecular Chaperone by the Antitumor Antibiotics Radicicol and Geldanamycin. *Journal of Medicinal Chemistry*, *42*(2), 260–266.

Rudolf, S., Kaempf, K., Vu, O., Meiler, J., Beck-Sickinger, A. G., & Coin, I. (2022). Binding of Natural Peptide Ligands to the Neuropeptide Y5 Receptor. *Angewandte Chemie International Edition*, *61*(5), e202108738.

Rulten, S. L., Kinloch, R. A., Tateossian, H., Robinson, C., Gettins, L., & Kay, J. E. (2006). The human FK506-binding proteins: characterization of human FKBP19. *Mammalian Genome*, *17*(4), 322–331.

Ryan, D. P., & Matthews, J. M. (2005). Protein–protein interactions in human disease. *Current opinion in structural biology*, *15*(4), 441-446.

Sabbagh, J. J., O'Leary III, J. C., Blair, L. J., Klengel, T., Nordhues, B. A., Fontaine, S. N., Binder, E. B., & Dickey, C. A. (2014). Age-associated epigenetic upregulation of the FKBP5 gene selectively impairs stress resiliency. *PLoS One*, *9*(9), e107241.

Sabers, C. J., Martin, M. M., Brunn, G. J., Williams, J. M., Dumont, F. J., Wiederrecht, G., & Abraham, R. T. (1995). Isolation of a Protein Target of the FKBP12-Rapamycin Complex in Mammalian Cells (∗). *Journal of Biological Chemistry*, *270*(2), 815–822.

Sakamoto, K., Hayashi, A., Sakamoto, A., Kiga, D., Nakayama, H., Soma, A., Kobayashi, T., Kitabatake, M., Takio, K., & Saito, K. (2002). Site-specific incorporation of an unnatural amino acid into proteins in mammalian cells. *Nucleic Acids Research*, *30*(21), 4692–4699.

Sato, S., Mimasu, S., Sato, A., Hino, N., Sakamoto, K., Umehara, T., & Yokoyama, S. (2011). Crystallographic study of a site-specifically cross-linked protein complex with a genetically incorporated photoreactive amino acid. *Biochemistry*, *50*(2), 250–257.

Scheufler, C., Brinker, A., Bourenkov, G., Pegoraro, S., Moroder, L., Bartunik, H., Hartl, F. U., & Moarefi, I. (2000). Structure of TPR domain–peptide complexes: critical elements in the assembly of the Hsp70–Hsp90 multichaperone machine. *Cell*, *101*(2), 199–210.

Schmidt, M. V., Paez-Pereda, M., Holsboer, F., Hausch, F., Paez-Pereda, M., Holsboer, F., & Hausch, F. (2012). The prospect of FKBP51 as a drug target. *ChemMedChem*, *7*(8), 1351–1359.

Schneider, C., Sepp-Lorenzino, L., Nimmesgern, E., Ouerfelli, O., Danishefsky, S., Rosen, N., & Hartl, F. U. (1996). Pharmacologic shifting of a balance between protein refolding and degradation mediated by Hsp90. *Proceedings of the National Academy of Sciences of the United States of America*, https://doi.org/10.1073/pnas.93.25.14536

Schülke, J.-P., Wochnik, G. M., Lang-Rollin, I., Gassen, N. C., Knapp, R. T., Berning, B., Yassouridis, A., & Rein, T. (2010). Differential impact of tetratricopeptide repeat proteins on the steroid hormone receptors. *PloS One*, *5*(7), e11717.

Schwarz, R., Tänzler, D., Ihling, C. H., Müller, M. Q., Kölbel, K., & Sinz, A. (2013). Monitoring conformational changes in peroxisome proliferator-activated receptor α by a genetically encoded photoamino acid, cross-linking, and mass spectrometry. *Journal of Medicinal Chemistry*, *56*(11), 4252–4263.

Seidel, L., Zarzycka, B., Zaidi, S. A., Katritch, V., & Coin, I. (2017). Structural insight into the activation of a class B G-protein-coupled receptor by peptide hormones in live human cells. *Elife*, *6,* e27711.

Serfling, R., & Coin, I. (2016). Incorporation of unnatural amino acids into proteins expressed in mammalian cells. In *Methods in enzymology* (Vol. 580, pp. 89–107). Elsevier.

Silverstein, A. M., Galigniana, M. D., Kanelakis, K. C., Radanyi, C., Renoir, J.-M., & Pratt, W. B. (1999). Different regions of the immunophilin FKBP52 determine its association with the glucocorticoid receptor, hsp90, and cytoplasmic dynein. *Journal of Biological Chemistry*, *274*(52), 36980–36986.

Sinars, C. R., Cheung-Flynn, J., Rimerman, R. A., Scammell, J. G., Smith, D. F., & Clardy, J. (2003). Structure of the large FK506-binding protein FKBP51, an Hsp90-binding protein and a component of steroid receptor complexes. *Proceedings of the National Academy of Sciences of the United States of America*, *100*(3), 868–873.

Sinha, A., & Mann, M. (2020). A beginner's guide to mass spectrometry–based proteomics. *The Biochemist*, *42*(5), 64–69.

Sivils, J. C., Storer, C. L., Galigniana, M. D., & Cox, M. B. (2011). Regulation of steroid hormone receptor function by the 52-kDa FK506-binding protein (FKBP52). *Current Opinion in Pharmacology*, *11*(4), 314–319.

Smith, D. F., Baggenstoss, B. A., Marion, T. N., & Rimerman, R. A. (1993). Two FKBP-related proteins are associated with progesterone receptor complexes. *Journal of Biological Chemistry*, 268(24), 18365-18371.

Smith, D. F., Faber, L. E., & Toft, D. O. (1990). Purification of unactivated progesterone receptor and identification of novel receptor-associated proteins. *Journal of Biological Chemistry,* 265(7), 3996-4003.

Smith, David F. (1993). Dynamics of heat shock protein 90-progesterone receptor binding and the disactivation loop model for steroid receptor complexes. *Molecular Endocrinology*, *7*(11), 1418–1429.

Smith, David F, & Toft, D. O. (2008). Minireview: the intersection of steroid receptors with molecular chaperones: observations and questions. *Molecular Endocrinology*, *22*(10), 2229–2240.

Stechschulte, L. A., & Sanchez, E. R. (2011). FKBP51—a selective modulator of glucocorticoid and androgen sensitivity. *Current Opinion in Pharmacology*, *11*(4), 332–337.

Steiner, J. P., Dawson, T. M., Fotuhi, M., Glatt, C. E., Snowman, A. M., Cohen, N., & Snyder, S. H. (1992). High brain densities of the immunophilin FKBP colocalized with calcineurin. *Nature*, *358*(6387), 584–587.

Storer, C. L., Dickey, C. A., Galigniana, M. D., Rein, T., & Cox, M. B. (2011). FKBP51 and FKBP52 in signaling and disease. *Trends in Endocrinology & Metabolism*, *22*(12), 481–490.

Sullivan, W. P., Owen, B. A. L., & Toft, D. O. (2002). The influence of ATP and p23 on the conformation of hsp90. *Journal of Biological Chemistry*, *277*(48), 45942–45948.

Takimoto, J. K., Adams, K. L., Xiang, Z., & Wang, L. (2009). Improving orthogonal tRNA-synthetase recognition for efficient unnatural amino acid incorporation and application in mammalian cells. *Molecular BioSystems*, *5*(9), 931–934.

Tanaka, H., Kuroda, A., Marusawa, H., Hatanaka, H., Kino, T., Goto, T., Hashimoto, M., & Taga, T. (1987). Structure of FK506, a novel immunosuppressant isolated from Streptomyces. *Journal of the American Chemical Society*, *109*(16), 5031–5033.

Tanaka, Y., Bond, M. R., & Kohler, J. J. (2008). Photocrosslinkers illuminate interactions in living cells. *Molecular BioSystems*, *4*(6), 473–480.

Touma, C., Gassen, N. C., Herrmann, L., Cheung-Flynn, J., Büll, D. R., Ionescu, I. A., Heinzmann, J.-M., Knapman, A., Siebertz, A., & Depping, A.-M. (2011). FK506 binding protein 5 shapes stress responsiveness: modulation of neuroendocrine reactivity and coping behavior. *Biological Psychiatry*, *70*(10), 928–936.

Van Duyne, G. D., Standaert, R. F., Karplus, P. A., Schreiber, S. L., & Clardy, J. (1991a). Atomic structure of FKBP-FK506, an immunophilin-immunosuppressant complex. *Science*, *252*(5007), 839–842.

Van Duyne, G. D., Standaert, R. F., Schreiber, S. L., & Clardy, J. (1991b). Atomic structure of the rapamycin human immunophilin FKBP-12 complex. *Journal of the American Chemical Society*, *113*(19), 7433–7434.

Venturi, E., Galfré, E., O'Brien, F., Pitt, S. J., Bellamy, S., Sessions, R. B., & Sitsapesan, R. (2014). FKBP12. 6 activates RyR1: investigating the amino acid residues critical for channel modulation. *Biophysical Journal*, *106*(4), 824–833.

Wang, L., Brock, A., Herberich, B., & Schultz, P. G. (2001). Expanding the genetic code of Escherichia coli. *Science*, *292*(5516), 498–500.

Wang, R. Y.-R., Noddings, C. M., Kirschke, E., Myasnikov, A. G., Johnson, J. L., & Agard, D. A. (2022). Structure of Hsp90–Hsp70–Hop–GR reveals the Hsp90 client-loading mechanism. *Nature*, *601*(7893), 460–464.

Wang, W., Takimoto, J. K., Louie, G. V, Baiga, T. J., Noel, J. P., Lee, K.-F., Slesinger, P. A., & Wang, L. (2007). Genetically encoding unnatural amino acids for cellular and neuronal studies. *Nature Neuroscience*, *10*(8), 1063-1072.

Weiss, M. S., Jabs, A., & Hilgenfeld, R. (1998). Peptide bonds revisited. *Nature Structural Biology*, *5*(8), 676.

Wen, Z., Zhang, Y., Zhang, B., Hang, Y., Xu, L., Chen, Y., Xie, Q., Zhao, Q., Zhang, L., & Li, G. (2023). Cryo-EM structure of the cytosolic AhR complex. *Structure*, 31(3) 295-308.

Whitesell, L., Mimnaugh, E. G., De Costa, B., Myers, C. E., & Neckers, L. M. (1994). Inhibition of heat shock protein HSP90-pp60(v-src) heteroprotein complex formation by benzoquinone ansamycins: Essential role for stress proteins in oncogenic transformation. *Proceedings of the National Academy of Sciences of the United States of America*, https://doi.org/10.1073/pnas.91.18.8324

Whitesell, Luke, & Cook, P. (1996). Stable and specific binding of heat shock protein 90 by geldanamycin disrupts glucocorticoid receptor function in intact cells. *Molecular Endocrinology*, https://doi.org/10.1210/me.10.6.705

Wilkins, B. J., Daggett, K. A., & Cropp, T. A. (2008). Peptide mass fingerprinting using isotopically encoded photo-crosslinking amino acids. *Molecular BioSystems*, *4*(9), 934–936.

Wilkins, B. J., Rall, N. A., Ostwal, Y., Kruitwagen, T., Hiragami-Hamada, K., Winkler, M., Barral, Y., Fischle, W., & Neumann, H. (2014). A cascade of histone modifications induces chromatin condensation in mitosis. *Science*, *343*(6166), 77–80.

Wittelsberger, A., Thomas, B. E., Mierke, D. F., & Rosenblatt, M. (2006). Methionine acts as a "magnet" in photoaffinity crosslinking experiments. *FEBS Letters*, *580*(7), 1872–1876.

Wochnik, G. M., Rüegg, J., Abel, G. A., Schmidt, U., Holsboer, F., & Rein, T. (2005). FK506-binding proteins 51 and 52 differentially regulate dynein interaction and nuclear translocation of the glucocorticoid receptor in mammalian cells. *Journal of Biological Chemistry*, *280*(6), 4609–4616.

Wu, B., Li, P., Liu, Y., Ding, Y., Shu, C., Ye, S., Bartlam, M., Shen, B., & Rao, Z. (2004). 3D structure of human FK506-binding protein 52: Implication for the assembly of the glucocorticoid receptor/Hsp90/immunophilin heterocomplex. *Proceedings of the National Academy of Sciences of the United States of America*, https://doi.org/10.1073/pnas.0305969101

Xie, J., & Schultz, P. G. (2006). A chemical toolkit for proteins—an expanded genetic code. *Nature Reviews Molecular Cell Biology*, *7*(10), 775.

Yang, Y., Song, H., He, D., Zhang, S., Dai, S., Lin, S., Meng, R., Wang, C., & Chen, P. R. (2016). Genetically encoded protein photocrosslinker with a transferable mass spectrometry-identifiable label. *Nature Communications*, *7*(1), 1–10.

Zhang, M., Lin, S., Song, X., Liu, J., Fu, Y., Ge, X., Fu, X., Chang, Z., & Chen, P. R. (2011). A genetically incorporated crosslinker reveals chaperone cooperation in acid resistance. *Nature Chemical Biology*, *7*(10), 671–677.

Zhang, Y., Fonslow, B. R., Shan, B., Baek, M.-C., & Yates III, J. R. (2013). Protein analysis by shotgun/bottom-up proteomics. *Chemical Reviews*, *113*(4), 2343–2394.

Ziemianowicz, D. S., Bomgarden, R., Etienne, C., & Schriemer, D. C. (2017). Amino acid insertion frequencies arising from photoproducts generated using aliphatic diazirines. *Journal of the American Society for Mass Spectrometry*, *28*(10), 2011–2021.

6. Materials and methods

6.1. Materials

6.1.1. General chemicals

Acetic acid 99-100% (C. Roth, 7332.2), Adenosin-5'-triphosphat disodium salt (C. Roth, HN35.1), Agar-Agar, Kobe I (C. Roth, 5210.3), Ampicillin sodium salt (C. Roth, K09.5), Bovine Serum Albumin (Sigma, A7030), Brilliant Blue G250 (C. Roth, 9598.1), Charcoal Activated (C. Roth, X865.1), cOmplete Mini Protease inhibitor cocktail (Roche, 11836153001), Coomasie Brilliant Blue R250 (C. Roth, 9598.1), Deoxyribonuclease I from bovine pancreas (DNAse I) (Sigma, DN25-1G), Dexamethasone 21-phosphate disodium salt (dissolved in DMSO, Sigma, D1159), Dimethylsulfoxid (DMSO) (C. Roth, 4720.4), Dithiothreitol (DTT) (C. Roth, 6908.1), di-Potassium hydrogen phosphate (C. Roth, P749.1), Ethanol 70% DAB (C.Roth, 7301.1), Ethanol denatured (C. Roth, K928.4), FK506 Tacrolimus (Beta Pharma, 56-01267), Formaldehyde 37% (C. Roth, 4979.3), Glycerol 86% (C. Roth, 4043.2), Glycine (C. Roth, 3908.2), Hepes (C. Roth, 9105.3), Kanamycin sulphate (C. Roth, T832.1), LB Broth (Luria/Miller) (C. Roth, X968.2), Nonidet® P-40 substitute (VWR Life Science, E109-50mL), Phenymethyl suphonyl fluoride (C. Roth, 6367.2), Ponceau S (C. Roth, 5938.2), Potassium carbonate (Alfa Aesar, A16625.36) Potassium dihydrogen phosphate (C. Roth, 3904.1), Potassium hydroxide (C. Roth, 6751.1), Powdered milk (C. Roth, T145.3), Propan-2-ol (AppliChem, 603-117-00-0), Rapamycin (Alfa Aesar, J62473), Rotiophorese® Gel 30 (37.5:1) (C. Roth, 3029.1), SDS (C. Roth, 0183.3), Silver nitrate (C. Roth, 9370.1), Sodium Chloride (C. Roth), TEMED (C. Roth, 2367.3), tetra-Sodium pyrophosphate decahydrate (Na_4PP_i) (Fluka, 71515), Sodium thiosulfate (Sigma Aldrich, 217263), Trichloroacetic acid (C. Roth, 8789.2), TRIS (C. Roth, 4855.2), TRIS hydrochloride (C. Roth, 9090.3), Triton X-100 (C. Roth, 3051.4), Tween 20 (C. Roth, 9127.2)

6.1.2. General plastics and materials

Eppendorf Tubes 5.0 mL (Eppendorf, 0030119401), Micro tube 1.5 mL (Sarstedt, 72.690.001), Microtube 1.5 mL protein LB (Sarstedt, 72.706.600), Micro tube 2.0 mL (Sarstedt, 72.691), Micro tube 2.0 mL LB (Sarstedt, 72.695.600), Pipette Tips – various volumes (Sarstedt), ProteinLoBind Tubes 5.0 mL (Eppendorf, 003010832), white 96 well half-area plate (Greiner bio-one, 392-0287), gel drying frame and cellophane (C. Roth), Amersham™ Protran™ 0.2 μm

Nitrocellulose (GE Healthcare Life Sciences, 10600001), Rotilabo®-Blottingpapiere, 0.35 mm (C. Roth, CL65.1)

6.1.3. Cell culture plastics

TC Dish 100 Standard (Sarstedt 83.3902), Combitips advanced 1.0 mL (Eppendorf BIOPUR 0030 089.642), Combitips advanced 5 mL (Eppendorf BIOPUR 0030 089.669), CryoPure Tubes 1.8 mL white (Sarstedt, 72.379), TC Testplate 96F (TPP, 92096), TC Plate 24 Well Standard F (Sarstedt, 83.3922.005), 12 Well Cell Culture Plate (Greiner bio-one, 665 180), TC – Plate sterile with lid single packed (Greiner bio-one, 657 160)

6.1.4. Devices

Biofuge Pico (Heraeus), Biometra TAdvanced Twin 48, 230 V (Analytic Jena), Electrophorese Powersupply (EPS series, Amersham), CVC 3000 Vacuum pump (vacuubrand), DS11+ Spectrophotometer (Denovix), Duomax 1030 and Polymax 1040 (Heidolph), EMB500-1 scale (KERN), IKA Kombimak REO stirring device, RM5 Rollenmischgerät, Light Microscope WILOVERT S (hund), Microwave (Samsung), Mixing Block MB-102 (BIOER) Multichannel Pipette 8 – 100 μL (Eppendorf), Pipette Matrix Multichannel 16 – 125 μL (Thermo Scientific), Pipettes – various volumes (Gilson), Reax 1 Vortexer (Heidolph), Rotilabo-Block-Heater H250 (Roth), RS-T170S Rollenmischgerät (PHOENIX Instrument), Sartorius Analytic Scale, Sprout Minifuge (Biozym), Tecan (GENiosPro or SPARKS) Waterbath-GFL-Typ-1002

6.1.5. Software

Microsoft Office 360, GraphPad Prism9, Biorander, Xcalibur Version 2.0 and 4.1, MaxQuant 2.0.1.0, MeroX 2.0, Pymol 2.4.2.

6.1.6. Antibodies

Name	Species	Dilution	Manufacturer
FLAG (HRP), A8592	Mono, mouse	1:5000 in 5% BSA in TBS	Sigma-Aldrich
HA (HRP)	Mono, rat	1:2000 in 5% milk in TBS	Roche
HIS (HRP), (27E8)	Mouse	1:1000 in 5% milk in TBS	CST
Hsp90AA1/AB1 MAB6457	Poly, mouse	1:1000 in 5% milk in TBS	Abnova
Hsp70 (C92F3A-5) SC66048	Mono, mouse	1:1000 in 5% milk in TBS	Santa Cruz Biotechnology
p23, JJ6, SC101496 (HRP)	Mono, mouse	1:1000 in 5% milk in TBS	Santa Cruz Biotechnology
HOP (DS14F5)	Mouse	1:1000 in 5% milk in TBS	Novus
Mouse (HRP) (7076S)	Poly, goat	1:1000 in 5% milk in TBS	CST

6.2. Generation of the TAG library by Golden Gate reaction

For generation different TAG mutants of FKBP51 and Glucocorticoid receptor, a TAG amber stop codon is cloned at the desired portion within the gene by Golden Mutagenesis (Püllmann et al., 2019). Mutant specific primers were designed with the webtool https://msbi.ipb-halle.de/GoldenMutagenesisWeb/.

6.2.1. PCR

The first step of Golden mutagenesis is the generation of two PCR fragments. The PCR was done in 96 well format with a final volume of 30 μL or single tubes with a final volume of 25 μL. Therefore, a reaction mix containing 5 μL of template plasmid DNA (HP 709 pBlueScript_FKBP51_FLAG for FKBP51 or HP 1504 pRK5 HA-GR BSA ex for glucocorticoid receptor, 10 ng/μL), 5 μL dNTPs (NEB N0447S, 200 μM), 1× Q5 buffer (NEB B9027S) and 0.5 μL Q5 polymerase (HF NEB M0491S, 2000 U/mL) was prepared. For generating the first fragment 5 μL of N- or C-terminal forward primer (HP921 for FKBP51 or HP 1781 or 1783 for

GR, 10 μM) and 5 μL of the mutant specific reverse primer (100 μM) were used. For generating the second fragment 5 μL N- or C-terminal reverse primer (HP922 for FKBP51 or HP 1782 or 1784 for GR, 100 μM) as well as 5 μL of the mutant specific forward primer (10 μM) were added.

Table 3: PCR program.

program	
1. 95 °C	2:00
2. 95 °C (cyclic denaturation)	0:45
3. 56 °C (annealing)	0:30
4. 72 °C (extending)	2:30
5. Repeat 2-4 30×	
6. 72 °C	5:00
7. 4 °C	∞

To analyze the samples an agarose gel electrophoresis was performed, followed by a PCR Clean Up in 96 well format or single tube format.

6.2.2. Agarose gel electrophoresis

For analysis by gel electrophoresis an 0.5% Agarose gel was prepared (0.5% w/w Agarose in 150 mL 1× TAE buffer with 15 μL Midori Green Advance DNA Stain) (Nippon Genetics Europe GmbH MG03). A sample of 5 μL of the PCR product was mixed with 1 μL 6×Gel loading Dye Purple (NEB B7024S) and loaded onto the gel. A sample of 4 μL 1 kBp DNA Ladder (NEB N0468S) was used as ladder. The gel was running for 45 min at 120 V in TAE buffer.

6.2.3. Golden Gate reaction

Golden Gate reaction was carried out in a final volume of 15 μL. A reaction mix containing the PCR Fragment 1 and Fragment 2 generated in 3.1.2, 0.3 μL of the Golden Gate Vector (HG 1467 or 1495, 760 ng/μL), was adjusted to a volume of 12 μL with MilliQ water. Additionally, 1 μL T4 Ligase (NEB M0202S, lot: 10024947), 1.5 μL 10× concentrated T4 ligase buffer and 0.5 μL Esp3I for FKBP51 or BSA HFv2 for GR was added. Reaction was performed in a thermos cycler using the following program

Table 4: Program for Golden Gate reaction.

program	
1. 37 °C	3:00
2. 16 °C	3:00
3. Repeat 1–2 30×	
4. 37 °C	3:00
5. 80 °C	20:00

Golden Gate reaction was used for transformation.

6.2.4. Transformation

An aliquot of 50 μL chemically competent *Escherichia coli* DH5α cells were thawed on ice. 15 μL of the Golden Gate reaction mixture, generated in 6.2.3, were added to the aliquot and incubated on ice for 30 min. Cells were heat shocked at 42 °C for 45 s followed by an incubation for 2 min on ice. 500 μL SOC medium were added and cells were shaken at 37 °C for 1 h. After incubation, 100 μL of transformed cells were plated into a well of a 6 well plate that is covered by LB agar containing 100 μg/mL ampicillin + 125 μM IPTG + 66 μg/mL X-Gal. Agar plates were then incubated overnight at 37 °C. The correct insertion of TAG mutation was verified by overnight sequencing by *E. coli* NightSeq from Microsynth Seqlab GmbH Göttingen. For generating glycerol stocks of bacterial culture, 1 mL culture was added to 500 μL 5% glycerol and stored at −80°C.

6.2.5. Plasmid DNA isolation

White colonies were picked (alternatively a bacterial cryo stock was used as inoculum) and transferred in 6 mL TB-medium with 100 ng/mL kanamycin or with 100 ng/mL ampicillin and incubated overnight at 37 °C. The plasmids were then extracted using High Copy Plasmid protocol of FastGene Plasmid Mini Kit (Nippon Genetics) or the QIAquick 96 PCR Purification Kit. Concentration was measured with NanoDrop and adjusted to 100 ng/μL. For larger plasmid DNA extraction 6 mL inoculated TB-medium with 100 ng/mL kanamycin or with 100 ng/mL ampicillin was used a preculture for a 50 mL TB-medium with 100 ng/mL kanamycin or with 100 ng/mL ampicillin culture which was incubated overnight at 37 °C. The plasmids were then extracted using a Medi-Prep Kit (Invitrogen)

6.2.6. Production of the FKBP51 TAG Twin Strep FLAG library

FKBP51 TAG mutants were clone into a pEGFP-C1 based Golden Gate vector with a C-terminal twin Strep FLAG tag (Gloeckner et al., 2009) (HP 1467). The cloning was performed using a Golden Gate approach and the FKBP51 TAG library as template. Therefore, one fragment was generated not two, for the rest the procedure the Golden Gate mutagenesis was the same as described in 6.2.

6.3. Cell culture

Cell culture experiments were performed with Human embryonic kidney (HEK) 293 cells that were cultured in Dulbecco's modified Eagle's medium (DMEM) with 10% fetal bovine serum (FBS) and 1% penicillin-streptomycin solution at 37 °C with 5% CO_2. All incubation steps took place in a HERAcell 160vi (ThermoFisher) at 37 °C and 5% CO_2 or CellXpert C170i (Eppendorf) 37 °C and 5% CO_2. All work was performed using sterility guidelines. Cell culturing and cellular assays were generally accompanied by the observation of the cells via light microscopy to assure confluency, cell shape, surface effects and the absence of contaminations.

6.3.1. Growth condition and cell passaging

Cells were grown in 10 cm TC-dishes for 3 to 4 days. For passaging, the cell culture media was aspirated and the cells were washed with 5 mL prewarmed PBS. 1 mL of prewarmed Trypsin-EDTA solution was added and equally distributed on the surface. The dish was placed in the incubator for 5 min. Cells were removed from the surface by resuspension in 5 mL culture media and spun down for 2 min at 1000 rpm. The supernatant was removed and cells were resuspended with 5 mL culture growth media. 250 μL of this suspension were added to 10 mL cell culture media in a fresh 10 cm TC plate.

6.3.2. Cell counting

For seeding cells were first counted to ensure experimental stability. For the cell suspension obtained in 6.3.1 10 μL of cells and 10 μL Trypan Blue solution were mixed in a tube. 10 μL were then transferred to a Neubauer Counting Chamber (Marienfeld). All non-blue cells in the four major quadrants were counted. Cell count in resuspension was calculated: 1 Neubauer count ≙ 5,000 cells / mL in the primary resuspension.

6.3.3. Cell culture plate coating

Cell culture dishes and multiwell plates used for assays were coated with poly-L-Lysine (PLL, 0.002%(v/v), 1:50 dilution in water). Half of the volume of the recommended culture volume was added to each cavity and placed in the incubator for 2 h up to 24 h. Afterwards, the solution was removed and all cavities were washed with an equal amount of water. Plates were dried in a sterile bank for 1 h and stored tape sealed at 4 °C until usage. Surface coating was performed for all cell culture assay experiments.

6.3.4. Amber suppression of FKBP51 mutants

In a poly-L-lysine coated 10 cm plate, 12 well plate or 96 well plate 1.5 million, 100.000 or 10.000 human embryonic kidney (HEK) 293 cells were seeded and cultured in Dulbecco's modified Eagle's medium (DEMEM) with 10 % fetal bovine serum (FBS) and 1% penicillin-streptomycin solution at 37°C with 5% CO_2 overnight. According to Lipofectamin 2000 cell transfection protocol, two mixtures were prepared. The first one contains a specific amount of Opti-MEM (0.5×volume of the transfection mix), plasmid DNA encoding for the FKBP51 TAG mutant either pTarget based or pCAG based, plasmid DNA encoding for (para-(benzoyl)-phenylalanine (pBpa) synthetase (HP 761) + the tRNA cassette and depending on the experiment plasmid DNA encoding for HA-tagged GR (HP124) or not. The second mixture contains Opti-MEM and Lipofectamin 2000 (volume of Lipofectamin2000: number of wells × 50 μL/48 × 0.8). Both mixtures were incubated at least for 5 min, mixed together (1:1) and were incubated for 25 min. Cell media was discarded and 80% fresh media containing 500 μM para-(benzoyl)-phenylalanine (50 mM in 100 mM NaOH, sterile filtered) as well as the prepared transfection mix was added. Cells were incubated for 42 h at 37 °C and 5% CO_2.

6.3.5. Amber suppression with isotopically labelled pBpa

In 2× poly-L-lysine coated 10 cm plate, 1.5 million human embryonic kidney (HEK) 293 cells were seeded each and cultured in Dulbecco's modified Eagle's medium (DEMEM) with 10 % fetal bovine serum (FBS) and 1% penicillin-streptomycin solution at 37 °C with 5% CO_2 overnight. According to Lipofectamin 2000 cell transfection protocol, two mixtures were prepared. For the isolation of FKBP51-Hsp90 crosslinks, the first one contains a specific amount of Opti-MEM (0.5×volume of the transfection mix), plasmid DNA encoding for the FKBP51 A398TAG (HP802) or M412TAG (HP927), plasmid DNA encoding for (para-(benzoyl)-

phenylalanine (pBpa) synthetase (HP 761. The second mixture contains Opti-MEM and Lipofectamin 2000 (volume of Lipofectamin2000: number of wells × 50 μL/48 × 0.8). Both mixtures were incubated at least for 5 min, mixed together (1:1) and were incubated for 25 min.

For the isolation of FKBP51-GR crosslink, the first one contains a specific amount of Opti-MEM (0.5×volume of the transfection mix), plasmid DNA encoding for the FKBP51 E75TAG (HP894), plasmid DNA encoding for (para-(benzoyl)-phenylalanine (pBpa) synthetase (HP 761, p_NEU_EBpaRS_4xBstYam, CMV promoter controlled enhanced pBpaRS and four copies of U6-BstYam expression cassettes (kind gift of Irene Coin, Leipzig) and the plasmid encoding HA-GR (HP124). The second mixture contains Opti-MEM and Lipofectamin 2000 (volume of Lipofectamin2000: number of wells × 50 μL/48 × 0.8). Both mixtures were incubated at least for 5 min, mixed together (1:1) and were incubated for 25 min. Cell media was discarded and 80% fresh media containing 250 μM *para*-(benzoyl)-phenylalanine (50 mM in 100 mM NaOH, sterile filtered) and 250 μM $^{13}C_6$ labelled *para*-(benzoyl)-phenylalanine (synthesized by Tim Heymann, The250, 50 mM in 100 mM NaOH, sterile filtered) as well as the prepared transfection mix was added. Cells were incubated for 42 h at 37 °C and 5% CO_2.

6.3.6. Amber suppression of glucocorticoid receptor mutants

In a poly-L-lysine coated 10 cm plate, 12 well plate or 96 well plate 2 million, 200.000 or 20.000 Human embryonic kidney (HEK) 293 cells were seeded and cultured in Dulbecco's modified Eagle's medium (DEMEM) with 10 % fetal bovine serum (FBS) and 1% penicillin-streptomycin solution at 37 °C with 5% CO_2 overnight. According to Lipofectamin 2000 cell transfection protocol, two mixtures were prepared. The first one contains a specific amount of Opti-MEM (0.5×volume of the transfection mix), plasmid DNA encoding for the SF GR TAG mutant, plasmid DNA encoding for (para-(benzoyl)-phenylalanine (pBpa) synthetase (HP 761) and depending on the experiment plasmid DNA encoding for HA-tagged FKBP51 (Tab.3).

Table 5: Amount of plasmid DNA for transfection in 10 cm plate, 12 well plate and 96 well plate.

	10 cm plate	12 well plate	96 well plate
SF TAG mutant plasmid DNA	2000 ng	200 ng	20 ng
Synthetase plasmid DNA	4000 ng	400 ng	40 ng
FKBP51-HA plasmid DNA	2000 ng	200 ng	20 ng
Optimen	1000 μL	100 μL	10 μL

The second mixture contains Opti-MEM and Lipofectamin 2000 (volume of Lipofectamin 2000: number of wells × 50 μL/48 × 0.8). Both mixtures were incubated at least for 5 min, mixed together (1:1) and were incubated for 25 min. Cell media was discarded and 80% fresh media containing 500 μM para-(benzoyl)-phenylalanine (50 mM in 100 mM NaOH, sterile filtered) as well as the prepared transfection mix was added. Cells were incubated for 42 h at 37 °C and 5% CO_2.

6.3.7. UV crosslinking and cell lysis

Cell medium was discarded and cells in a 10 cm plate were washed with 10 mL PBS. For UV treatment PBS were discarded and 1 mL fresh PBS were added. Cells in 12 well or 96 well plates were not washed. Here, 100 μL or 10 μL PBS were added before UV treatment. For UV crosslinking, plates were placed on ice under UV lamp (2× 15W, Conso VL-215.L) and irradiate with 365 nm for 30 min or 0 min. For cell lysis, PBS was discarded and either 70 μL (96 well plate), 100 μL (12 well plate) or 1000 μL (10 cm plate) NETN buffer + PMSF (1 mM) was added. Cells were shaken on ice for 1h, afterwards scratched from the well, transferred to a 1.5 mL tube and centrifugated for 15 min at 15.000 rpm.

6.4. Western blot

For SDS Page, 20 μL 4× Lämmli buffer were added to 50 μL cell lysate and heated for 5 min at 95°C. 15 μL were loaded onto an 8% SDS-PAGE gel. Gel was running for 90 min at 150 V and afterwards transferred into a blotting chamber (30 V for 75 min). The membrane was then blocked with 5% milk powder in 1×TBS buffer for 30 min at rt and incubated in the antibody solution (Anti-FLAG 1:1000, Sigma A8592-.2MG, monoclonal ANTI-FLAG M" Peroxidase, lot 059K6059) in 5% BSA 0.5% Tween or Anti-HA (1:1000, Roche, rat 12 013 819 001) overnight at 4°C. Washing was performed by incubation for 5 min in TBS, 5 min in in 1×TBS/0.1% Tween and again 5 min in 1×TBS. For imaging, samples were treated with 1 mL ECS solution (Millipore, P90720, 1:1).

6.5. Immunoprecipitation

Anti-FLAG M2 Magnetic beats (Sigma Aldrich, M8823) were used for FLAG immunoprecipitation. For 1000 μL cell lysate from 6.3.7 50 μL magnetic beats were prepared as recommended in the technical bulletin, in short magnetic beats were washed 2× with 1000 μL 1×TBS buffer. Cell lysate was incubated with the beads for overnight at 4°C on a roller

shaker. The beats were washed 1× 1000 µL TBS, 1× 1000 µL TBS + 0.1% Tween, 1× 1000 µL TBS. FLAG tagged protein was eluted with 150 µL 3× FLAG peptide (Sigma Aldrich, F4799) or 2× 250 µL for 6.8. Samples were analyzed by Western blot 6.4.

6.6. Coomassie staining and gel drying

SDS-page gels, which were not transferred for Western Blotting, were stained in Coomassie stainer (40% v/v ethanol, 10% v/v acetic acid, 1 g/L Coomasie Brilliant Blue R250) for at least 15 min. Destaining was performed in two steps: 1) at least 30 min in destaining solution (40% v/v ethanol, 10% v/v acetic acid) and 2) in water at 4 °C overnight. Optionally, gels were dried for at least two days in cellophane using a gel drying frame.

6.7. Size exclusion chromatography

After immunoprecipitation, usually cell lysate of 2×10cm plate eluted with 2× 250 µL, elute was concentrated using spin column to 50 µL and 3× washed with 150 mM sodium phosphate (pH 7.0). For size exclusion chromatography a HPLC system Agilent 1260, column: AdvanceBio 300A, 2.7 µm Serial no 0006436100-23 was used and the column was primed with MilliQ water with a flow rate of 200 µL/min for 15 min and 300 µL/min with freshly prepared 150 mM sodium phosphate (pH 7.0) for 30 min. The system was operated with a flow rate of 300 µL/min with freshly prepared 150 mM sodium phosphate (pH 7.0) and fraction collector was set to 100 µL fraction in 96 well plate Greiner white round bottom constant collecting. 10 µL sample was injected and a 12 min run was performed.

6.8. Sample preparation for mass spectrometry analysis

6.8.1. SDS PAGE

After immunoprecipitation, usually cell lysate of 2×10cm plate eluted with 2× 250 µL, elute was concentrated using spin column to 30 µL and 15 µL Lämmli buffer was added for denaturation and sample was boiled at 95°C for 5 min. Reduced with 10 mM TECP (0.5 M stock) at 56°C for 30 min. Alkylated for 30 min in the dark with 40 mM chloroacetamide (Stock 0.5 M). Sample was boiled at 95°C for 5 min. Samples was added to an 8% SDS PAGE for 90 min at 150 V. For SDS PAGE Coomassie staining 6.6 was performed. Bands were cut out into small pieces (1−2 mm^3), transferred into a 1.5 mL tube and in gel digest was performed.

6.8.2. In gel digest

Prepared gel pieces were washed 3× with 200 µL 50 mM ammonium bicarbonate (ABC)/ 40% acetonitrile, dehydrated for 10 min with 150 µL 100% acetonitrile and dried for 10 min. 10 µL of 12.5 ng/µL Trypsin (Pierres) in 50 mM ABC was added. Gel pieces were swelled for 30 min at 4°C and 25 µL 50 mM ABC was added to cover the pieces completely with buffer. Gel pieces were incubated overnight at 37°C.

6.8.3. Peptide isolation

To the digested gel pieces 50 µL 50% isopropanol/ 0.5% TFA was added and shaken for 30 min at rt. The supernatant was transferred into a 1.5 mL low binding tube (Eppendorf). To the gel pieces 40 µL 50% isopropanol/ 0.5% TFA was added and shaken for 30 min at rt. The supernatant was removed and pool with the supernatant from above. To the gel pieces 20 µL pure isopropanol with 1% TFA was added and shaken for 30 min at rt. The supernatant was removed and pool with the supernatant from above. The supernatant was added to StageTips (IBA) and centrifuged at 2000 rpm until all liquid has passed. 200 µL pure isopropanol with 1% TFA was added and centrifuged at 2000 rpm until all liquid has passed.
200 µL MilliQ water with 0.2% TFA was added and centrifuged at 2000 rpm until all liquid has passed.
Peptides were eluted with 50 µL 80% acetonitrile with 1.25% ammonia and centrifuged at 2000 rpm until all liquid has passed. The solvent was removed by speed-vac (Eppendorf) to dryness.

6.8.4. Mass spectrometry analysis at the Munch Group in Frankfurt

Mass spectrometry analysis was carried out by Dr. Georg Tascher by the following protocol: Peptides were resuspended in 0.1% formic acid and separated on an Easy nanoLC 1200 (ThermoFisher Scientific) and a 40-cm-long, 75-µm-inner-diameter fused-silica column, which had been packed in house with 1.9-µm C18 particles (ReproSil-Pur, Dr. Maisch), and kept at 45 °C using an integrated column oven (Sonation). Peptides were eluted by a nonlinear gradient from 5–38% acetonitrile over 120 min and directly sprayed into a QExactive HF mass spectrometer equipped with a nanoFlex ion source (ThermoFisher Scientific) at a spray voltage of 2.3 kV. Full-scan MS spectra (350–1,400 *m/z*) were acquired at a resolution of 120,000 at *m/z* 200, a maximum injection time of 100 ms and an AGC target value of 3×10^6. Up to 20

most intense peptides per full scan were isolated using a 1 Th window and fragmented using higher-energy collisional dissociation (normalized collision energy of 35). MS/MS spectra were acquired with a resolution of 45,000 at *m/z* 200, a maximum injection time of 80 ms and an AGC target value of 1×10^5. Ions with charge states of 1 and >6 as well as ions with unassigned charge states were not considered for fragmentation. Dynamic exclusion was set to 20 s to minimize repeated sequencing of already acquired precursors. The raw data were analyzed using MaxQuant version 2.0.1 using the Swiss-Prot data base with the default settings. Fixed modifications were set as carbamidomethyl at cysteine residues and methionine oxidation as static modification.

6.8.5. Data analysis

Raw data files were converted to mzXML files using ProteoWizard 3.0.18199 and subjected to MeroX (Götze et al., 2011) version 2.0 analysis for the identification of crosslinked peptides. MS/MS spectra were matched with FKBP51, Hsp90, or the GR, using the following parameters: full trypsin digest with maximum 2 missed cleavages, static modification carbamidomethylation of cysteine, as well as dynamic modification oxidation of methionine, acetylation of protein N-terminus and phosphorylation of serine, threonine and tyrosine. Precursor mass tolerance was 10 ppm and product ions fragment ion tolerance were 15 ppm.

6.8.6. In-house mass spectrometry analysis

Peptides were resuspended in 10 μL 2% acetonitrile with 0.1% formic acid. For bottom-up proteomics measurements a LTQ Orbitrap XL was used. The mass spectrometer is operated in a data dependent top 10 mode, performing one precursor scan at a resolution of 60000 at 400 *m/z* with maximum injection time of 500 ms and the AGC is set to 1×10^6, followed by 10 data dependent CID scans of the ten most intense ions in the ion trap with a maximum injection time of 100 ms and the AGC is set to 1×10^4. Samples are then analyzed by using an in-house bomb loaded capillary with ReproSil-pur C18 1.9 μm silica column with a tapered tip provided by MS Wil with an easy nLC1200 system using a 90 min gradient starting at 0% B to 40% B in 50 min to a 60 % B in 20 min and then to 100% B in 10 min followed by a 10 min hold at 100% B. The column is equilibrated with 3 μl pure A and sample was loaded at a constant pressure of 500 bar. Solvent A consists of water with 2% acetonitrile and 0.1 % formic acid and solvent B consists of 80 % acetonitrile, 20 % water and 0.1 % formic acid. For the nanoLC an in-house built nano ion source is used where a high voltage of 2 kV is applied to the T-union connecting

the LC to the analytical column. The mass spectrometer is controlled using Xcalibur version 2.1 and the nanoLC is controlled using Xcalibur 4.2. The raw data were analyzed using MaxQuant version 2.0.1 using the Swiss-Prot data base with the default settings. Fixed modifications were set as carbamidomethyl at cysteine residues and methionine oxidation as static modification.

6.9. Silver staining

Silver staining was carried out using the "Short" Silver Nitrate Staining from Chevallet *et al.* 2006 (Chevallet et al., 2006). 20 μL of each sample from 6.3.7 was mix with 5 μL Lämmli buffer and 20 μL were loaded onto 12 comb 8% SDS-PAGE freshly casted. 5 μL unstained marker A26630 Thermo 1:50 were used as molecular marker. Gel was running for 90 min at 150 V. All used staining boxes were rinsed with MilliQ-H_2O, all new boxes were rinsed with acetone, 70% EtOH and MP-H_2O. For fixation, the gel was treated with fixation solution 30% (v/v) EtOH/ 10% (v/v) acetic acid 3× 30 min and incubated overnight in fixation solution. For washing, the gel was rinsed 2× in 20% (v/v) EtOH for 10 min and 2× in MilliQ-H_2O for 10 min. For sensitizing, the gel was soaked 1 min in 0.8 mM $Na_2S_2O_3$ for 1 min and washed 2× in MilliQ-H_2O for 1 min. For impregnating, the gel was soaked in 12 mM $AgNO_3$. For development, the gel was taken out of the silver nitrate bath, dip in a water bath for 10 s and transfer it into the basic developer solution 3% (w/v) K_2CO_3, 0.25‰ Formalin, 0.125‰ of a 10% (w/v) $Na_2S_2O_3$ solution. When the desired staining degree was achieved, the gel was transferred into the stop solution 4% (w/v) Tris, 2% (v/v) acetic acid for 45 min.

6.10. ELISA

6.10.1. ELISA coating

ELISA plates (Maxisorp, 96 well plate, Nunc from Invitrogen, M9410-1CS) were coated by diluting 1.5 ng/μL or 7.5 ng/μL Streptactin (IBA, lot:1204-0031) in 1×PBS. 100 μL were added to each well and the plates incubated at 4°C overnight. Plates were washed 4× with 200 μL in 1×PBS/0.05% Tween20 (ELISA washer: BioTek ELx405 Select CW) and blocked with 100 or 200 μL of 5% milk powder in 1×TBS at 4°C overnight. Plates were washed 4× with 200 μL PBS/0.05% Tween20 (ELISA washer: BioTek ELx405 Select CW) and plates were stored at 4°C.

6.10.2.ELISA

For ELISA, first 70 μL PBS were added to each well then30 μl of cell lysate according to 6.3.7 were added and the plate was incubated at 4° C overnight. ELISA plates were washed with ELISA washer 4× with 200 μL 1×PBS/0.05% Tween20. Then, 100 μL antibody solution (1:2000 anti-FLAG in BSA in 1×TBST, 1:1000 anti-HA in 1×PBS) were added and the plate was incubated for 2 h at rt. Plates were again washed 4× with 200 μL in 1×PBS/0.05% Tween20 and 100 μL TMB substrate were added. After 10 min incubation in the dark, enzymatic reaction were stopped by adding 100 μL 0.18 M H_2SO_4. Absorption was measured at 450 nm and 465 nm (Genius Pro Tecan, Infinite M1000). Data were analyzed by GraphPad Prism 9.

7. Extended Figures

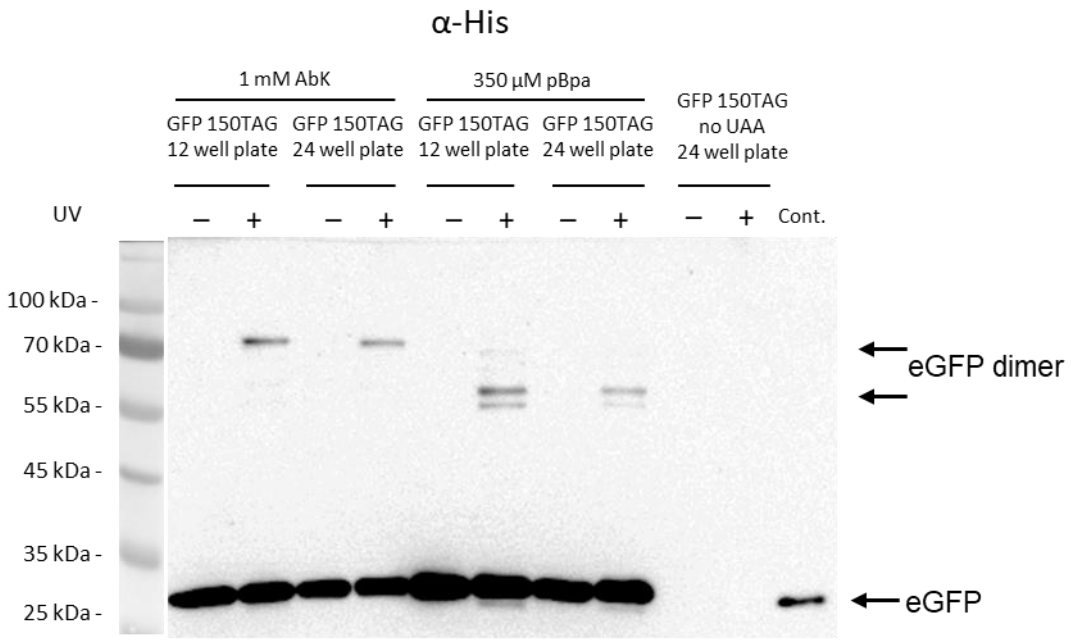

Extended Figure 1. Incorporation experiments to test both AbK and pBpa for amber suppression using the eGFP G150TAG mutant. Cont. = eGFP WT. Two different plate sizes were tested, amber suppression in 12 well and 24 well.

A

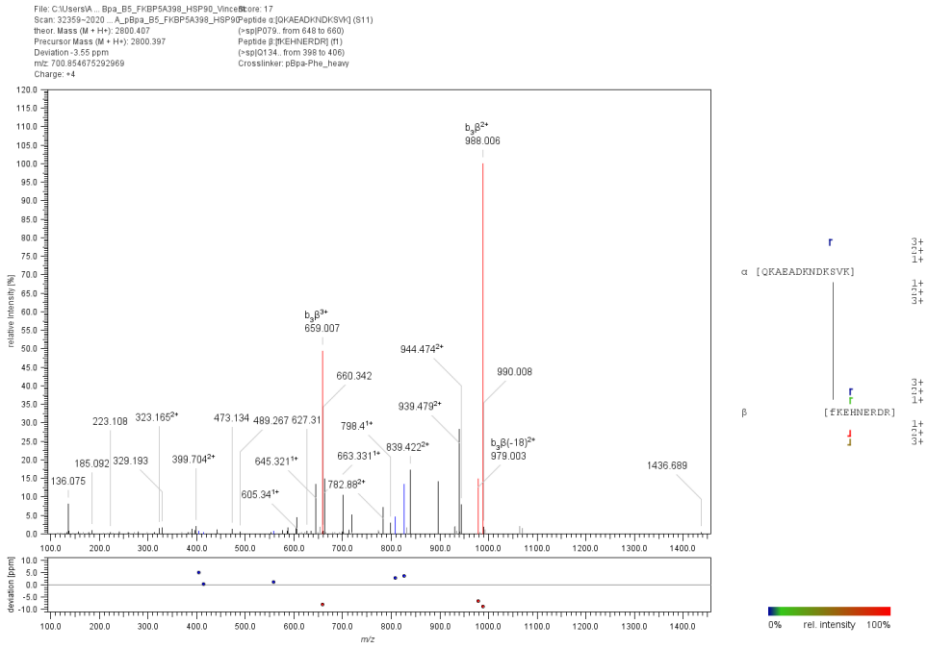

B

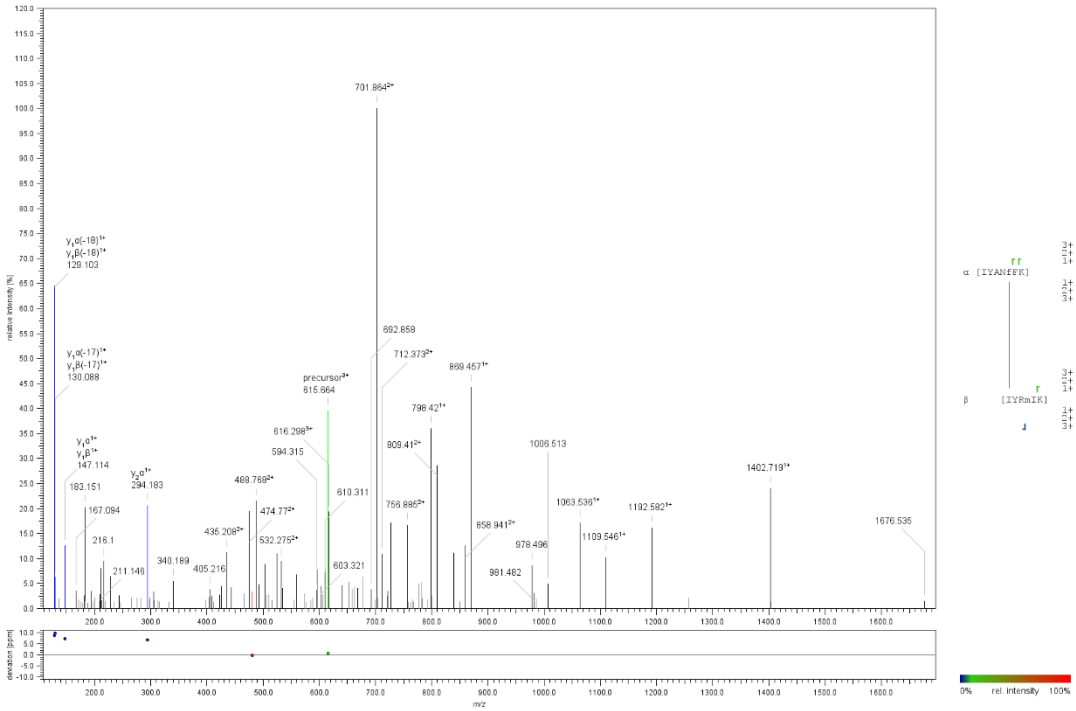

Extended Figure 2: MeroX output. Identification of crosslinked peptides by MeroX. A, MS/MS spectrum of a potential crosslinked FKBP51 A398pBpa→Hsp90 peptide of m/z = 701.1052. C, MS/MS spectrum of a potential crosslinked FKBP51 M412pBpa→Hsp90 peptide of m/z = 615.6642.

α-FLAG

FKBP51-FLAG	E75 pBpa		Q85 pBpa		P123 pBpa		T127 pBpa		G158 pBpa	G178 pBpa		K232 pBpa	
UV	–	+	–	+	–	+	–	+	–	+	–	+	–	+
	+ HA-Hsp90													

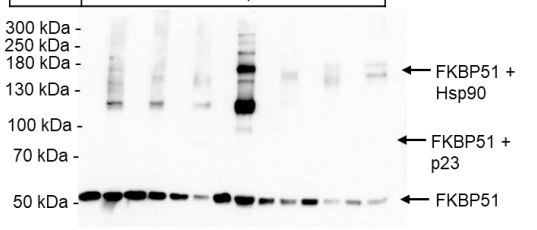

α-HA

FKBP51-FLAG	E75 pBpa		Q85 pBpa		P123 pBpa		T127 pBpa		G158 pBpa	G178 pBpa		K232 pBpa	
UV	–	+	–	+	–	+	–	+	–	+	–	+	–	+
	+ HA-Hsp90													

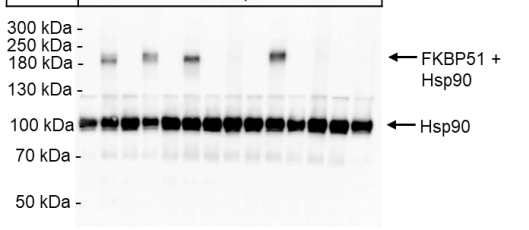

α-FLAG

FKBP51-FLAG	N238 pBpa		D260 pBpa		G281 pBpa		G303 pBpa		L362 pBpa	
UV	–	+	–	+	–	+	–	+	–	+
	+ HA-Hsp90									

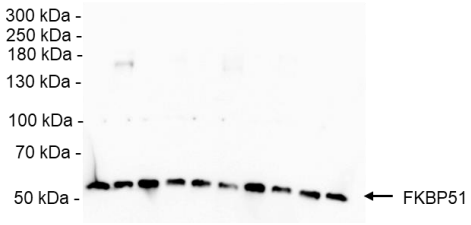

α-HA

FKBP51-FLAG	N238 pBpa		D260 pBpa		G281 pBpa		G303 pBpa		L362 pBpa	
UV	–	+	–	+	–	+	–	+	–	+
	+ HA-Hsp90									

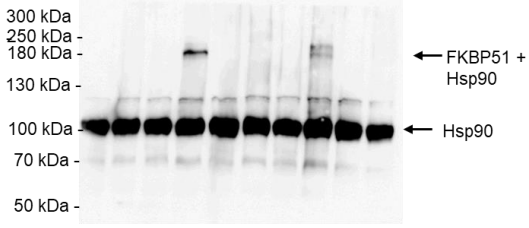

α-FLAG

FKBP51-FLAG	G64 pBpa		R73 pBpa		F77 pBpa		V78 pBpa		F79 pBpa		T96 pBpa		K108 pBpa	
UV	–	+	–	+	–	+	–	+	–	+	–	+	–	+
	+ HA-Hsp90													

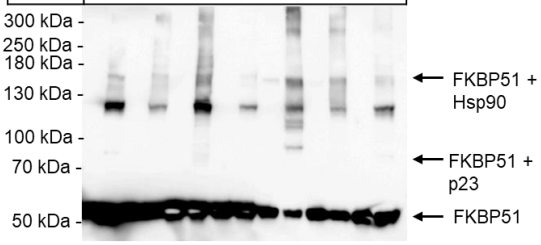

α-HA

FKBP51-FLAG	G64 pBpa		R73 pBpa		F77 pBpa		V78 pBpa		F79 pBpa		T96 pBpa		K108 pBpa	
UV	–	+	–	+	–	+	–	+	–	+	–	+	–	+
	+ HA-Hsp90													

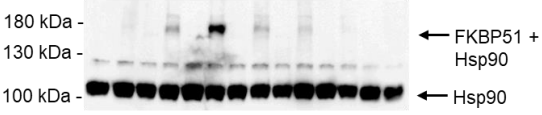

α-FLAG

FKBP51-FLAG	I122 pBpa		P123 pBpa		N125 pBpa		T127 pBpa		G158 pBpa	N161 pBpa		G178 pBpa	
UV	–	+	–	+	–	+	–	+	–	+	–	+	–	+
	+ HA-Hsp90													

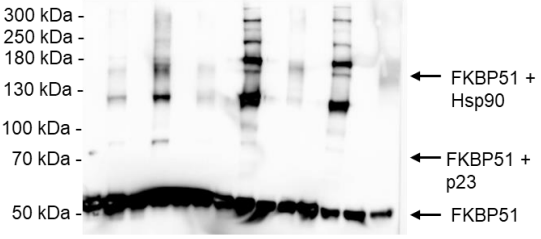

α-HA

FKBP51-FLAG	I122 pBpa		P123 pBpa		N125 pBpa		T127 pBpa		G158 pBpa	N161 pBpa		G178 pBpa	
UV	–	+	–	+	–	+	–	+	–	+	–	+	–	+
	+ HA-Hsp90													

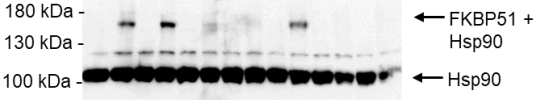

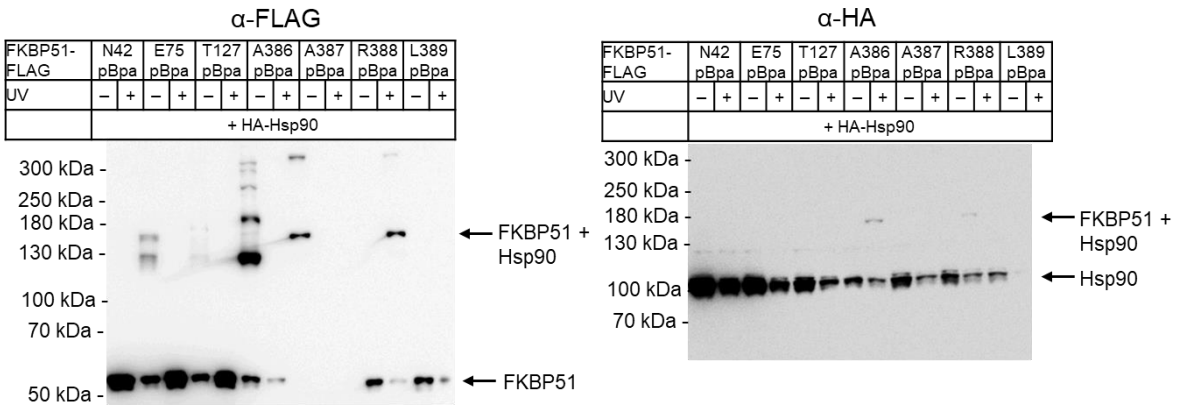

Extended Figure 3: In-cell photocrosslinking confirms multiple interaction sites between FKBP51 and Hsp90. Western blots of FKBP51 pBpa mutants expressed and photocrosslinked in HEK293 cells co-expressing HA-tagged Hsp90. UV light-induced HA-reactive bands at a size of ~160 kDa are indicative of the mutated position being in proximity to Hsp90.

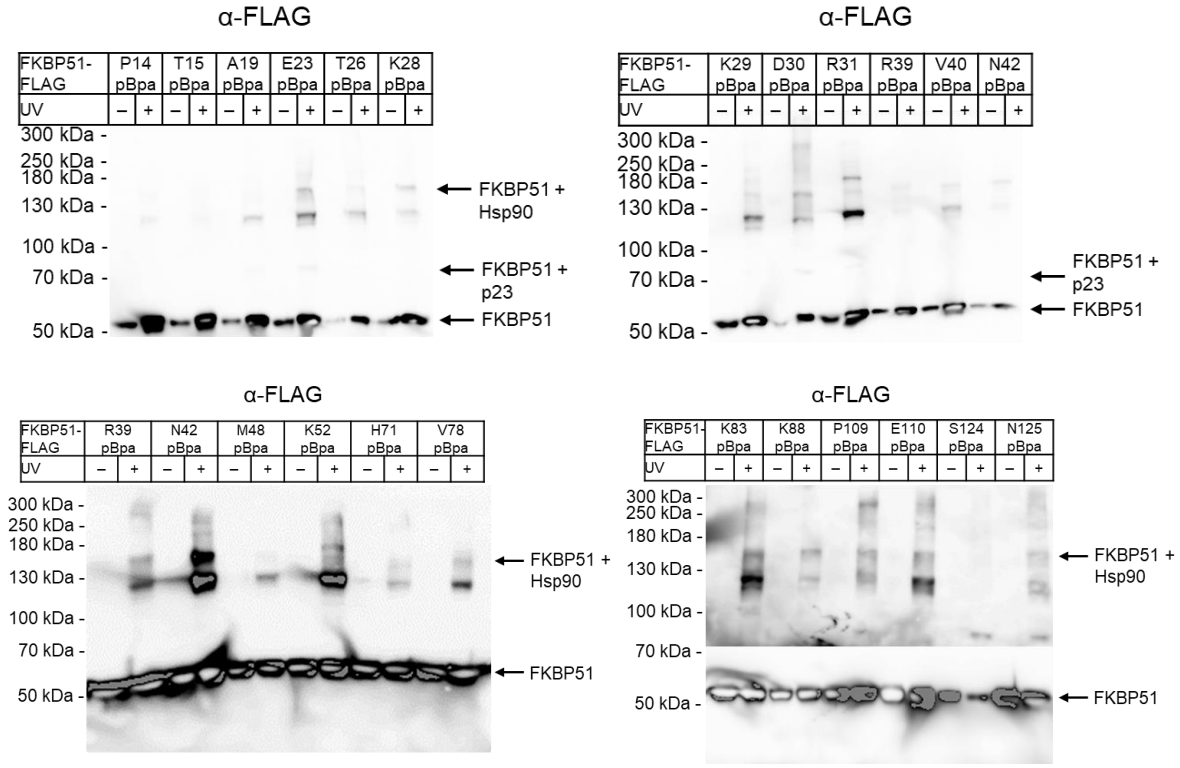

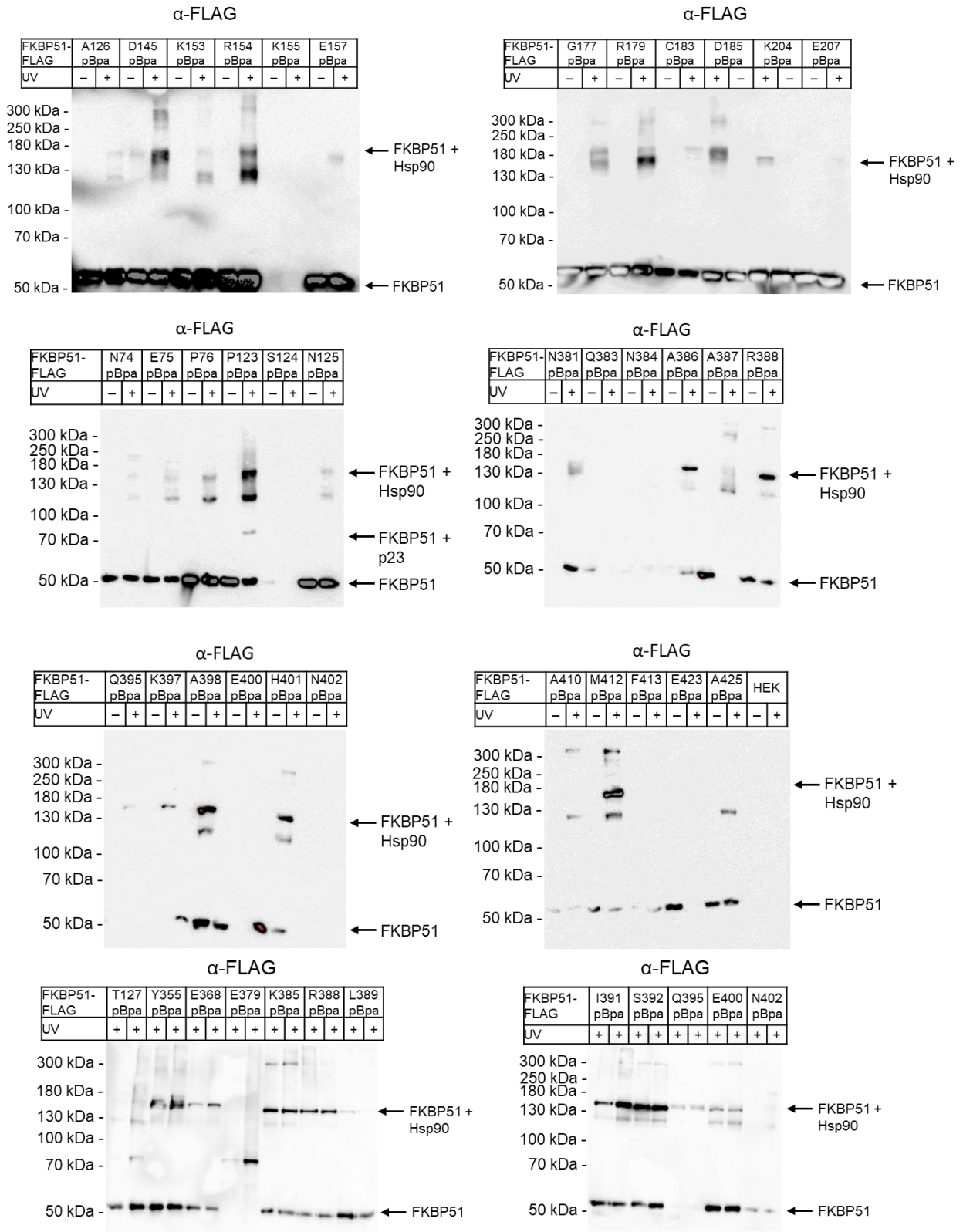

Extended Figure 4: In-cell photocrosslinking confirms multiple interaction sites between FKBP51 and Hsp90. Western blots of FKBP51 pBpa mutants expressed and photocrosslinked in HEK293 cells. UV light-induced FLAG-reactive bands at a size of ~160 kDa are indicative of the mutated position being in proximity to Hsp90 and bands at a size of ~70 kDa are indicative of the mutated position being in proximity to p23.

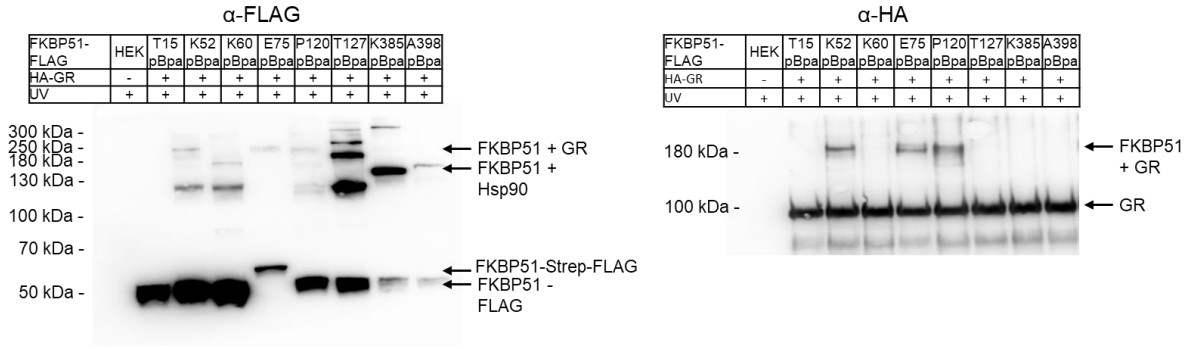

Extended Figure 5: In-cell photocrosslinking of selected FKBP51 pBpa mutants reveals direct FKBP51-GR interaction. Western blots of FKBP51 pBpa mutants in the FK1 domain expressed with HA-tagged GR overexpressed and photocrosslinked in HEK293 cells. UV light-induced HA-reactive bands at a size of ~180 kDa are indicative of the mutated position being in proximity to GR.

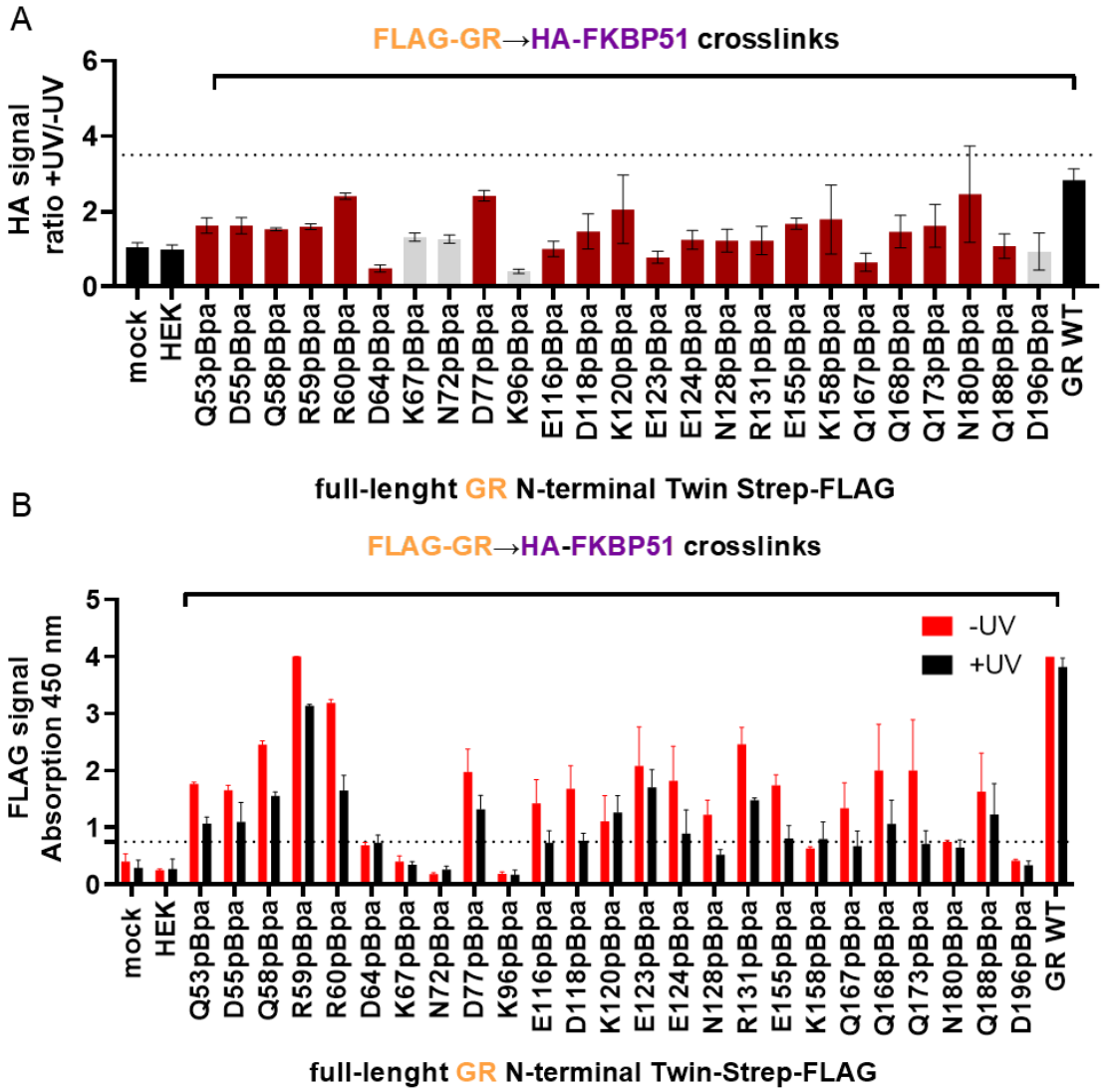

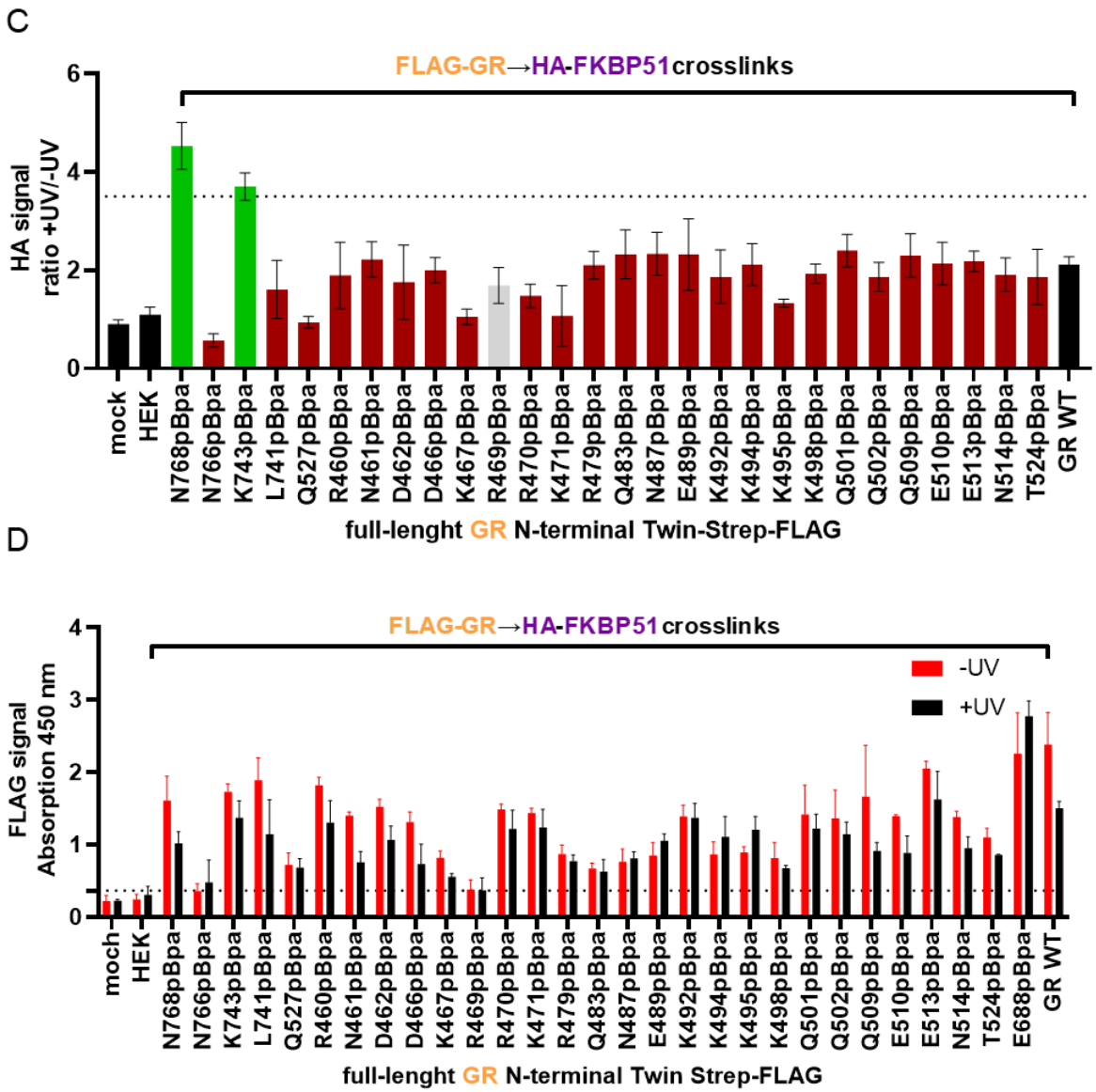

Extended Figure 6: Large scale GR→FKBP51 crosslinking screening by ELISA. A + C, ELISA data for selected full-length N-terminal Twin-Strep-FLAG GR pBpa mutants expressed and photocrosslinked in HEK293 cells co-overexpressing HA-tagged FKBP51. Irradiated cells and matched non-irradiated control cells are lysed, lysates are absorbed to Streptactin-coated 96 well plates, washed, and coated with HRP-coupled anti-HA antibodies to detect GR→FKBP51 crosslinks. The depicted values represent signal ratios of irradiated vs non-irradiated samples. HA ratios >3.5 are indicative of the mutated position being in proximity to FKBP51. Crosslinks detected by ELISA are highlighted in green and positions below the threshold are shown in red. Mock, non- or $GR^{wildtype}$-transfected HEK293 cells were included as background controls (black bars). B + D, A aliquot of each lysate was absorbed to separate Streptactin-coated 96 well plates, washed, and coated with HRP-coupled anti-FLAG antibodies to control for adequate GR expression levels. Grey sample (A + C) indicated amber suppression ratio signal/WT <25% (B + D), which were excluded from further analyses. Each bar represents data from biological replicates (n=3).

8. Abbreviations

ATP	Adenintriphosphat
Ca^{2+}	Calciumions
C-terminus	Carboxy-terminus
DAG	Diacylglycerol
DMSO	Dimethylsulfoxid
DTT	Dithiothreitol
EC_{50}	Concentration at which the effect is half maximal
EDTA	Ethylendiamintetraacetat
EtOH	Ethanol
Em	Emission
Ex	Excitation
FCS	Fetale Calf Serum
FKBP	FK506 binding Protein
FL	Full Length
FRET	Förster Resonance Energy Transfer
GAPDH	Glyceraldehyde 3-phosphate dehydrogenase
GR	Glucocorticoid Receptor
HEK	Human embryonal kidney cells
HP	Hausch Primer/Plasmid
HTRF	Homogenous Time Resolved Fluorescence
Hsp90	Heat shock protein HSP 90
IPTG	Isopropyl β-D-1-thiogalactopyranoside
NaAc	Sodium acetate
$NaPP_i$	sodium pyrophosphate
NMR	Nuclear magnetic resonance spectroscopy
N-terminus	Amino-terminus
PMSF	Phenylmethylsulfonylfluorid
SDS	Sodium dodecyl sulfate
TBS(-T)	Tris-buffered saline (-Tween)
TC	Tissue Culture

9. Bibliography

Baischew, A., Engel, S., Geiger, T. M., Taubert, M. C., & Hausch, F. (2023). Structural and biochemical insights into FKBP51 as a Hsp90 co-chaperone. *Journal of Cellular Biochemistry*.

Baischew, A*., Engel, S.*, Geiger, T. M., & Hausch, F. (2023). Large-scale in-cell photocrosslinking at single residue resolution reveals the molecular basis for glucocorticoid receptor regulation by immunophilins. *bioRxiv*, 2023-01.

* Equal contribution

10. Acknowledgment

I am thankful to my supervisor Prof. Dr. Felix Hausch who provided me with the opportunity to work in his group and on such a great topic. I also thank Prof. Dr. Harald Kolmar who agreed to be the second supervisor of this work. Thank you to all members of the Hausch lab for the great working environment in the lab. I also appreciate that all members of the biochemistry lab listened to my scientific fun facts. A special thanks goes to Sarah Engel, with whom I had the pleasure to work on deciphering the FKBP-GR interaction at single residue resolution. I want to thank Dr. Alexander Schießer for providing the Orbitrap mass spectrometer and splendid technical support and Dr. Tim Heymann for helping to set up an MS platform in the Hausch lab as well as for synthesizing the isotopically labeled pBpa. I am thankful to Dr. Georg Tascher and Dr. Vivien Schoonenberg for providing insights into mass spectrometry and for measuring my samples.

I am forever in debt to all the great students who helped me during this project: Kim Ziebner, Monika Gnatzy, Karola Bahrami, Luisa-Marie Pfeiffer, Sarah Engel, Jan-Philipp Kahl, Constanze Sixt, Lara Stolz, Malin Wilfinger and Janna Treber. The exciting discussions with you and your terrific commitment in the individual projects have contributed substantially to the results of this work.

I am grateful to my wife and partner Luisa Baischew for her love and support.